ALMA MATER STUDIORUM
UNIVERSITÀ DI BOLOGNA

DOTTORATO DI RICERCA IN

SCIENZE BIOTECNOLOGICHE, BIOCOMPUTAZIONALI, FARMACEUTICHE E FARMACOLOGICHE

Ciclo 38

Settore Concorsuale: 05/E1 - BIOCHIMICA GENERALE

Settore Scientifico Disciplinare: BIO/10 - BIOCHIMICA

THERAPEUTIC POTENTIAL OF UBIQSOME® SUPPLEMENTATION IN CONTRASTING ATORVASTATIN-INDUCED CYTOTOXICITY IN VITRO AND CDKL5 DEFICIENCY IN VIVO

Presentata da: Francesca Valenti

Coordinatore Dottorato

Maria Laura Bolognesi

Supervisore

Romana Fato

Co-supervisore

Christian Bergamini

Esame finale anno 2026

Therapeutic potential of Ubiqsome® Supplementation in contrasting Atorvastatin-induced cytotoxicity *in vitro* and CDKL5 deficiency *in vivo*

Abstract

Statins are the primary treatment for managing elevated cholesterol levels linked to acute cardiovascular risk. However, their use can lead to side effects, likely due to depletion of Coenzyme Q_{10} (CoQ_{10}), a crucial part of the mitochondrial electron transport chain and an antioxidant in membranes. Our study shows that Atorvastatin causes cytotoxic effects in human dermal fibroblasts by inducing oxidative stress and mitochondrial dysfunction. Supplementation with a formulated CoQ_{10} named Ubiqsome® in statin-treated cells considerably reduced ROS levels and restored mitochondrial oxygen consumption and the ATP/ADP ratio in the cells. Additionally, the data suggest that at high doses, Atorvastatin's off-target effects involve inhibition of mitochondrial respiratory complexes I and III, triggering reverse electron transport and ROS production at Complex I. These findings highlight the benefits of CoQ_{10} supplementation for reducing statin-induced cytotoxicity and propose a mechanism explaining the adverse effects of Atorvastatin treatment.

Ubiqsome® was also tested *in vivo*, to ameliorate the oxidative stress related to the CDKL5 deficiency disorder (CDD), a developmental encephalopathy caused by mutations in the cyclin-dependent kinase-like 5 (CDKL5) gene, characterized by a complex and severe clinical presentation, including early-onset epilepsy, cognitive, motor, visual, and gastrointestinal impairments. Currently, there is no available medical treatment to mitigate, reverse, or improve the course of this disease and enhance the patient's quality of life. Although CDD is primarily a genetic disorder affecting the brain, evidence suggests the presence of systemic abnormalities, such as a redox imbalance in plasma and skin fibroblasts derived from CDD patients, as well as in cardiac myocytes of a mouse

model of CDD. To elucidate the role of oxidative stress in CDD pathophysiology, this study aimed to investigate the therapeutic potential of Coenzyme Q_{10}, known for its potent antioxidant properties, using both *in vitro* and *in vivo* models of CDD. Our findings demonstrated that CoQ_{10} supplementation decreased general and mitochondrial reactive oxygen species (ROS) levels and restored glutathione homeostasis *in vitro*, using a neuronal cell model lacking the *CDKL5* gene. Notably, CoQ_{10} administered as Ubiqsome® provided a protective effect against lipid peroxidation and DNA damage in the heart tissue of a murine CDD model, the $Cdkl5^{+/-}$ female mouse, even though no alterations in CoQ_{10} or CoQ_9 content were observed in heart tissues.

Table of contents

Abstract 1

Statins are the primary treatment for managing elevated cholesterol levels linked to acute cardiovascular risk. However, their use can lead to side effects, likely due to depletion of Coenzyme Q_{10} (CoQ_{10}), a crucial part of the mitochondrial electron transport chain and an antioxidant in membranes. Our study shows that Atorvastatin causes cytotoxic effects in human dermal fibroblasts by inducing oxidative stress and mitochondrial dysfunction. CoQ_{10} supplementation in statin-treated cells considerably reduced ROS levels and restored mitochondrial oxygen consumption and the ATP/ADP ratio in the cells. Additionally, the data suggest that at high doses, Atorvastatin's off-target effects involve inhibition of mitochondrial respiratory complexes I and III, triggering reverse electron transport and ROS production at Complex I. These findings highlight the benefits of CoQ_{10} supplementation for reducing statin-induced cytotoxicity and propose a mechanism explaining the adverse effects of Atorvastatin treatment.

Abstract 2

CDKL5 deficiency disorder (CDD), a developmental encephalopathy caused by mutations in the cyclin-dependent kinase-like 5 (CDKL5) gene, is characterized by a complex and severe clinical presentation, including early-onset epilepsy, cognitive, motor, visual, and gastrointestinal impairments. Currently, there is no available medical treatment to mitigate, reverse, or improve the course of this disease and enhance the patient's quality of life. Although CDD is primarily a genetic disorder affecting the brain, evidence suggests the presence of systemic abnormalities, such as a redox imbalance in plasma and skin fibroblasts derived from CDD patients, as well as in cardiac myocytes of a mouse model of CDD. To elucidate the role of oxidative stress in CDD pathophysiology, this study aimed to investigate the therapeutic potential of Coenzyme Q_{10}, known for its potent antioxidant properties, using both *in vitro* and *in vivo* models of CDD. Our findings

demonstrated that CoQ_{10} supplementation decreased general and mitochondrial reactive oxygen species (ROS) levels and restored glutathione homeostasis *in vitro*, using a neuronal cell model lacking the *CDKL5* gene. Notably, CoQ_{10} administered as Ubiqsome® provided a protective effect against lipid peroxidation and DNA damage in the heart tissue of a murine CDD model, the $Cdkl5^{+/-}$ female mouse, even though no alterations in CoQ_{10} or CoQ_9 content were observed in heart tissues or in striated muscle. The results underscore the potential of the antioxidant supplement CoQ_{10} as a therapeutic strategy for counteracting the harmful oxidative stress associated with *CDKL5* deficiency, or other diseases displaying oxidative stress; however, they also remark the challenge linked to the biodistribution of CoQ_{10} to peripheral tissues.

1 Introduction

1.1. Cardiovascular diseases and Hypercholesterolemia

Cardiovascular diseases (CVD), consisting of ischemic heart disease, stroke, heart failure, peripheral arterial disease, and a number of other cardiac and vascular conditions (ASCVD) [1], remains a major cause of premature mortality, contributing to reduced quality of life, and rising health care costs [2]. Dyslipidaemia, and in particular hypercholesterolemia, is recognised as one of the most important risk factors associated with an increased risk of cardiovascular events [3]. Hypercholesterolemia is quite a common complex lipoprotein disorder defined by elevated plasma concentrations of total cholesterol. While the focus is generally on low-density lipoprotein-associated cholesterol (LDL-C) [4], there is an increased interest in the consideration of other apoB-containing lipoproteins in the development of ASCVD (VLDL, IDL, lipoprotein A), with the potential atherogenic actions of the individual components of the lipidome and proteome of LDL, that goes beyond cholesterol and apoB [5 6].

Sustained hypercholesterolemia drives pathological outcomes through the retention and alteration of apolipoprotein B-rich lipoproteins in the arterial intima, which incites endothelial dysfunction, draws monocytes, fosters foam cell development, and promotes smooth muscle cells proliferation—key features of atherogenesis. Over time, these processes culminate in the development of atherosclerotic plaques, which can progress to unstable lesions prone to rupture, thrombotic occlusion, and acute clinical events such as myocardial infarction, ischemic stroke, or sudden cardiac death [7]. Epidemiological and mechanistic studies have established a linear relationship between LDL-C exposure and ASCVD risk, with each 38.7 mg/dL (1 mmol/L) reduction in LDL-C associated with a ~21% relative risk reduction in major vascular events [8]. Globally, 4.4 million deaths were attributed to high LDL-C in 2019, which accounted for 12.6% of all risk-related deaths and had risen by 46.7% compared to 1990 [9] (Figure.1) . In 2019, 44% of global deaths from ischemic heart disease

was attributable to high LDL cholesterol [10]. While the advisable total cholesterol level should be about 150 mg/dL, with LDL-C at or below 100 mg/dL according to the American Heart Association [11], it's hard to precisely define the upper limits of cholesterol in plasma, since lipid profiles are continuous variable that depend on sex, age, pre-existent conditions, used drugs, pregnancy, etc [12]. Although there is no threshold cholesterol below which CVD risk ceases to exist, its incidence is higher in countries where mean adult levels of serum cholesterol are higher [13]. According to the 2025 Consensus on the Clinical Pathway of Blood Cholesterol Management in Taiwan [14], the recommended LDL-C target values are < 130 mg/dL, < 115 mg/dL, < 100 mg/dL, < 70 mg/dL, and < 55 mg/dL for those at low, moderate, high, very high, and extremely high risk, respectively. Some doubts have recently emerged about the actual link between high LDL-C blood levels and the insurgence of cardiovascular events [15], however, the evidence from randomised controlled trials of statins users demonstrates the benefit from lowering LDL-C levels to less than 1.8 mmol/l (70 mg/dl), when absolute CVD risk is high [16] [17] [18].

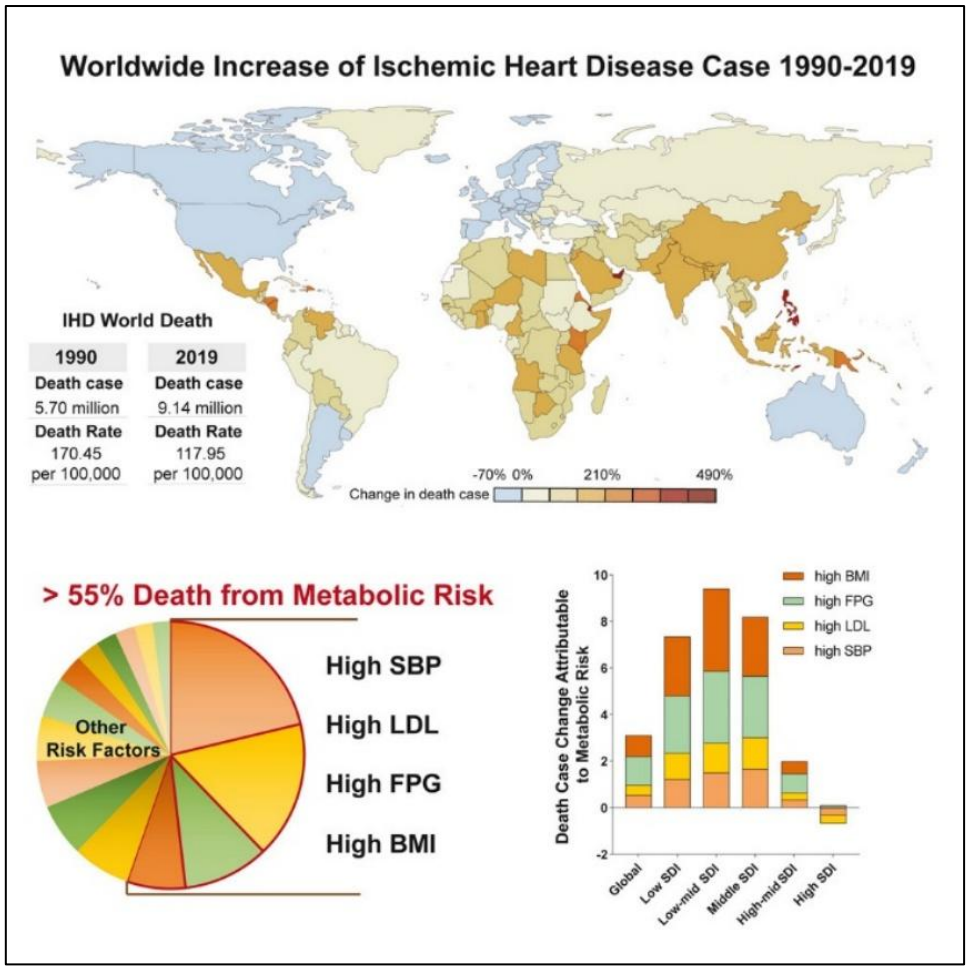

Figure 1. Worldwide increase of ischemic heart disease 1990-2019. Over recent decades, rapid economic development and social advancements have greatly increased the incidence of metabolic risk factors, which include high systolic blood pressure (SBP), high low-density lipoprotein cholesterol (LDL-c), high fasting plasma glucose (FPG), and high body mass index (BMI). Source: "Global Burden of Disease Study 2019 suggests that metabolic risk factors are the leading drivers of the burden of ischemic heart disease" by W. Wang et al. – Cell metabolism [19].

Disorders of cholesterol and lipoprotein metabolism may be the result of unhealthy dietary habits and physical inactivity [20], uncontrolled diabetes mellitus [21], and genetics [22]. From a pure etiological perspective, the commonest cause of hypercholesterolaemia is overproduction of LDL, mainly from VLDL, and a scarce clearance of these lipoproteins from the bloodstream, due to polymorphisms in certain genes, and in the presence of nutritional excess over energy expenditure [23] [24].

Hypercholesterolemia is in fact an heterogeneous disorder, with several subtypes identified, including familial hypercholesterolemia (FH), polygenic hypercholesterolemia, and secondary hypercholesterolemia due to underlying conditions or lifestyle factors.

Primary hypercholesterolemia is primarily driven by mutations in one (monogenic) or more (polygenic) genes involved in lipoproteins metabolism, or can be idiopathic. Genes involved comprise: LDL receptor, apolipoproteins APOB, APOA1, APOC2, APOA5, APOE, tribbles homolog 1 (TRIB1), and hepatic lipase (LIPC) [25] [26] [27] [28] [29].

It can be pure or combined, as the disorder can be characterized by solely increase of cholesterol, or also triglycerides.

Primary hypercholesterolemia comprises:

* Common hypercholesterolemia: polygenic, 70% of prevalence.
* Familiar hypercholesterolemia (FH, 0.2% prevalence): monogenic (dominant) homozygous or heterozygous. Most cases are due to mutation of the LDL receptor, with a smaller proportion due to mutations of the apoB100 gene, and gain-of-function mutations of proprotein convertase subtilisin kexin 9 (PCSK9).
* Autosomal recessive hypercholesterolemia: rare, due to dysfunction of an adaptor protein (ARH protein) required for receptor-mediated hepatic uptake of LDL.
* type III hyperlipoproteinemia caused by a defect in the ApoE2 protein, which prevents efficient clearance of VLDL remnants.

Acquired or secondary hypercholesterolemia is a lipid disorder characterized by elevated cholesterol levels that develop as a consequence of other underlying diseases or conditions, that interfere with lipid regulation [30]. Common causes of secondary hypercholesterolemia include endocrine disorders such as hypothyroidism, metabolic diseases like diabetes mellitus, kidney-related conditions including nephrotic syndrome and chronic renal failure, liver diseases (such as cholestasis or primary biliary cholangitis), and certain medications like steroids, thiazide diuretics, beta-blockers, and others [30] [31]. Lifestyle factors including unhealthy diet, obesity, and excessive alcohol intake also contribute.

INTRODUCTION

Therapeutic strategies for hypercholesterolemia are stratified according to ASCVD risk and LDL-C targets, as outlined by international guidelines (e.g., ESC/EAS, ACC/AHA) [32]. Dietary intervention is a first-line therapeutic approach to manage pure or combined hypercholesterolemia and reduce cardiovascular risk at all ages; adopting a heart-healthy habits such as dietary patterns (Mediterranean, Portfolio, and DASH diets) with a focus on reducing saturated fats intake, increasing viscous fibres, and the introduction of a regular physical activity, have demonstrated to ameliorate the lipid profile [33]. The decision to go beyond dietary advice and introduce lipid-lowering medications is based on an assessment of risk, and takes account for the severeness of the biochemical picture, comorbidities, age [34].

Pharmacological treatments include statins and non-statin drugs, such as ezetimibe, bile acid sequestrants, and PCSK9 inhibitors.

Statins are the first-line, most effective prescribed therapy, used for primary or secondary prevention, able to reduce LDL-C up to 60% through upregulation of hepatic LDL receptor (LDLR) expression and increased LDL clearance [35]. Used in case of detected hypercholesterolemia, or in presence of risk factors that can increase cholesterol or cardiovascular factors (preventive approach), their mechanism of action relies on the inhibition of the HMG-CoA reductase, mainly in the liver [36]. There is general agreement in Europe and the USA that the threshold for initiating statin treatment (for very high risk patients) should be that of LDL-C > 1.8 mmol/l (> 70 mg/dl), and the target of treatment should be LDL-C < 1.8 mmol/l (< 70 mg/dl) [37] [38]. Patients that would benefit from statin treatment, according to guidelines, are people with :

- known atherosclerotic CVD (coronary heart disease, stroke, and peripheral arterial disease);
- Type 1 diabetes for longer than 10 years, age ≥ 40 years, presence of microalbuminuria, or established nephropathy or other major cardiovascular risk factors;

- Monogenic hyperlipidaemias (which include familial hypercholesterolaemia) and very high cholesterol (defined by the European recommendations as ≥ 8 mmol/l (309 mg/dl);
- patients with chronic kidney disease.

The different statin therapies lower LDL-C levels with different magnitude, depending on the type, dose, individual response/tolerance [36].

When statin treatment is not sufficient, or tolerated, other non-statin medications are prescribed, alone or in combination with statins or other cholesterol-lowering drugs.

Ezetimibe reduces the absorption of cholesterol by specifically targeting the Niemann-Pick C1-Like 1 protein (NPC1L1) in the small intestine, a transmembrane protein located at the apical membrane of enterocytes that mediates the absorption of cholesterol (both derived from dietary intake and biliary) and phytosterols from the gut lumen [39]. When intestinal absorption of cholesterol is reduced, chylomicrons with a reduced amount of cholesterol are formed, thus cholesterol delivery to the liver is decreased. This leads to the activation of the SREBPs elements, that eventually lead to an increased expression of LDLR [40]. However, ezetimibe is less effective than statins, and only reduces LDL-C by about 20% [35].

Proprotein convertase subtilisin/kexin type 9 (PCSK9) inhibitors are used when the maximal tolerated dose of statin is not effective. PCSK9 is involved in the turnover of LDL, specifically promoting the degradation of LDLR [41]; moreover, recent studies have highlighted its role in exacerbating atherosclerosis through a mechanism independent of LDLR [42]. PCSK9 inhibitors include monoclonal antibodies or small interfering RNA, and lower LDL-C by 50-60% by decreasing PCSK9 and Lipoprotein A levels.

Bempedoic acid lowers LDL-C by 15-25% by inhibiting the hepatic ATP citrate lyase (ACLY) activity resulting in a decrease in cholesterol synthesis in the liver, and an up-regulation of LDL receptors. It's employed when statin therapy is not efficient or tolerated.

Lomitapide and evinacumab are approved for lowering LDL levels in patients with homozygous familiar hypercholesterolemia, as they are not dependent on LDL receptors for decreasing LDL levels. Lomitapide inhibits microsomal triglyceride transfer protein (MTP), essential for the assembly and secretion of very low-density lipoproteins (VLDL) and chylomicrons by the liver and intestine, respectively. Evinacumab is a monoclonal antibody that inhibits the activity of angiopoietin-like protein 3 (ANGPTL3), which regulates the body's lipid profile by inhibiting lipoprotein lipase (LPL) and endothelial lipase (EL); its inhibition results in the increased activity of LPL and EL, and a decrease in LDL-C, HDL-C, and triglyceride levels. – ref

This thesis will discuss and explore in detail statins.

1.2. Statins

Statins are the treatment of choice for the management of hypercholesterolemia, because of their safety profile and proven efficacy in preventing the risk of cardiovascular acute events in patients with an assessed risk and/or a clinical history of CVDs [43].

This class of drugs includes several compounds that differ in how effective they are, chemical structures, pharmacokinetic profiles, and tolerability; however, they all share a common mechanism of action, as they all are competitive inhibitors of the HMG-CoA reductase, the rate-limiting enzyme of the mevalonate pathway, that leads to cholesterol biosynthesis [44].

After the discovery that HMGR was the "pacemaker for cholesterol biosynthesis" by Nancy Bucher in the 1960's [45], Akira Endo and collaborators started postulating that some microbes may produce secondary metabolites that could inhibit the enzyme, as a defence mechanism against other microbes that required sterols and/or other mevalonate-derived isoprenoid compounds for their growth. In the early 1970s they isolated the first statin, mevastatin (named compactin back then), from *Penicillium citrinum* [46]; the compound was a potent inhibitor of HMG-CoA reductase (HMGCR)

enzyme and active *in vivo*, but toxicology studies demonstrated evidence of lymphomas in dogs receiving 200 mg/kg/day for 2 years [47]. Pravastatin was serendipitously discovered as an active metabolite of mevastatin found in dogs urines [48], followed by lovastatin (at first studied as monacolin K) introduction by Merck [49]. Other statins, such as simvastatin, are also derivatives of fungal products, but are chemically modified [50] [51]. Fluvastatin, cerivastatin, atorvastatin, rosuvastatin, and pitavastatin are completely synthetic, and all contain a fluorophenyl-substituted indole ring [52].

1.2.1. Chemistry, pharmacodynamics, and pharmacokinetics of statins

The chemical structure of a statin can be broadly divided into three parts:

1. the pharmacophore, a modified hydroxyglutaric acid structure, specifically a 3,5-dihydroxyheptanoic acid unit (3R,5R stereochemistry is critical for activity) that closely resembles the endogenous substrate HMG-CoA and the mevaldyl-CoA transition state intermediate. This mimicry allows statins to competitively bind to the active site of the enzyme HMG-CoA reductase, by forming polar interactions with the enzyme. The moiety can be present in an active hydroxy-acid form, or an inactive lactone form, hydrolysed *in vivo* to the respective active hydroxy-acid form;
2. an hydrophobic ring structure covalently linked to the pharmacophore, involved in the binding of the statin to the enzyme; the ring can be a partially reduced hexahydronaphthalene (lovastatin, simvastatin, pravastatin), a pyrrole (atorvastatin), an indole (fluvastatin), a pyrimidine (rosuvastatin), a pyridine (cerivastatin), or a quinoline (pitavastatin);
3. side groups on the rings that define the solubility properties of the drugs, and therefore many of their pharmacokinetic properties.

Type 1 statins have a substituted decalin ring structure similar to the natural statin mevastatin. They include lovastatin, pravastatin, and simvastatin. These statins are either naturally derived or semi-synthetic, often existing as inactive lactones that require metabolic activation to the active hydroxy-acid form.

Type 2 statins are fully synthetic and have larger, more complex ring structures with additional groups such as a fluorophenyl moiety replacing the butyryl group found in type 1 statins. This group enables additional polar interactions, leading to tighter binding to the HMG-CoA reductase enzyme. Examples include fluvastatin, atorvastatin, cerivastatin, and rosuvastatin [53] [54].

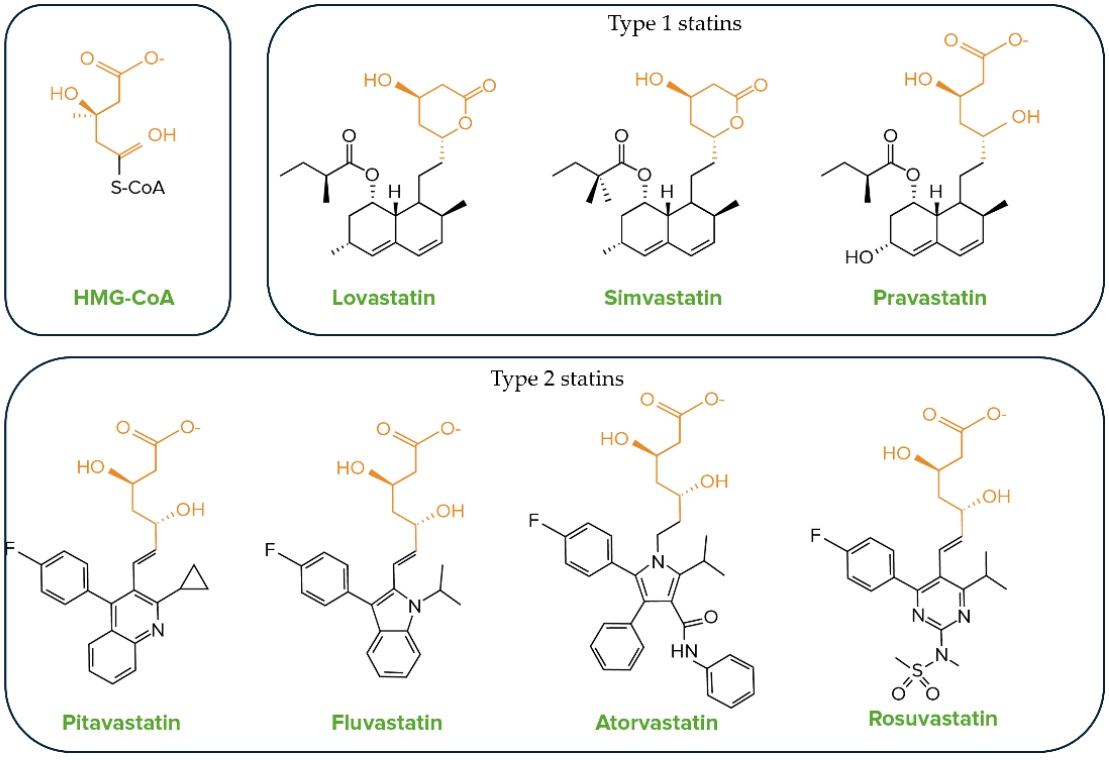

Figure 2. Chemical structures of HMG-CoA (natural substrate of HMG-CoA reductase) and different statins. Type 1 and type 2 statins are represented. The pharmacophore is represented in orange, the additional groups in black.

Notably, statins do not compete for the binding of the co-factor NADPH. Because statins are competitive with respect to HMG-CoA, it appeared likely that their HMG-like moieties might bind to the HMG-binding portion of the enzyme active site. However, in this binding mode their bulky hydrophobic groups would clash with residues that compose the narrow pocket which

accommodates the pantothenic acid moiety of CoA. By exploiting the conformational flexibility of HMGR to create a hydrophobic binding pocket near the active site, the bulky, hydrophobic compounds of statins occupy the HMG-binding pocket and part of the binding surface for CoA, contacting residues within helices Lα1 and Lα10 of the enzyme's large domain. Thus, access of the substrate HMG-CoA to the active site of the enzyme is blocked. The tight binding of statins is likely due to the large number of polar and non-polar interactions between the inhibitors and the active site of HMGR, which allows for the formation of hydrogen bonds. [55]. The structurally diverse, rigid hydrophobic groups of the statins are accommodated in a shallow non-polar groove that is present only when COOH-terminal residues of HMGR are disordered [56].

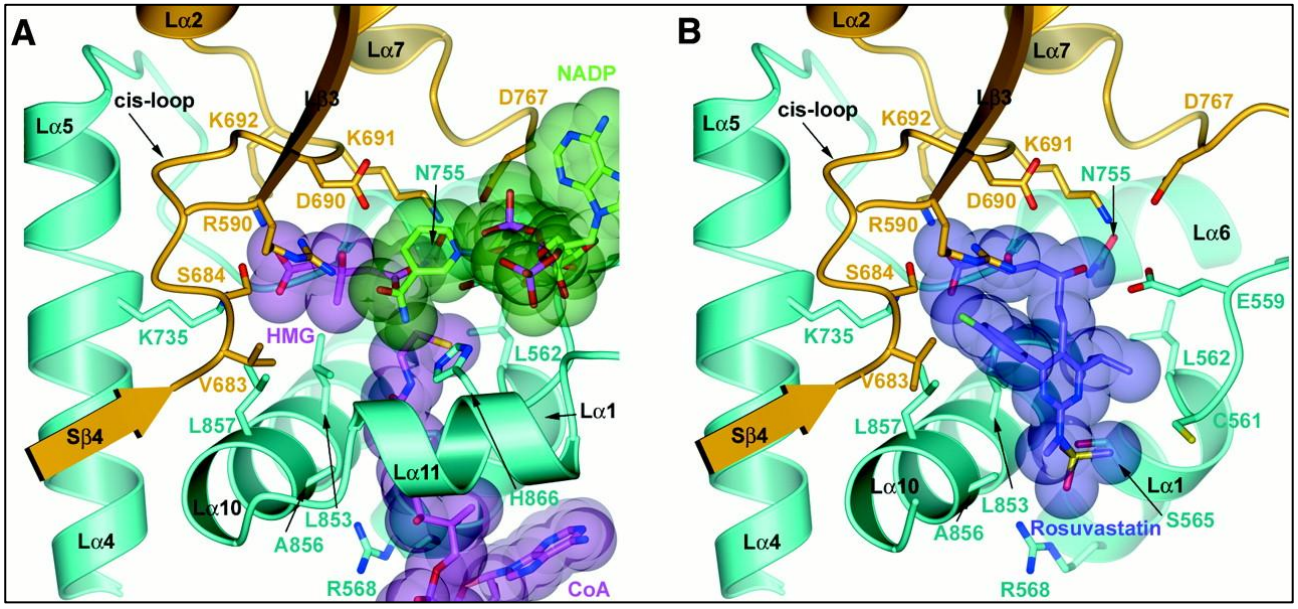

Figure 3. Interaction of the cis-loop (residues 682–694 within helices Lα1 and Lα10 of the enzyme's large domain) with the endogenous substrates HMG, CoA, and NADP (A) and with Rosuvastatin (B). The active site is located at a monomer-monomer interface. One monomer is coloured yellow, the other monomer is in green. Selected side chains of residues that contact the substrates or the statin are shown in a ball-and-stick representation. HMG and CoA are coloured in magenta; NADP is coloured in green, Rosuvastatin is coloured in purple. Source "Structural Mechanism for Statin Inhibition of HMG-CoA Reductase" by Eva S. Istvan and Johann Deisenhofer – Science [57]

Enzyme activity assay of HMG-CoA reductase substrate catalytic fragments indicates that statins, including simvastatin, pravastatin, fluvastatin, cerivastatin, atorvastatin and rosuvastatin, have a

high affinity for HMG-CoA reductase with inhibition constants (K_i) of 5–44 nM while the Michaelis constant (K_m) of HMG-CoA is 4 μM, suggesting that all statins are potent inhibitors of this enzyme [58] [59] [60].

Statins are also classified in "hydrophobic" and "hydrophilic"; this definition is mainly based on experimental partition coefficients [61]. The log *P* partition coefficient (commonly water–n-octanol) for un-ionized drugs (or where the pH is adjusted to ensure the predominant species is un-ionized) and the log *D* for ionized drugs (pH-dependent), are taken as measures of the lipophilicity of drugs. Log *D* is usually measured at pH = 7.4 (the physiological pH of blood serum). For un-ionized compounds, log *P* = log *D* at any pH [62].

The lipophilicity (log *D* at pH 7.4) of some of the most prescribed statins are reported in Table 1.

Table 1. Relative lipophilicity (log D and log P at pH 7.4) of some of the most prescribed statins. Source: "Cognitive effects of statin medications" by B. J. Kelley et al. – CNS Drugs [63].

Statin	Log *D* at pH 7.4	Log *P* at pH 7.0	Comparative lipophilicity	Protein binding (%)
Simvastatin	1.50 – 1.75	2.06	+++++	95-98
Lovastatin		1.70	+++++	>95
Atorvastatin	1.00 – 1.25	1.61	++++	98
Fluvastatin	1.00 – 1.25	1.67	++++	98
Rosuvastatin	-0.25 – 0.50	0.13	++	88
Pravastatin	-0.75 – 1.0	-0,23	+	43-67

Based on such data, rosuvastatin and pravastatin are commonly referred to as hydrophilic statins, while simvastatin, lovastatin, fluvastatin, and atorvastatin are called hydrophobic statins [64].

Depending upon their chemical structures, statins have different affinities for HMG-CoA reductase, which determines their pharmacological effects, and different pharmacokinetic properties (i.e. tissue distribution, metabolic stability, enzymes and transporters involved in their metabolism) [51]. These characteristics may also be related to the adverse effects of statins, that will be discussed later.

All statins currently on the market are well absorbed from the intestine. The mechanism for the intestinal absorption of statins varies from one drug to another, involving passive diffusion and/or specific transport systems [64]. The main target of statins is the liver, as the homeostasis of the body cholesterol is controlled by this organ, although other tissues may be reached. To date the human transporters involved in the uptake of statins have been characterized: pravastatin, cerivastatin, pitavastatin, rosuvastatin and atorvastatin are substrates of human OATP1B1 (also referred to as OATP-C/OATP2/LST-1, SLCO1B1/SLC21A6) [65] [66] [67]. The hepato-selectivity of the statins is related to the distribution of these transporters (also present in the intestine, where statins are first absorbed), but also to their lipophilicity. The more lipophilic statins (especially those in lactone form) tend to achieve higher levels of exposure in non-hepatic tissues, passively and non-selectively diffusing, while the hydrophilic statins tend to be more hepato-selective [68].

Metabolism occurs in different ways. Lipophilic statins undergo hepatic and enteric metabolism via cytochrome P450 (CYP450 family of enzymes) whereas the water soluble statins are excreted largely unchanged. Pravastatin and rosuvastatin are mainly eliminated from the body by a transporter-mediated excretion mechanism in the liver, and excreted in the urines; these statins have been not shown to participate in any clinically relevant drug–drug interactions with CYP450 agents. Other statins are excreted with the bile [69] [70] [71] [72].

To respect to the closed or open form of the pharmacophore, statins in the acid form undergo lactonization, via acyl glucuronide, and the lactonized form can be converted again to the open acid form by carboxy esterase; subsequently, the compounds are metabolized or excreted into the bile or urine, or directly metabolized by P450 as the lactone forms [64].

1.2.2. Inhibition of the Mevalonate pathway

Statins are competitive reversible inhibitors of HMG-CoA reductase (HMGR) [73]. The mevalonate pathway is an essential anabolic pathway, crucial for cell growth, differentiation and structure of cell membranes; it uses acetyl-CoA, NADPH and ATP to produce sterols and isoprenoid metabolites that are essential for a variety of biological processes [74]. The synthesized compounds include: cholesterol and its derivatives (bile acids and steroid hormones), dolichols (essential for protein glycosylation), heme A (part of the respiratory chain) and the isoprenoid sidechain of ubiquinone (potent membrane antioxidant, and key component of the electron transport chain).

The efficiency of the pathway partially relies on the availability of the various substrates, that derive from different processes in the cell: acetyl-CoA is produced following glucose, glutamine or acetate metabolism; NADPH is produced from the pentose phosphate pathway, isocitrate dehydrogenase, malic enzyme; ATP production relies on the oxidation of substrates as glucose or fatty acid, therefore on the mitochondrial function.

The main steps of the pathway are represented in Figure 4:

1. Condensation of two acetyl-CoA molecules to form acetoacetyl-CoA, catalysed by acetyl-CoA acetyltransferase.
2. Addition of a third acetyl-CoA to acetoacetyl-CoA, forming 3-hydroxy-3-methylglutaryl-CoA (HMG-CoA), catalysed by HMG-CoA synthase.
3. Reduction of HMG-CoA to mevalonate by HMG-CoA reductase, using NADPH. This is the rate-limiting and key regulatory step.
4. Phosphorylation of mevalonate to mevalonate-5-phosphate by mevalonate kinase.
5. Further phosphorylation to mevalonate-5-diphosphate by phosphomevalonate kinase.
6. Decarboxylation and phosphorylation of mevalonate-5-diphosphate to isopentenyl pyrophosphate (IPP), releasing CO2, catalysed by mevalonate-5-diphosphate decarboxylase.

7. Isomerization of IPP to dimethylallyl pyrophosphate (DMAPP) by isopentenyl-diphosphate isomerase. IPP and DMAPP serves as monomeric units for the consequent synthesis of all downstream metabolites in a so-called "head-to-tail" manner, such as 15-carbon intermediate farnesyl pyrophosphate (FPP).
8. FPP constitutes the major branch-point in polyisoprene biosynthesis. This compound can participate in three different sets of enzymatic reactions. In the first set two FPP units, thanks to repeated "head-to-head" condensations, form squalene, the first intermediate for the sterol pathway. In the second set of reactions, FPP molecules are converted into long-chain polyisoprene alcohols. In the third set FPP condensate with isopentenyl, through "head-to-tail" polymerizations, producing long chain isoprenoids. The main features of these long-chain polyprenols are that double bonds are in the trans configuration. Once the chain length reaches 10 isoprene units in human cells, the polyisoprenil tail is transferred to the benzoquinone head in order to initiate COQ_{10} biosynthesis.

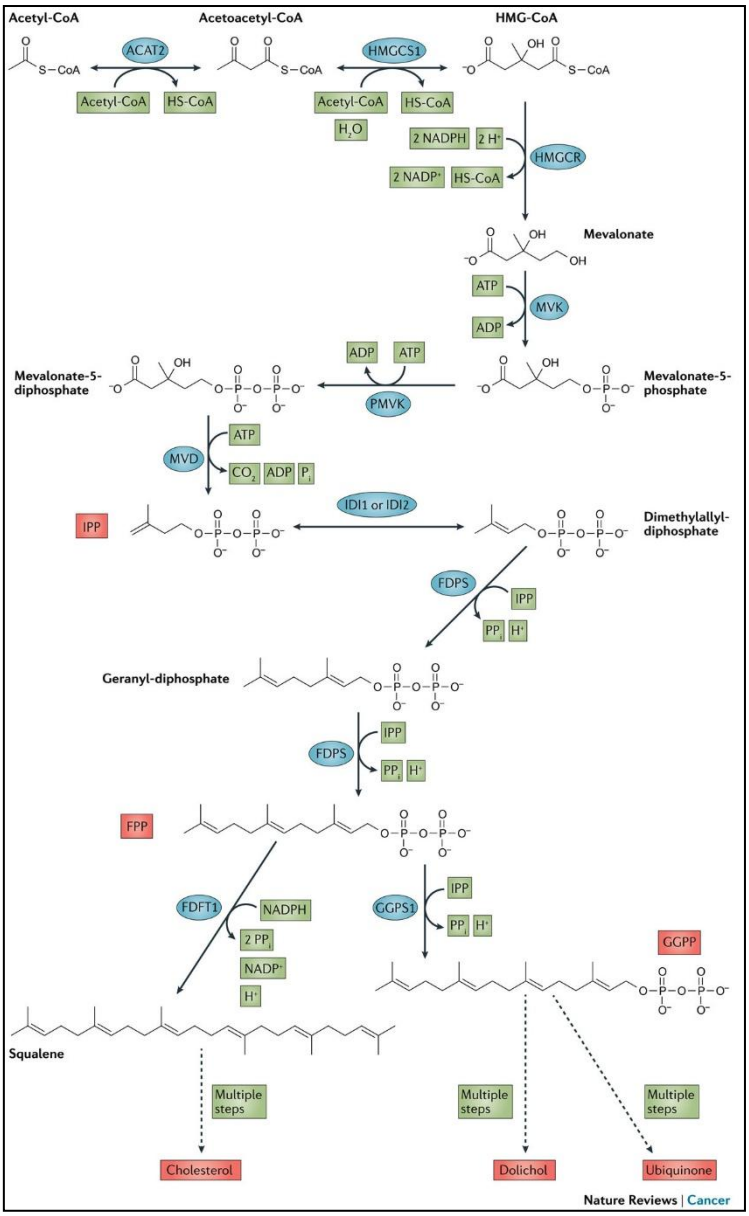

Figure 4. Key biochemical reactions of the mevalonate pathway. Mevalonate (MVA) pathway enzymes condense three acetyl-CoA molecules in a two-step reaction to produce 3-hydroxy-3-methylglutaryl CoA (HMG-CoA). Both reactions are reversible and in equilibria, with the intracellular concentration of acetyl-CoA being the primary driver. HMG-CoA is then reduced by HMG-CoA reductase (HMGCR) to produce MVA via an irreversible reaction. MVA is then converted into isopentenyl-diphosphate (IPP) through a series of enzymatic steps, which serves as a monomeric unit for the consequent synthesis of all downstream metabolites (metabolites discussed in this Review are highlighted in pink). Dashed arrows indicate multiple steps. ACAT2, acetyl-CoA acetyltransferase 2; FDFT1, farnesyl-diphosphate farnesyltransferase 1; FDPS, farnesyl diphosphate synthase; FPP, farnesyl diphosphate; GGPP, geranylgeranyl-diphosphate; GGPS1, geranylgeranyl diphosphate synthase 1; HMGCS1, HMG-CoA synthase 1; IDI, isopentenyl diphosphate isomerase; MVD, mevalonate-diphosphate decarboxylase; MVK, mevalonate kinase; PMVK, phosphomevalonate kinase. Source "The interplay between cell signalling and the mevalonate pathway in cancer" by P.J. Mullen – Nature Reviews Cancer [75].

The reduction of the HMG-CoA to mevalonate by the HMG-CoA reductase is the limiting step of the pathway, meaning the activity of HMGCR controls the overall speed of the pathway. The

reaction lead by HMGCR is a four-electron reductive deacylation of HMG-CoA to CoA and mevalonate that proceeds as follows:

$$(S)\text{HMG-CoA} + 2\text{NADPH} + H^+ \rightarrow (R)\text{mevalonate} + 2\text{NADP}^+ + \text{CoA-SH}\ .$$

HMGCR activity and levels are tightly regulated through feedback mechanisms to maintain lipid homeostasis. The regulation proceeds at four levels:

1. transcriptional: when cholesterol levels are low, Sterol Regulatory Element-Binding Proteins (SREBPs) bind to the promoter of the HMGR gene, activating its transcription and increasing enzyme production;
2. translational: high levels of farnesol inhibit the translation of HMGR mRNA;
3. post-translational: low ATP levels activate AMPK, which phosphorylates HMGR at serine 871/872, inhibiting the enzyme;
4. turnover: when high sterol levels are detected through the sterol-sensing domain, the enzyme is ubiquitinated on specific lysine residues, and degraded in the proteasome system [76].

The inhibition of HMGR efficiently decreases the enzyme activity, blocking the mevalonate pathway upstream. This translates into a lower synthesis of all the metabolic intermediates, starting from mevalonate, including cholesterol.

1.2.3. Cholesterol-lowering effect *in vivo*

About 50% or more of the total cholesterol in the body is endogenous and it is mainly synthesized in the liver, so the liver is the target organ of statins [77].

The associated reduction in intracellular cholesterol concentration induces the activation of the SREBPs elements, that leads to an increased transcription and expression of LDL-receptor on the hepatocyte cell surface; this results in an increased extraction of LDL-C from the bloodstream.

SREBPs activation also leads to an increase in the expression of the HMGR as a feedback mechanism, which can sound contradictory in terms of efficacy of the therapy; however, cytochrome P450 7A1 (CYP7A1, cholesterol 7α-hydroxylase), which is specific to the liver, transforms intracellular cholesterol to bile acids, leading to a reduction of cholesterol in hepatocytes, although it is taken up via upregulated LDL-receptors. Biodegradation of cholesterol in the liver and excretion of bile acids results in a reduction of total cholesterol in the body. [78]

Statins have beneficial effects on plasma lipid profiles beyond lowering LDL-cholesterol: they modestly increase high-density lipoprotein-cholesterol (HDL-C) blood concentration by approximately 4% to 10%, and the change is greater in patients with lower baseline HDL-C levels and in those with the combination of high triglycerides and low HDL-C.

Statins also reduce triglyceride concentrations, which contributes to improved lipid profiles [79]. Statins also exert beneficial cardiovascular effects that go beyond their lipid-modifying properties. These non-lipid effects are often referred to as pleiotropic effects. One key mechanism involves inhibiting the synthesis of non-steroidal isoprenoid compounds, such as farnesyl-pyrophosphate (FPP) and geranyl-geranyl-pyrophosphate (GGPP), important for the post-translational modification of proteins such as prenylation, which is crucial for the function of various proteins involved in cell signalling and survival [80].

Anti-atherosclerotic effects of the statins include:

- Inhibition of migration and proliferation of arterial myocytes
- Inhibition of macrophage growth
- Inhibition of cholesterol accumulation in macrophages
- Inhibition of cell adhesion
- Induction of myocytes apoptosis in proliferative lesions
- Inhibition of tissue factor expression and activity [81].

1.2.4. Side effects of statins

Statins are the most prescribed drugs worldwide, since they are considered safe and effective in reducing the risk of occlusive vascular events, as reported by meta-analyses of individual participant data from randomised trials [82]. Nonetheless, many statin users – 30% or more – abandon the therapy within 1 year, due to adverse effects, raising the risk of cardiovascular acute events. The reasons behind discontinuation of the therapy are many, as statins are associated with an increased risk of diabetes mellitus (a 10% proportional increase, primarily affecting patients with pre-existing diabetes risk factors), hepatic transaminase elevations, cognitive dysfunction and several symptoms such as myalgia, even if a causal link between statin use and these symptoms is still debated [83].

Statin-associated muscle symptoms (SAMS) is the most prevalent registered adverse effect related to statins. Observational studies indicate an incidence of SAMS of 30%, while on the other hand, randomized clinical trials suggest a much lower rate (about 5%) [83] [84] [85]. Muscle symptoms include myalgia (intended as muscle pain or aching, stiffness, tenderness, or cramp), myopathy, and myositis with or without creatine kinase (CK) elevation, and in the most severe cases as rhabdomyolysis (1-2 cases per 10,000 person-years of statin use) [86].

SAMS are the most important and commonly reported side effect of statins primarily because they are the leading cause of statin intolerance, non-adherence, and discontinuation. This is critical because discontinuing statins due to these symptoms can increase the risk of adverse cardiovascular outcomes due to inadequate lipid management. Because SAMS can lead to stopping or switching statins, they represent a major clinical challenge in managing patients requiring long-term cardiovascular protection [87].

1.2.5. Molecular basis of SAMS

How statins injure skeletal muscle is not clear, as the pathophysiology of SAMS is not fully understood. Several and controversial mechanisms have been proposed. Data and speculations result from observational studies in statin users or *in vitro* studies in cell models.

A first factor to take into account is the chemical properties of the statins that influence their pharmacokinetics. Higher lipophilicity in statins is associated with lower hepato-selectivity because lipophilic statins more readily cross cell membranes and thus distribute more widely into extrahepatic tissues, including muscle and other organs, rather than remaining concentrated in the liver. This broader tissue distribution contrasts with hydrophilic statins, which are more hepato-selective due to their limited ability to diffuse across cell membranes, leading to preferential uptake by liver cells. Therefore, a higher hepato-selectivity is believed to reduce the risk of adverse side effects such as SAMS because this selectivity limits the drug's accumulation in muscular tissue. This relationship is supported by studies showing that muscle side effects are more common with lipophilic statins like simvastatin and atorvastatin, compared to hydrophilic ones like pravastatin and rosuvastatin. The mechanism appears to be multifactorial but includes the dosage, the degree of uptake and clearance, and a possible accumulation in muscle tissue due to an increase of systemic exposure, influencing toxicity such as muscle pain, inflammation, and damage [88] [89].

The pleiotropic effects displayed by the statins can be attributed to the consequences of the inhibition of the mevalonate pathway (on-target effects), that causes decreased biosynthesis of many key molecules, or to off-target effects.

<u>On-target effects</u>.

The mevalonate pathway is a critical metabolic route responsible for the biosynthesis of cholesterol, and other essential intermediate metabolites, such as isoprenoids, dolichols, heme A. By inhibiting

the pathway upstream, at the rate-limiting enzyme level – by a competitive inhibition of HMGR – statins decrease biosynthesis of multiple intermediate metabolites, essential for the cell homeostasis. The reduction in cholesterol biosynthesis in muscle cells by statins leads to a reduction in their cholesterol contents of the plasma membrane. This may cause breakdown of the T-tubular system and subsarcolemmal rupture, as reported by *Draeger et al*. [90]. However, this hypothesis conflicts with the fact that cholesterol reduction obtained by squalene synthase or PCSK9 inhibition does not trigger myotoxicity, suggesting that the toxic effect may derive from the accumulation of intermediate metabolites, or other off-target effects [91] [92].

Some reports support the hypothesis of the lower prenylation of small GTP-binding proteins (Ras, Rac, Rho) which can lead to altered homeostasis and apoptosis of myocytes [93] [94] [95].

Many authors support the hypothesis of the secondary deficiency of CoQ_{10} as the leading cause for SAMS. CoQ_{10}, a lipophilic molecule located in the membranes, plays a pivotal role in the inner mitochondrial membrane, taking part of the electron transport chain and ATP production. Moreover, it's a potent membrane antioxidant and has a role in the biosynthesis of pyrimidines. In some studies myopathy has been reported to be associated with muscle CoQ_{10} deficiency, while some other studies question this point, as collected data are contradictory [96] [97] [98]. For example, *Laakson et al*. reported that CoQ_{10} in the skeletal muscle is not reduced by administration of statins while *Paiva et al*. showed that it is reduced in patients taking a high dose of simvastatin [99] [100].

Off-target effects.

Pleiotropic effects of statins have been described as independent of cholesterol lowering outcomes. Statins have been described as powerful antagonists of the chloride (Cl^-) channel in the muscle membrane, *Pierno et al*. reported a marked reduction of the resting chloride conductance (gCl) with

an increase of sarcolemma excitability that shifted the mechanical threshold for contraction towards more negative potentials [101].

A recent study revealed that SAMS is associated with the off target inhibition of mitochondrial complex III by statin lactones [102]. This last remark opens the question about the diverse mechanisms of action that the different statins may exert. In fact, it's widely discussed that the pleiotropic observed effects may depend on the chemical structure of the compound, and specifically be characteristic of the lipophilic statins [103] [104]. Lipophilic statins have higher pro-apoptotic activity than hydrophilic statins, which is likely due to differential transmembrane uptake [105]. Lipophilicity is related to hepato-selectivity: the more lipophilic statins tend to achieve higher levels of exposure in non-hepatic tissues, such as muscle tissue. Rosuvastatin and pravastatin, which mainly rely on active transport into the liver, tend to display less collateral effects, especially regarding muscle symptoms, although no statin treatment is recommended in case of rhabdomyolysis. Finally, interindividual difference in the pharmacological and/or toxic side effects have been associated to genetic variability, as for example some patients may be more susceptible to SAMS due to polymorphisms in genes encoding proteins involved in statin uptake and metabolism, such as the solute carrier organic anion transporter family member 1B1 (SLCO1B1) or cytochrome P450 (CYP2D6, CYP3A4, CYP3A5) [106]. An altered metabolism and clearance of lipophilic statins (hydrophilic are expelled almost unaltered) may increase their concentration in tissues. Moreover, it has recently been identified that pravastatin, simvastatin, and fluvastatin inhibit human OATs (organic anion transporters) activity [107].

In this thesis we will discuss the statin-induced side effects in relation to Coenzyme Q_{10} deficiency. Statins reduce CoQ_{10} levels in blood and muscle tissue, which can impair mitochondrial function and reduce cellular energy production. This mitochondrial dysfunction leads to muscle symptoms like fatigue, pain, and in severe cases, rhabdomyolysis. Several studies have shown statin therapy causes a significant drop in CoQ_{10} levels, correlating with the severity of muscle symptoms [108].

One prospective study specifically on atorvastatin revealed a nearly 50% reduction in plasma CoQ_{10} levels after 30 days of treatment [109]. This reduction is relevant since CoQ_{10} is essential for mitochondrial energy production in muscle cells, and its deficiency is linked to muscle-related side effects like myalgia and exercise intolerance. Supplementation with CoQ_{10} has shown promise in alleviating these muscle symptoms by helping restore mitochondrial function, though more research is still needed for definitive conclusions. Some meta-analyses have found mixed results, with certain studies not demonstrating significant benefits, indicating that more research is needed to define the precise role of CoQ_{10} supplementation in statin therapy [110].

1.3. Coenzyme Q_{10}

There is consensus that CoQ_{10} depletion may be a plausible, though not fully proven, mechanism behind muscle-related SAMS [111]. Case reports and clinical studies have shown muscle symptoms improving with CoQ10 supplementation in mitochondrial and primary CoQ_{10} deficiency myopathies, but results in SAMS-suffering patients are inconsistent, with some trials showing benefit and others not [112].

Coenzyme Q, also named Ubiquinone (CoQ), is a highly hydrophobic molecule ubiquitously distributed in every eukaryotic cell membrane. Chemically, it's a 2,3-dimethoxy, 5-methyl, 6-polyisoprene parabenzoquinone, in which the polyisoprene tail can vary in length, depending on the species. In humans, coenzyme Q10 (CoQ_{10}) is therefore a 1,4-benzoquinone, in which "Q" refers to the quinone chemical group and "10" refers to the number of isoprenyl chemical subunits. The benzoquinone group cycles between a reduced (ubiquinol) and an oxidized (ubiquinone) form: each carbonyl group can accept one electron, and the redox cycle occurs by the transfer of one electron at the time, a process that generates a semiquinone intermediate. The tail helps

anchoring CoQ_{10} firmly within the lipid bilayer of cell membranes, maintaining the molecule's proper orientation and mobility within the membranes.

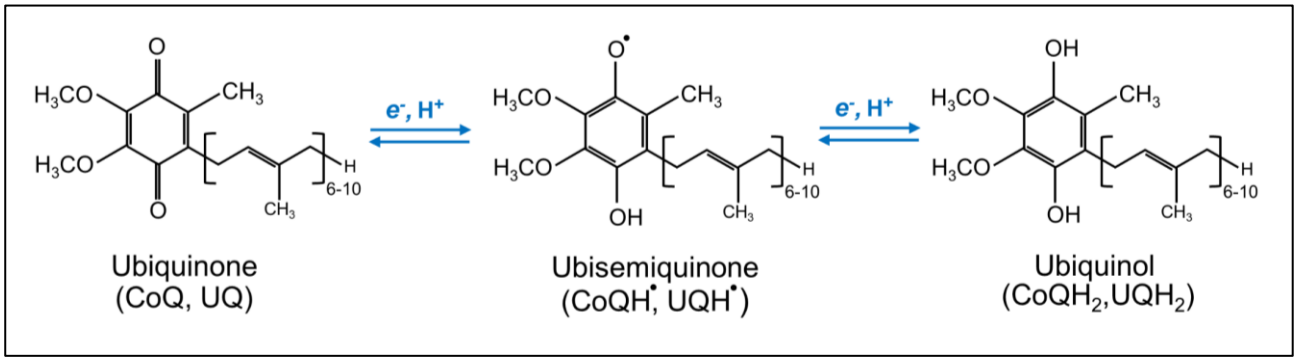

Figure 5. Coenzyme Q chemical structure and single electron transfer redox reactions of the CoQ head group, whereby CoQ can cycle through the oxidized (CoQ), radical ($CoQH^{\bullet}$), and fully reduced ($CoQH_2$) forms. Source "Understanding coenzyme Q" by Y. Wang et al. – Physiological Reviews [113].

The CoQ_{10} head group is derived from the essential amino acid phenylalanine, which is converted into tyrosine and, subsequently, 4-hydroxybenzoate (4-HB). Despite this, biosynthetic details of 4-HB production biosynthesis from tyrosine remain still unclear. The tail is attached to the ring precursor 4-HB in the matrix side of the inner mitochondrial membrane, through an aromatic substitution, catalysed by the mitochondrial enzyme COQ2, which represents the rate-limiting enzyme for the biosynthesis of CoQ_{10}, although it has been speculated that Ubiad1, a prenyl-transferase in the Golgi, may be responsible for this reaction, to produce the pool of non-mitochondrial CoQ_{10} [114]. The head group is then modified by other components of the COQ-synthome, the multiprotein biosynthetic complex involved in CoQ_{10} biosynthesis. The ring is hydroxylated at positions 5 and 6 by COQ6 and COQ7 respectively, O-methylated by COQ3 at positions 5 and 6, and C-methylated at position 2 by COQ5. The sequences of these reactions follow the chemical logic of electrophilic aromatic substitution (EAS) reactions on the aromatic ring. Finally, COQ4 is required for the oxidative decarboxylation of the C1 carbon [115].

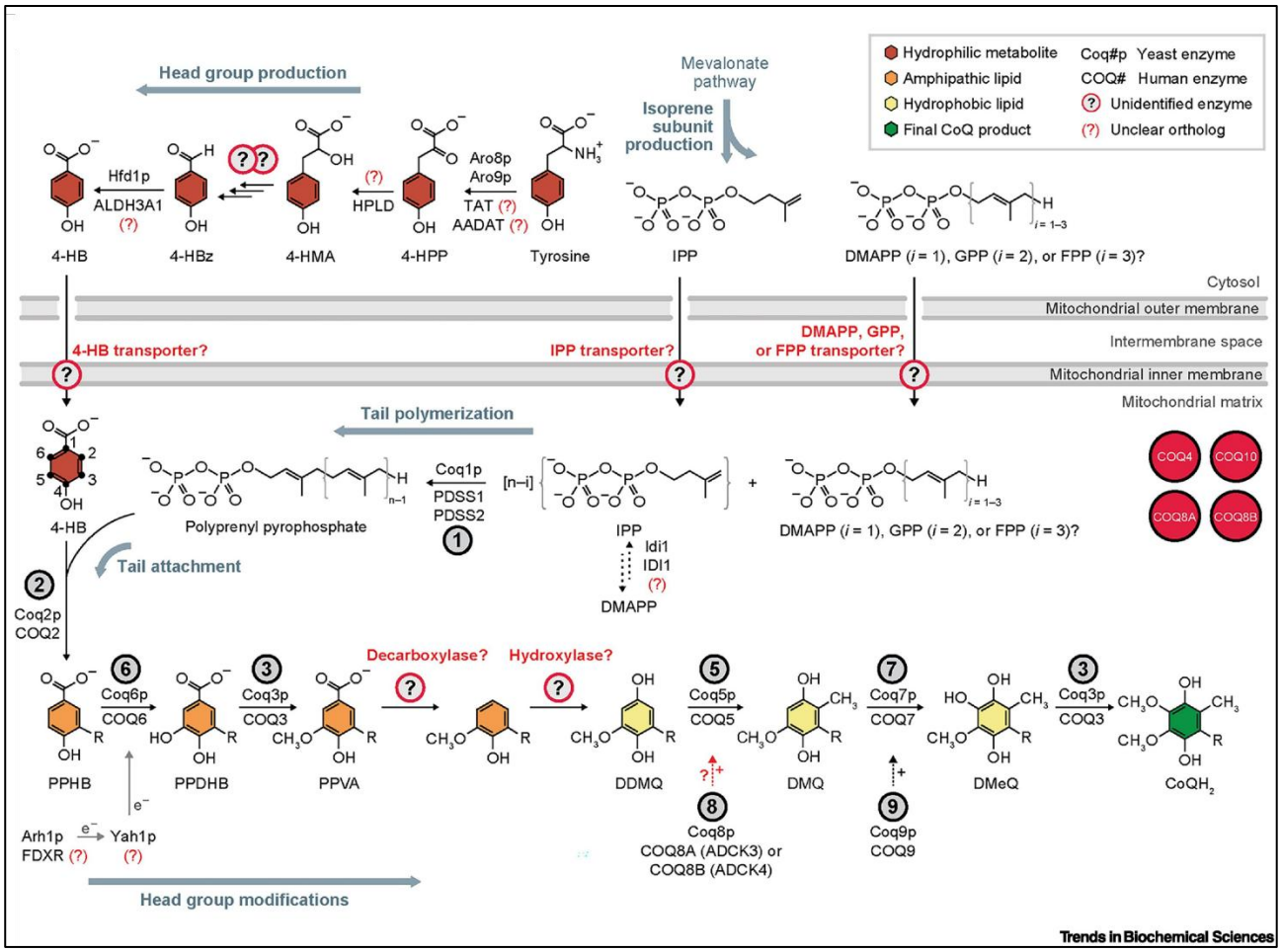

Figure 6. The primary eukaryotic pathway, conserved from Saccharomyces cerevisiae to humans, of CoQ biosynthesis. CoQ production begins with the head group precursor 4-HB, derived from tyrosine, and tail subunit IPP, derived from the mevalonate pathway, which are both transported into the mitochondrial matrix by unknown means. Following tail polymerization and head group attachment, CoQ intermediates are processed through a series of head group modifications to yield mature CoQ. Biosynthetic enzymes that catalyze each reaction are denoted by the circled number above each arrow. Unidentified enzymes and transporters are indicated by circled question marks. Auxiliary proteins with some unclear involvement in CoQ biosynthesis are depicted in red circles. '+' symbol near dashed arrows designates a hypothesized supportive role for the indicated reaction. Abbreviations: 4-HBz, 4-hydroxybenzaldehyde; 4-HMA, 4-hydroxymandelate; 4-HPP, 4-hydroxyphenylpyruvate; AADAT, mitochondrial alpha-aminoadipate aminotransferase; ALDH3A1, aldehyde dehydrogenase 3A1; DDMQ, demethoxy-demethyl-coenzyme Q; DMQ, demethoxy-coenzyme Q; DMeQ, demethyl-coenzyme Q; DMAPP, dimethylallyl pyrophosphate; FDX2 (FDX1L), mitochondrial ferredoxin 2 (ferredoxin 1-like); FDXR, ferredoxin reductase; FPP, farnesyl pyrophosphate; GPP, geranyl pyrophosphate; HPLD, hydroxyphenylpyruvate dioxygenase-like protein; IDI1, isopentenyl-diphosphate delta isomerase 1; IPP, isopentenyl pyrophosphate; PDSS1, prenyl (decaprenyl) diphosphate synthase subunit 1; PPDHB, polyprenyl-dihydroxybenzoate; PPHB, polyprenyl-hydroxybenzoate; PPVA, polyprenyl-vanillic acid; TAT, tyrosine aminotransferase. Source "Coenzyme Q biochemistry and biosynthesis" by R.M. Guerra et al. – Trend in Biochemical Sciences [116].

CoQ_{10} plays different important roles in the cells.

1. It's a crucial component of the electron transport chain in the inner membranes of mitochondria. It shuttles electrons from Complex I (NADH dehydrogenase) and Complex II (succinate dehydrogenase) to the cytochrome bc1 complex (Complex III), where it is

oxidized. This electron transfer process at Complex III is called the Q cycle. During the Q cycle, a ubiquinol molecule ($CoQH_2$) binds to the Qo site of Complex III and donates two electrons: one electron is transferred to cytochrome c (which then leaves Complex III) via the Rieske iron-sulfur protein and cytochrome c1; the other electron is transferred to a bound ubiquinone (CoQ) at the Qi site via the two cytochromes b, partially reducing it to a semiquinone radical ($CoQH^{\bullet -}$). Two protons from ubiquinol are released into the intermembrane space. A second ubiquinol molecule binds to the Qo site and donates two electrons analogously; at this point the ubiquinol at the Qi site dissociates and two other protons are released into the intermembrane space. Thus, the Q cycle couples electron transfer with proton translocation (four in total), and the proton pumping contributes directly to the proton motive force used by ATP synthase to generate ATP, but also to maintain the mitochondrial redox balance and to prevent oxidative stress.

2. Coenzyme Q_{10} in its reduced form is a potent antioxidant involved in multiple antioxidant systems and processes:
    - it directly scavenges reactive oxygen species (ROS) and prevents lipid peroxidation in mitochondrial and cellular membranes, protecting them from oxidative damage. This process is directly linked to the maintenance of a forward electron flow in the mitochondrial respiratory chain.
    - acts as indirect antioxidant, by helping regenerating other key antioxidants such as α-tocopherol (vitamin E) and ascorbate (vitamin C).
    - can increase the production and activity of enzymes like superoxide dismutase (SOD) and glutathione peroxidase, which are crucial for detoxifying ROS and preventing ferroptosis.

- influences gene expression related to antioxidant responses via pathways like Nrf2/Keap1/ARE, promoting the synthesis of detoxifying and antioxidant enzymes.

3. CoQ_{10} acts as an electron acceptor and obligatory cofactor of other mitochondrial dehydrogenases, including:
    - dihydroorotate dehydrogenase (DHODH), for pyrimidine nucleotides biosynthesis;
    - glycerol 3-phosphate dehydrogenase (G3PDH), a part of the glycerophosphate shuttle;
    - the electron transport flavoprotein dehydrogenase (ETFDH), a key enzyme of fatty acid β-oxidation and amino acid catabolism;
    - proline dehydrogenase (PRODH) and proline dehydrogenase 2 (PRODH2), both of which are involved in proline, glyoxylate, and arginine metabolism;
    - choline dehydrogenase (CHDH), which is primarily found in liver and kidney in humans and catalyzes the oxidation of choline to glycine betaine;
    - sulfide-quinone oxidoreductase (SQOR), which is essential for detoxification of hydrogen sulfide [113].

At the same time CoQ is involved in ROS production in the ETC. It remains to be established to what extent the amount of CoQ and its redox state contributes to total mitochondrial ROS in a given cell or cell type in a particular physiological state [117]. In the ETC, Complex I and Complex III are generally detected as sources of ROS. At Complex I, electrons move from NADH to the flavin mononucleotide (FMN, the I_F site) to iron-sulfur clusters, and finally to CoQ. The CoQ reduction site (the I_Q site) is located at the junction of the hydrophobic membrane arm and the hydrophilic matrix arm [118]. Complex I-linked substrates (i.e., glutamate, malate or pyruvate) provide NADH that feed electrons to the respiratory chain in the forward direction, contributing to the generation of ROS possibly from

the I_F site, the N2 centre, or the $CoQ^{\bullet-}$ [119] [120]. Complex I can also produce ROS when electrons flow through Complex I in the reverse direction, in which electrons flow back from $CoQH_2$ to Complex I and reduce NAD+ to NADH. In this scenario, a highly reduced CoQ pool (that provides the electrons) and a high protonmotive force are necessary, but it is still debated which site actually contributes to the ROS generation [121]. Complex III catalyses a reaction of net oxidation of $CoQH_2$ and reduction of Cyt c, in a process (the Q cycle) that may involve single electron transfers, according to some authors. The formation of a $CoQ^{\bullet-}$ intermediate after the first electron transfer (Qo site) has been postulated but not demonstrated [122] [123]; however, blocking Qo with inhibitors such as stigmatellin, prevents ROS formation. On the other hand, X-ray and cryo-EM structural studies have documented a CoQ occupancy within the Qi site [123] [124]. Mechanistically, heme bH reduces CoQ to $CoQ^{\bullet-}$ after an electron is transferred from the first $CoQH_2$, and reduces $CoQ^{\bullet-}$ to $CoQH_2$ after a second oxidation event. As the $CoQ^{\bullet-}$ intermediate that is formed after every first electron transfer needs to remain at the Qi site until the second electron transfer, the $CoQ^{\bullet-}$ in the Qi site is predicted to be tightly bound and stable. Antimycin A, the best-known Qi site inhibitor, blocks the electron transfer from heme bH to the Qi site and thus inhibits the reduction of the CoQ pool at the Complex III [125] [126].

CoQ_{10} is unevenly distributed in cells and tissues, with higher concentrations found in tissues with greater energy demands. The highest levels of CoQ_{10} are present in the heart, liver, kidneys, and muscles, which require more ATP for their functions. These tissues contain higher amounts of CoQ_{10} per gram of protein to support the intense mitochondrial activity needed for energy production.

CoQ_{10} in muscle cells is predominantly located in the mitochondria, where it plays a critical role in the oxidative phosphorylation process necessary for ATP production. Muscles with a high oxidative metabolism, such as those composed mainly of slow-twitch (type I) fibers, contain higher concentrations of CoQ_{10} compared to muscles with predominantly fast-twitch (type II) glycolytic

fibers. This distribution reflects the higher mitochondrial content in oxidative muscle fibers [127]. Studies show that mitochondrial CoQ_{10} levels increase with muscle maturation and are correlated with markers of oxidative metabolism such as succinate dehydrogenase (SDH) activity and slow ATPase activity. Muscles relying on oxidative metabolism have more CoQ_{10} to support their greater energy needs and protect against oxidative damage, especially with aging.

Therefore, given the importance of CoQ_{10}, and given the high energy demand of muscle cells, it can be easily asserted that statin-induced CoQ_{10} depletion may impair mitochondrial respiratory capacity, leading to reduced energy availability and increased oxidative stress in muscle fibers, and that this alteration of homeostasis can contribute to symptoms such as muscle pain, weakness, cramps, and fatigue observed in many patients on statins.

Besides, there is a clear analogy between the symptoms experienced by patients with primary Coenzyme Q_{10} deficiency and those seen in statin users. Primary CoQ_{10} deficiency is a rare, inherited disorder characterized by low levels of CoQ_{10} in tissues, particularly affecting the brain, muscles, kidneys, and heart, due to mutations in one or more genes involved in CoQ_{10} biosynthesis.

Symptoms of primary CoQ_{10} deficiency often include muscle weakness, exercise intolerance, muscle pain, and elevated creatine kinase levels, closely mirroring the muscle symptoms seen in statin-treated patients. The impact of creatine kinase levels, which are index of cell damage, is still debated, as observational studies cannot directly link high levels of creatine kinase to the insurgence of SAMS [128] [129]. In both conditions, the underlying issue seems to be an impaired mitochondrial energy production due to insufficient CoQ_{10}, that leads to muscle dysfunction and damage. This similarity supports the idea that statin-induced CoQ_{10} depletion (secondary deficiency) contributes to the development of SAMS. This analogy strengthens the rationale for considering CoQ_{10} supplementation to potentially alleviate muscle symptoms associated with statin therapy, though clinical response can vary [130]. In primary CoQ_{10} deficiency, supplementation is critical to prevent

progression, highlighting the essential role of CoQ_{10} in muscle and systemic health. However, response to CoQ_{10} supplementation can vary, likely depending on the cause of CoQ_{10} deficiency, individual polymorphisms, dosage and duration of treatment [130].

CoQ_{10} is absorbed primarily through the small intestine, with some authors highlighting that the bioavailability of the reduced form is superior over the oxidized form. Once absorbed, it is incorporated into chylomicrons and transported to the liver via the lymphatic system. In the liver, CoQ_{10} is then redistributed into the bloodstream, where it binds predominantly to lipoproteins including very low-density lipoproteins (VLDL), low-density lipoproteins (LDL), and high-density lipoproteins (HDL) [131]. CoQ_{10} molecules maintain their original form (reduced or oxidized) when incorporated into the lipoproteins after intestinal absorption [132]. Once incorporated into lipoproteins, they are transported through the bloodstream via VLDL, LDL, and HDL to various tissues. The main pathways of CoQ_{10} elimination are through the bile ducts and feces; a small fraction is eliminated in the urine [133]. However, exogenous supplementation may not always work effectively due to several reasons related to its absorption, metabolism, and delivery to tissues. CoQ_{10} is highly hydrophobic and tends to crystallize, which limits its absorption in the gastrointestinal tract, where it needs to dissolve into a watery environment before absorption [134]. Some individuals inherently have a low capacity to absorb Coenzyme Q_{10} (CoQ_{10}) due to genetic variations and other factors influencing its metabolism and transport. For example, genetic polymorphisms in genes such as NQO1 (NAD(P)H quinone dehydrogenase 1 and apoE have been shown to affect CoQ_{10} levels in the body and its response to supplementation. Certain genotypes are associated with lower baseline CoQ_{10} levels and altered metabolism, which can lead to reduced absorption efficiency or altered distribution of CoQ_{10} in tissues [135] [136]. Even when blood CoQ_{10} levels rise, its transport into tissues and cells is complex and not fully understood. Cellular uptake mechanisms may involve endocytosis of lipoprotein particles or interaction with specific plasma membrane transport proteins, but the exact pathways remain

unclear. Efficient delivery to mitochondria in target tissues remains a challenge [137]. Effective supplements often require crystal modification or formulations to enhance bioavailability [138].

1.3.1. CoQ_{10} formulations

To overcome the issue of its low adsorption and bioavailability, various formulations of CoQ_{10} have been conceived. For example, CoQ_{10} dissolved in oils such as soybean or palm oil [116 117 141], medium-chain triglycerides oleogels [142], or other vegetable oils tends to have better stability and absorption than powder-based forms.

Liposomes, nanocapsules, and nanoemulsions are advanced pharmaceutical and nutraceutical delivery systems designed to enhance the solubility, bioavailability, and targeted delivery of drugs and nutrients like Coenzyme Q_{10}.

Liposomes are spherical vesicles composed of one or more phospholipid bilayers, mimicking natural cell membranes that can encapsulate both hydrophilic compounds (in the aqueous core) and lipophilic compounds (within the lipid bilayer). **Nanocapsules** are nano-scaled vesicular systems where the drug is confined to a cavity surrounded by a polymeric membrane. They offer protection of sensitive drugs and controlled release profiles; polymers can be natural or synthetic, biodegradable or non-biodegradable. **Nanoemulsions** and microemulsions are oil-in-water emulsions with droplet sizes typically below or over 200 nm respectively, stabilized by surfactants.

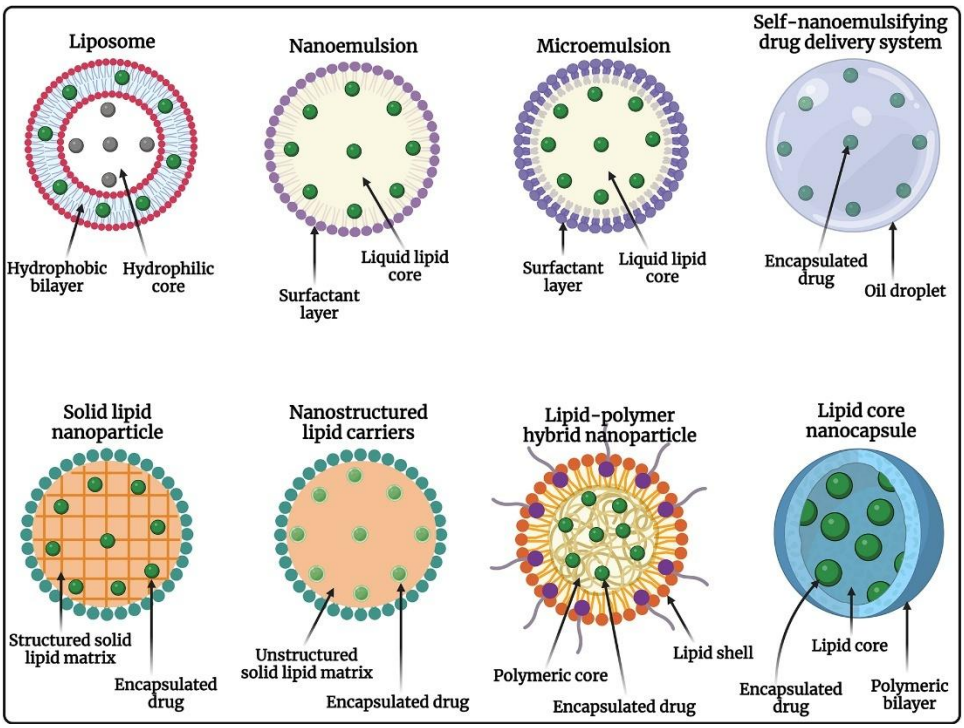

Figure 7. Schematic representation of different types of lipid-based nanoparticles for drug delivery. Source: "Exploring the therapeutic potential of lipid-based nanoparticles in the management of oral squamous cell carcinoma" by A. Chaudhary - Exploration of Targeted Anti-tumor Therapy [143].

Examples of advanced CoQ_{10} formulations designed to improve bioavailability are Qter®, LiBADDS and Ubiqsome®.

Qter® is a water-soluble CoQ_{10} formulation, obtained by terclatration of native CoQ_{10}. This technique involves grinding native CoQ_{10} with a pharmaceutically inactive matrix of maltodextrins to maintain CoQ_{10} in its monomeric form, which significantly enhances its bioavailability and biological efficacy. Research by Bergamini et al. demonstrated that Qter® has much better cellular uptake compared to native CoQ_{10}, requiring doses 10 to 100 times lower to achieve similar intracellular and mitochondrial CoQ_{10} levels. Unlike native CoQ_{10}, which tends to accumulate in extra-mitochondrial membranes and has limited mitochondrial availability, Qter® effectively reaches and integrates into the inner mitochondrial membrane where it exerts its functional roles [144].

In LiBADDS (Lipid-Based Auto-Emulsifying Drug Delivery System), CoQ_{10} is dissolved in medium-chain triglycerides and other lipids and is absorbed on a solid mixture composed mainly of

maltodextrin and sodium starch octenyl succinate under mechanical stirring. In this formulation, the maltodextrin matrix acts as a carrier supporting CoQ_{10} in a dispersed state, improving its dissolution profile when in contact with gastrointestinal fluids [145].

For the study presented in this thesis, we have tested CoQ_{10} formulated as Ubiqsome®, provided by Indena S.p.A., which co-funded the Ph.D. project.

1.3.2. Ubiqsome®

Ubiqsome® is a lipid-based formulation that encapsulates CoQ_{10} in liposome-like phospholipid vesicles named Phytosome®. The basic difference between liposomes and Phytosomes® is that, in liposomes, the active biomaterial is dissolved in the central cavity containing or in the layers of the membrane(s), in Phytosomes®, it is an integral part of the membrane, being the carried molecules stabled through chemical bonds to the polar head of the phospholipids [146].

Another substantial difference is the preparation.

Liposomes are formed by physically encapsulating the active compound inside phospholipid bilayer vesicles. The process generally involves hydrating a thin lipid film formed of phospholipids, followed by mechanical dispersion and sonication. **Phytosomes®** are prepared by chemically complexing (binding) phytoconstituents with phospholipids, usually phosphatidylcholine. This process is done in an aprotic organic solvent where phospholipids and the active compounds interact to form a molecular complex typically in a 1:1 or 2:1 molar ratio. After complex formation, solvent removal and drying methods like vacuum evaporation, precipitation, lyophilization, or spray drying isolate the Phytosome® complex. The resulting chemical bonding between phospholipid polar heads and the phytochemical is key to enhance stability and bioavailability.

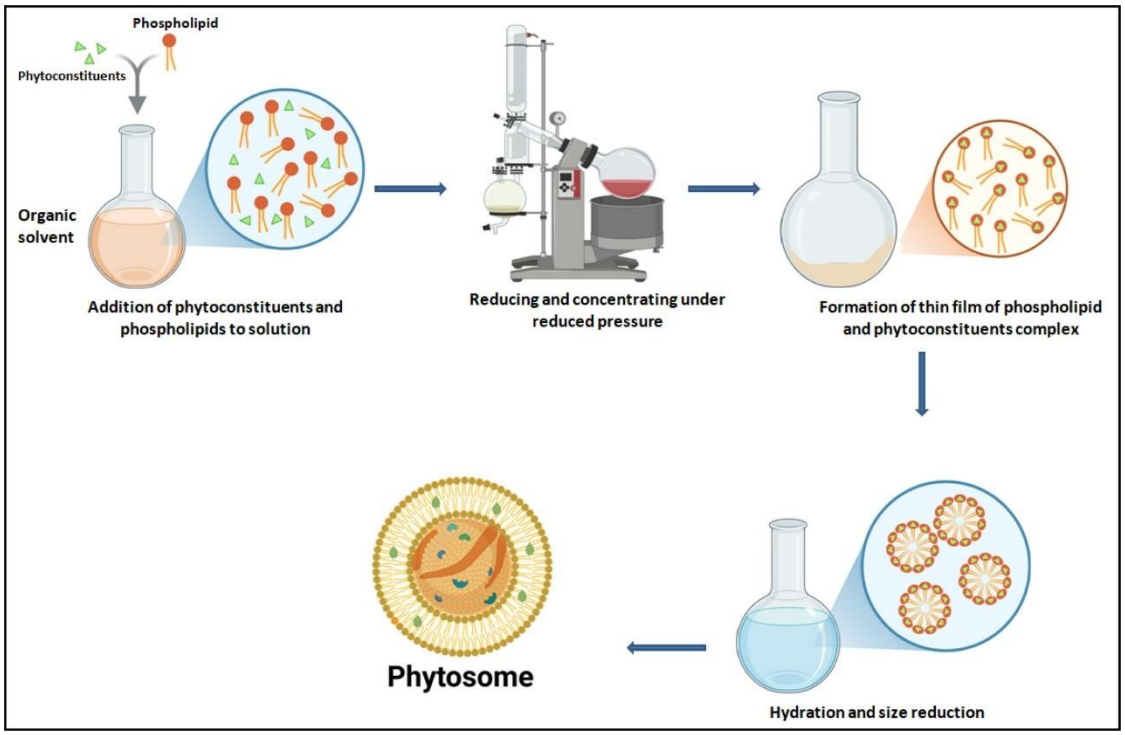

Figure 8. Schematic representation of Phytosome® preparation. Phospholipids (commonly phosphatidylcholine) and the phytochemical (bioactive plant compound) are each dissolved in suitable organic solvents such as dichloromethane or methanol. The two solutions are mixed by gentle stirring, allowing the phytochemical to form a chemical complex with the polar head groups of the phospholipids via hydrogen bonding. Lastly, the solvent mixture is evaporated under vacuum or rotary evaporation to form a thin, dry film of the Phytosome® complex. Source "Phytosomes as a New Frontier and Emerging Nanotechnology Platform for Phytopharmaceuticals: Therapeutic and Clinical Applications" by S. Koppula et al. – Phytotherapy Research [147].

The bioactive compound is chemically bound to the phospholipid, forming a stable complex [146] [148]. Ubiqsome® has already been studied *in vitro* by Rizzardi et al. [149], who investigated the bioenergetic and antioxidant effects of Ubiqsome® in human intestinal (I407) and rat muscle (H9c2) cell lines. The study found that Ubiqsome® significantly increases cellular and mitochondrial CoQ_{10} content, improving mitochondrial function and antioxidant capacity compared to equivalent concentrations of standard CoQ_{10}. Cicero et al. [150], conducted a double-blind, randomized, placebo-controlled crossover study that showed that Ubiqsome® improved plasma total antioxidant capacity and endothelial reactivity in healthy subjects, supporting cardiovascular health benefits.

1.4. CDKL5 deficiency disorder

CDKL5 (cyclin-dependent kinase-like 5) deficiency disorder (CDD) is a rare and severe X-linked developmental encephalopathy caused by mutations in the CDKL5 gene, with an estimated incidence of approximately 1 in 40,000 to 60,000 live births and a female-to-male ratio of 4:1 (males rarely survive fetal development) [151]; clinically overlapping with the Rett syndrome, CDD is considered a different disease, even though CDKL5 mutations can arise also in patients suffering from Rett syndrome. CDD manifests with profound neurological symptoms including early-onset seizures, intellectual disability, cortical visual impairment, disrupted sleep patterns, and significant motor deficits. Advances in clinical characterization have expanded the phenotypic spectrum to include frequent peripheral manifestations such as gastrointestinal dysfunction, irregular respiration, hypotonia, and scoliosis [152]. The CDKL5 gene encodes a serine-threonine kinase highly expressed in neurons, particularly localized within axons, dendrites, and dendritic spines [153]. Mouse models of CDD demonstrate that loss of CDKL5 expression in the central nervous system results in impairments across motor, sensory, cognitive, and socio-emotional behaviours, mirroring the human clinical phenotype. Studies using Cdkl5-deficient mice and neuronal cultures have consistently implicated CDKL5 in critical neuronal processes including survival, dendritic branching, axonal growth, and synaptic functionality [154]. Recent evidence indicates that the role of CDKL5 extends beyond the CNS, affecting non-neuronal tissues. Notably, heterozygous Cdkl5 +/− female mice exhibit cardiac structural and functional abnormalities, including QTc interval prolongation, elevated heart rate, fibrosis, mitochondrial dysfunction, and increased reactive oxygen species (ROS) production - markers commonly associated with cardiac aging. Correspondingly, Cdkl5-null brains display features of accelerated neuronal senescence, encompassing elevated DNA damage and mitochondrial deficits. These findings correlate with reports of systemic redox imbalance observed in plasma samples from CDD patients. Oxidative stress, is increasingly

recognized as a common pathogenic mechanism in various neurodevelopmental disorders. Besides, CDKL5 deficiency is associated with mitochondrial dysfunction: studies in patient-derived neuronal cells and Cdkl5-null mouse models reveal significant impairments in mitochondrial bioenergetics [155]. Coenzyme Q_{10} plays a crucial role as antioxidant, protecting mitochondrial and cellular membranes from free radical damage, and ameliorates mitochondrial functions [156]. CoQ_{10} supplementation is still debated, given its poor bioavailability, even if some studies report benefits in terms of protection from oxidative stress in neurodegenerative diseases, cardiomyopathies, and metabolic disorders, although no direct correlation between the onset of the disease and CoQ_{10} levels have been reported [157] [158].

Aim of the study

Statins are the cornerstone therapy for the primary and secondary prevention of cardiovascular disease due to their potent LDL-cholesterol-lowering effects. However, their use is associated with a range of adverse effects, most notably statin-associated muscle symptoms (SAMS), which can lead to discontinuation and compromised cardiovascular protection. The pathogenesis of SAMS is multifactorial, but a leading hypothesis implicates that statin-induced depletion of Coenzyme Q_{10} (CoQ_{10}), a critical cofactor in mitochondrial respiration and antioxidant defence, may be one of the main causes. CoQ_{10} depletion, in fact, may contribute to mitochondrial dysfunction, oxidative stress, and muscle damage. While CoQ_{10} supplementation in statin users has been proposed as a strategy to mitigate side effects and gain compliance, clinical evidence remains inconsistent, partly due to variability in formulations and dosing regimens. This study aimed to investigate how Atorvastatin exerts toxic effects in human dermal fibroblasts. Atorvastatin is one of the most prescribed statins and is associated with a range of side effects, some of which are reported more frequently or severely than with other statins. Atorvastatin is administered as a prodrug, since the pharmacophore is in lactone form. The lactone ring of statins has been implicated in the drug's lipophilicity and a possible accumulation in peripheral tissues, due to a scarce hepato-selectivity, may be responsible for side effects. Moreover, the lactone ring may be display off-target effects, as already demonstrated by Schirris et al. [102], who have reported that these drugs can inhibit the Qo centre of complex III. Here we investigated the effects linked to CoQ_{10} deficiency and off-target effects likely due to a high concentration used. We used the potential beneficial effects of Ubiqsome®, a CoQ_{10} formulation to alleviate Atorvastatin-induced side effects, addressing a significant unmet need in statin therapy. Moreover, the collaboration with another team of researchers, gave us the opportunity to test the efficacy of Ubiqsome® treatment *in vivo*, establishing an additional objective for this thesis. This side project served as a complementary endeavour to the main study, providing an opportunity to

address a significant challenge: the biodistribution of CoQ_{10} in peripheral tissues, and the effectiveness of the oral supplementation.

2. Materials and Methods

2.1. Cell Cultures and Treatments

Human dermal fibroblasts (HDF) from a healthy middle aged donor, were cultured in Dulbecco's Modified Eagle Medium (DMEM, Euroclone, Milan, Italy), supplemented with 10% fetal bovine serum (FBS), 100 I.U./mL Penicillin and 100 μg/mL Streptomycin, and grown at 37 °C in 5% CO2 with saturating humidity. For drug treatment, cells were seeded on an appropriate support and grown for 24 hours in complete culture medium before treatment. Cell count for seeding was performed by using the Trypan blue exclusion method [159]; protein content was assessed by using the Lowry method [160]. Treatments were performed using Atorvastatin Calcium, Ubiqsome® (UBQ) or a combination of the two. Atorvastatin Calcium was purchased at Sigma-Aldrich (St. Louis, MO, USA), and dissolved in bi-distilled water-prepared 10% Bovine Serum Albumin (BSA, Sigma-Aldrich, St. Louis, MO, USA) for cell treatments, or DMSO for enzymatic assays; UBQ was provided by Indena S.p.A., Milan, Italy; concentrations of UBQ used are referred to the equivalent CoQ_{10} present in the formulation.

HDF from a patient handling a mutation in the enzyme COQ7 (patient P118 [161]) were cultured in Dulbecco's Modified Eagle Medium (DMEM, Euroclone, Milan, Italy), supplemented with 10% fetal bovine serum (FBS), 100 I.U./mL Penicillin and 100 μg/mL Streptomycin, and grown at 37 °C in 5% CO2 with saturating humidity. Cell count for seeding was performed by using the Trypan blue exclusion method [159]; treatments were performed using Atorvastatin Calcium (Sigma-Aldrich St. Louis, MO, USA), with or without UBQ, for 24 hours.

Wild type and CDKL5-KO (CRISPR-Cas9 generated [162]) SH-SY5Y neuroblastoma cells (ECACC, Sigma-Aldrich, St. Louis, MO, USA) cells were cultured in Dulbecco's modified Eagle's medium

(DMEM; Euroclone, Milan, Italy). Cell count for seeding was performed by using the Trypan blue exclusion method [159]; treatments were performed using Ubiqsome® (UBQ, Indena, Milan, Italy) or Phytosome® alone for 24 hours.

2.2. Viability assay

For Atorvastatin treatments 3×10^3 HDF per well were seeded on a multi-96 well plate and let attach for 24 hours before treatment. For the treatments, cells were incubated with a range of concentrations between 3 μM and 100 μM of Atorvastatin for 24 hours, and co-treated with 10 nM, 50 nM or 100 nM of UBQ. For the cell viability analysis, cells were subjected to the MTT colorimetric assay [163]. Briefly, cells were incubated with 300 μM MTT dissolved in non-complete DMEM for 2 h at 37°C; after this time, medium was aspirated, the wells were then gently washed with PBS and 150 μl of DMSO per well were added to dissolve formazan salts. Absorbance was read at λ=570 nm using a Victor Nivo multiplate reader spectrophotometer (PerkinElmer, Waltham, MA, USA).

HDF-P118 were seeded at a density of 5×10^3 HDF per well on a multi-96 well plate and let attach for 24 hours before treatment. Cells were incubated with a range of concentrations between 3 μM and 300 μM of Atorvastatin for 24 hours, or Atorvastatin + 10 nM UBQ, and viability was evaluated via MTT.

2.3. Oxygen consumption rate

Oxygen consumption rate was measured in HDF using a Seahorse XF24 Extracellular Flux Analyzer (Agilent, Santa Clara, CA, USA). 1×10^4 cells per well were seeded onto a Seahorse XF24 cell culture microplate and incubated for 24 hours prior to treatment with 3 μM, 30 μM, 50 μM, 100 μM Atorvastatin with and without 10 nM UBQ. Plates were washed with Seahorse assay media

(Seahorse Bioscience, Billerica, MA, USA), supplemented with 1 g/L glucose, 1 mM sodium pyruvate, and 2 mM L-glutamine, and incubated in a CO2-free incubator at 37°C for 1 hour to allow temperature and pH equilibration before measuring in the Seahorse XF24. OCR was recorded in basal conditions and after the addition of inhibitors and effectors of the mitochondrial electron transport chain: oligomycin 0.4 μM to inhibit ATP synthase; FCCP (Carbonyl cyanide 4-(trifluoromethoxy) Phenylhydrazone) 2 μM to uncouple respiration; rotenone 1 μM and antimycin A 5 μM to block the mitochondrial chain at the end of the experiment. Cells were counted using Cell Imaging Reader BioTek Cytation 1 (Agilent, Santa Clara, CA, USA) prior to the analysis, to normalize data.

For SH-SY5Y and SH-SY5Y-KO, the cellular oxygen consumption was measured through polarography, using an oxygraph chamber (Instech Mod. 203, Plymouth Meeting, PA, USA), as reported in [164]. Briefly, SH-SY5Y and SH-*CDKL5*-KO cells were washed in NaCl 0.9% and trypsinized; cells were collected and centrifuged, and the pellet was resuspended in non-complete medium. The cell suspension was put in the oxygraphy chamber, and the oxygen consumption rate was measured in the basal condition and in presence of oligomycin A 0.4 μM, FCCP 2 μM, and rotenone 1 μM plus antimycin A 5 μM. The results were normalized on total protein content.

2.4. Nucleotides extraction

Nucleotides from cultured HDF were extracted following Jones et al. [165] with minor modifications and quantified by HPLC. Briefly, 1.5×10^5 cells were seeded in a T25 flask and let ad-here for 24 hours before treatments. Extracted nucleotides were injected in a two-pump system equipped with a photodiode array detector (Agilent, Santa Clara, CA, USA, 1100 series) and a C18 column (Kinetex, Phenomenex, Torrance, CA, USA, 2.6 μm, 250 × 4.6 mm), with λ=260 nm. ATP and ADP were

quantified by measuring the area under the curve of identified peaks and interpolating the result in a standard curve. Data were normalized on protein content.

Nucleotides from homogenized heart and muscle tissues were extracted similarly.

2.5. CoQ quantitation

2.5.1. Coenzyme Q_{10} content in Atorvastatin-treated HDF

CoQ_{10} was extracted from cultured cells as described by Takada et al. [166] with minor modifications. Briefly, cells were pelleted and resuspended in 200 µl PBS. 10 µl of internal standard CoQ_7, 10 µl of FeCl3 0.1%, and 5 volumes of a n-hexane/ethanol mixture (5:3) were added. The suspension was thoroughly vortexed for 2 minutes and centrifuged at 1800 g for 10 minutes. The upper layer from each sample was collected, and a second extraction was performed. The collected solutions were dried out in glass tubes by nitrogen flux, and the dry extracts were resuspended in 50 µl of ethanol. 20 µL of samples were injected into a two-pump HPLC system equipped with photodiode array detector (Agilent, Santa Cruz, CA, USA) and a C18 column (Kinetex, Phenomenex, 5 µm 100 A, 150 × 4.6 mm), using an ethanol/water mobile phase (96:4, v/v) at a 0.8 mL/min flow rate. The CoQ_7 and CoQ_{10} peaks at λ = 275 nm were identified and quantified by interpolating the area under the curve with a calibration curve. The results were normalized on protein content and extraction yield (based on extracted CoQ_7) .

2.5.2. Coenzyme Q content in plasma

Total plasma CoQ_9 and CoQ_{10} content was measured through high-performance liquid chromatography (HPLC) as described above, with minor modifications. 200 µL of plasma were diluted 1:1 with bi-distilled water before the application of the protocol.

2.5.3. Coenzyme Q content in tissues

Total CoQ_9 and CoQ_{10} levels were also measured in heart and muscle tissue homogenates. Briefly, tissues were homogenized using a Turrax; the homogenates were then subjected to 15 strokes in a glass potter and filtered with gauze. The resulting homogenates were extracted for CoQ_9 and CoQ_{10} as described above. All procedures were carried out at 4°C. The CoQ content was normalized to the protein content, measured with the Bradford method [167].

2.6. Mitochondrial mass

Mitochondrial mass was assessed by measuring the citrate synthase activity [168] in a a Jasco V-750 spectrofluorometer (Jasco, Tokyo, Japan) equipped with a stirring device and thermostatic control set up at 30 °C. Briefly, 30 μg of cell lysate were added to a 1 ml quartz cuvette containing a 100 mM TRIS + 0.1% Triton X-100 buffer (pH 7.4), 100 μM of acetyl-CoA, and 100 μM of 5,5′-dithiobis-2-nitrobenzoic acid (DTNB); 500 μM oxalacetate was used to start the reaction. The enzymatic activity was measured following the reduction of DTNB to TNB (ε = 13.6 mM-1 cm^{-1}) at λ=412 nm over time.

2.7. Mitochondrial chain functionality in permeabilized cells

Activity of the electron transport chain (ETC) was measured by OCR using a Sea-horse XF24 Extracellular Flux Analyzer (Agilent, Santa Clara, CA, USA) after 24 hours treatment with 30 μM Atorvastatin, 10 nM UBQ or both. 1.5×10^4 cells were seeded in a Seahorse XF24 cell culture microplate and incubated for 24 hours prior to treatment; the day of the experiment the plates were washed with Seahorse assay media (Seahorse Bioscience), and incubated in a CO_2-free incubator at 37°C for 1 hour to allow temperature and pH equilibration before measuring in the Seahorse XF24; cells were permeabilized with digitonin (25 μg/ml) and supplemented with substrates for Complex I or Complex II. Namely, to measure Complex I-driven OCR, cells were incubated with 2.5 mM

glutamate/malate and 40 μM malonate, while Complex II-related respiration was conducted adding 10 mM succinate and 1 μM rotenone to the medium. Basal oxygen consumption was measured.

A similar experiment was conducted by measuring Complex I and Complex II-driven OCRs after acute treatment with 30 μM of Atorvastatin. In this case 3×10^4 cells were seeded in a Seahorse XF24 cell culture microplate and incubated for 24 hours prior to treatment; the day of the experiment, the plates were treated as mentioned above, and substrates for Complex I or II were provided. After the initial basal respiration record, 30 μM of Atorvastatin, or an equal volume of Seahorse medium were injected and OCRs were recorded.

2.8. Mitochondrial chain functionality in isolated mitochondria

The activity of the mitochondrial chain was also measured in isolated freeze-thawed mouse liver mitochondria. Mouse liver mitochondria were isolated according to Bergamini et al. [169] with minor modifications; to permeabilize the membranes and provide substrates, isolated mitochondria were subjected to freeze-thaw cycles. Complex I-driven respiration was measured in a Jasco V-750 spectrofluorometer (Jasco, Tokyo, Japan) equipped with a stirring device and thermostatic control set up at 30°C. 50 μg of mitochondria were incubated with different concentrations of DMSO-dissolved Atorvastatin and diluted in a 1 ml solution containing 25 mM potassium phosphate buffer pH 7.5 and 1 mg/ml BSA in a quartz cuvette; the reaction was initiated by adding 70 μM of NADH. The enzymatic activity was measured following the extinction of NADH at λ=340 nm over time. Complex II-driven respiration was conducted in an oxygraphy chamber (Instech Mod.203, Plymouth Meeting, PA, USA). Briefly, 275 ug of mitochondria were added to the oxygraphy chamber containing a respiration buffer (0.25 M sucrose, 50 mM HEPES, 4 mM MgSO4, 10 mM KH2PO4, pH 7.4); the reaction was started by adding 20 mM of succinate to the chamber.

2.9. Complex I activity

Specific Complex I hydrogenase activity in the presence of Atorvastatin was assayed spectrophotometrically as in Spinazzi et al. [170] using a Jasco V-750 spectrofluorometer (Jasco, Tokyo, Japan) equipped with a stirring device at 30 °C. Briefly, 30 μg of isolated freeze-thawed mouse liver mitochondria were pre-incubated with Atorvastatin and then transferred in a 1 ml quartz cuvette containing 25 μM antimycin A, 1 mg/ml BSA and 70 μM NADH (ε = 6.22 mM-1 cm^{-1}) dissolved in a 50 mM potassium phosphate buffer; 50 μM decyl-ubiquinone (DB) was used to start the reaction and NADH consumption was followed over time at λ=340 nm. NADH dehydrogenase activity of Complex I was measured by following ferricyanide $[Fe(CN)_6]^{3-}$ (ε = 1 mM-1 cm^{-1}) reduction [171] in a Jasco V-750 spectrofluorometer (Jasco, Tokyo, Japan) equipped with a stirring device at 30 °C. Briefly, 30 μg of isolated freeze-thawed mouse liver mitochondria were pre-incubated with Atorvastatin and then transferred in a 1 ml quartz cuvette contain-ing a 50 mM potassium phosphate buffer, 1 mg/ml BSA and 25 μM antimycin A; 70 μM NADH and 250 μM of $[Fe(CN)_6]^{3-}$ were used to start the reaction and $[Fe(CN)_6]^{3-}$ re-duction was followed over time at λ=420 nm.

2.10. Complex II activity

Complex II activity in the presence of Atorvastatin was assayed spectrophotometrically as in Spinazzi et al. [170], using a Jasco V-750 spectrofluorometer (Jasco, Tokyo, Japan) equipped with a stirring device at 30°C. Briefly, isolated freeze-thawed mouse liver mitochondria were pre-incubated with Atorvastatin and then transferred in a 1 ml quartz cuvette containing 25 μM antimycin and 20 mM succinate dissolved in a potassium phosphate buffer at pH 7.5; 50 μM decyl-ubiquinone (DB) and 2,6-Dichlorophenolindophenol sodium salt hydrate (DCPIP, ε = 16 mM-1 cm^{-1}) were used to start the reaction; DCPIP reduction was followed over time at λ=600 nm.

2.11. Oxidative stress

2.11.1. Measurement of cytosolic ROS production

Reactive oxygen species (ROS) production was measured in cultured HDF using the chloromethyl derivative of 2′-7′-dichlorodihydrofluorescein diacetate, acetyl ester (CM-H_2DCFDA, Thermo Fisher Scientific, Waltham, MA, USA). 2×10^4 cells per well were seeded onto a 24 well plate and incubated for 24 hours with 30 μM of Atorvastatin, 10 nM UBQ or both. Positive controls were generated adding 300 μM of hydrogen peroxide. Then cells were loaded with 5 μM of the probe for 45 minutes at 37°C and washed twice with Hanks' Balanced Salt Solution (HBSS). Epifluorescence was captured using a Zeiss Celldiscoverer7 (Zeiss, Jena, Germany), in a controlled atmosphere (37°C, 5% CO_2), with the green channel. Single-cell fluorescence intensity was analysed with ImageJ Version 1.54p (National Institutes of Health, Bethesda, MD, USA).

Oxidative stress in SHSY-5Y and SH-CDKL5-KO was measured in intact cells using the reactive oxygen species indicator 2′,7′-dichlorodihydrofluorescein diacetate (DCF-DA, Thermo Fisher Scientific, Waltham, MA, USA), as previously described. Briefly, the cells were seeded in 96-well plates at 4×10^4 cells per well. After 24 hours to allow adhesion, the cells were incubated with 100 nM UBQ or Phytosome® dissolved in complete medium for 24 hours at 37 °C in 5% CO2. After this time, the cells were incubated with 10 μM DCF-DA in complete medium for 30 minutes, washed with Hank's balanced salt solution (HBSS), and the fluorescence value in each well was measured (λ_{ex} = 485 nm; λ_{em} = 535 nm) with a plate reader (Enspire, Perkin Elmer, Shelton, CT, USA). The fluorescence emission was normalized on protein content using the Lowry method.

2.11.2. Measurement of mitochondrial ROS production in intact cells

Mitochondrial ROS production (mROS) in HDF was measured using the dihydroethidium derivative MitoSOX Red or MitoSOX Green (Thermo Fisher, Waltham, MA, USA). For MitoSOX Red staining, 1×10^4 cells per well were seeded in a μ-Slide 8 Well (Ibidi, Martinsried, Germany) and incubated for 24 hours prior to treatment with 30 μM Atorvastatin or 10 nM UBQ. For mROS detection cells were loaded with 5 μM Mito-SOX Red for 30 minutes at 37°C and washed twice with HBSS before the measurement. The cells were then imaged using a Leica SPE confocal microscope at λ_{ex} = 396 nm; λ_{em} = 610 nm (Leica Microsystems, Wetzlar, Germany) and analysed using the ImageJ software Version 1.54p (National Institutes of Health, Bethesda, MD, USA). For MitoSOX Green staining, 3×10^4 cells per well were seeded in a multi-96 plate and incubated for 24 hours prior to treatment with 30 μM Atorvastatin. Cells were stained with 1 μM MitoSOX Green for 30 minutes at 37°C and washed twice with HBSS; 20 mM succinate in HBSS were added to each well before the measurement, in order to observe reverse electron transport. Green fluorescence was acquired using a multi plate reader spectrophotometer (PerkinElmer Victor Nivo, Waltham, MA, USA).

mROS in SHSY-5Y were measured by MitoSOX Green as described above, seeding 10×10^3 cells/well in a multi-96 plate, and using 5 μM of probe.

2.11.3. Measurement of membranes peroxidation in intact cells

The determination of membrane lipid peroxidation was performed using the lipid peroxidation sensor dye STY-BODIPY [172]. 1×10^4 cells per well were seeded in a μ-Slide 8 Well (Ibidi, Germany) and incubated for 24 hours prior to treatment with 30 μM Atorvastatin or UBQ. The day of the experiment, cells were incubated with 1 μM of the probe for 1 hour, washed with PBS, and fixed in 4% paraformaldehyde. Positive controls were generated using 500 nM of RSL3, an inducer of lipid peroxidation. Images were acquired using a Nikon C1si confocal microscope (Nikon, Tokyo, Japan)

and fluorescence intensities were quantified using the ImageJ software Version 1.54p. Fluorescence was acquired by two-channel imaging, as the probe emission peak shifts from λ=~590 nm to λ=~510 nm when oxidized. Data are reported as green/red fluorescence intensity ratio.

2.11.4. Glutathione content assay

The glutathione (GSH) levels were quantified using a bioluminescent GSH/GSSG-Glo® kit (Promega, Madison, WI, USA), following the manufacturer's instruction. Briefly, cells were seeded in 96-well plates at 4×10^4 cells per well and let adhere for 24 hours. The cells were then incubated with 100 nM UBQ or vehicle dissolved in complete medium for 24 hours at 37 °C in 5% CO_2. After this time, the cells were lysed with 25 μL GSH or GSSG lysis reagents, and luciferin generation reagent was added (50 μL), followed by luciferin detection regent (100 μL). The luminescent signal was measured with a Glomax microplate reader (Promega, Madison, WI, USA), and the GSH/GSSG ratio was calculated as [(net total glutathione RLU − net GSSG RLU)/(net GSSG RLU)] × 2, where RLU stands for Relative Light Units.

2.11.5. Measurement of lipid peroxidation products in tissue homogenates

Lipid peroxidation in the heart tissue homogenates from *Cdkl5*$^{+/-}$ and *Cdkl5*$^{+/+}$ female mice was assessed by measuring the biomarker Malondialdehyde (MDA) as in Reilly et al. [173]. Briefly, the quantification of MDA was performed through reaction with thiobarbituric acid (TBA), and the measurement of the TBA-MDA adduct was carried out at 535 nm using a Jasco V-750 spectrophotometer. 1,1,3,3-tetramethoxypropane (Sigma-Aldrich, St. Louis, MO, USA) was used as standard.

2.11.6. ROS production in isolated mitochondria

ROS production in isolated mouse liver mitochondria was followed over time as in Fato et al. [174] with minor modifications. 0.5 mg/ml mitochondria were energized with 70 μM NADH, or 20 mM succinate, in presence of different concentrations of DMSO-dissolved Atorvastatin ranging from 12.5 μM to 100 μM, and 5 μM of the fluorogenic dye 2′,7′-Dichlorodihydrofluorescein diacetate (DCFDA). Fluorescence of oxidized DCF was recorded every 5 minutes in a multi plate reader spectrophotometer (PerkinElmer Victor Nivo, Waltham, MA, USA).

2.12. Real time PCR

A set of genes central for mitochondrial function was tested with Real-Time PCR. Briefly, 2×10^5 cells were seeded in a multi-6 well plate and allowed to attach for 24 hours before treatment. Cells were incubated with 30 μM of Atorvastatin with and without 10 nM of UBQ for 6 hours. After the incubation period, cells were washed with cold PBS, detached by trypsin, and centrifuged at 7500 rpm at 4°C. The pellets were transferred into liquid nitrogen and stored at -80°C until processed. Gene expression analysis was used to quantify the possible change in expression of a selected set of genes: citrate synthase (CS), succinate dehydrogenase (SDH), peroxisome proliferator-activated receptor gamma coactivator 1-alpha (PGC-1α), and electron-transferring-flavoprotein dehydrogenase (ETFDH). SYBR-green Real-Time qPCR (PowerUp™ SYBR™ Green Master Mix; ThermoFisher) was used for gene expression analysis, using β-Actin and GAPDH as housekeeping genes. The 2-ΔΔCt method was used for relative gene expression quantification. Primer sequences are listed in Table 2.

Table 2. List of genes with relative accession numbers and primer sequences.

Gene	Gene accession number	Primer sequences
β-ACTIN	NM001101	Fw 5′-ACCTTCTACAATGAGCTGCG-3′ Rv 5′-CCTGGATAGCAACGTACATGG-3′
GAPDH	NM_002046	Fw 5′-ACATCGCTCAGACACCATG-3′ Rv 5′-TGTAGTTGAGGTCAATGAAGGG-3′
CS	NM_004077.3	Fw 5′-CATTGACTCTAACCTGGACTGG-3′ Rv 5′-ACTTACATTGCCACCCTCATG-3′
SDH	NM_004168.2	Fw 5′-TGGTTGTCTTTGGTCGGG-3′ Rv 5′-GCGTTTGGTTTAATTGGAGGG-3′
PGC1α	NM_013261.5	Fw 5′-ACCAAACCCACAGAGAACAG-3′ Rv 5′-GGGTCAGAGGAAGAGATAAAGTTG-3′
ETFDH	NM_004453.4	Fw 5′-TTCAACTTCTACTGTGCCTCG-3′ Rv 5′-GCCTGCACCAACTATTACAAC-3′

2.13. Lactate quantitation

Extracellular lactate quantitation was assessed by meaning of lactate dehydrogenase (LDH) activity measured in a Jasco V-750 spectrofluorometer (Jasco, Tokyo, Japan) equipped with thermostatic control and cuvette stirring device. Cells were treated with 30 μM of Atorvastatin with and without UBQ for 24 hours. The day of the experiment, cells were incubated with fresh untreated medium, and aliquots of media were collected after 3 hours and 6 hours. Briefly, the collected media were diluted 2:1 with perchloric acid (PCA) 1 M, vortexed and incubated for 2 hours at 4°C to allow protein precipitation. Samples were then centrifuged at 13.000g at 4°C and 100 μl of the supernatant were added to the cuvette containing 1 ml of buffer (10 mM Tris - 500mM Glycine pH 9.2, containing 1U/ml of rabbit muscle LDH type II) and 2,5 mM of NAD^+. NAD^+ reduction was followed over time as absorbance increase (ΔAbs/min) at $\lambda = 340$ at (37°C). Resulting ΔAbs/min values were interpolated on a standard curve, and data were normalized on protein content.

2.14. Mice treatment

For *in vivo* treatment, 6–8-month-old *Cdkl5*$^{+/+}$ and *Cdkl5*$^{+/-}$ female mice were provided with drinking water containing UBQ or vehicle (Phytosome®) for two weeks. The daily intake of UBQ for each mouse was equivalent to ~500 mg of UBQ (corresponding to 100 mg of CoQ_{10}) per kilogram of body weight. Considering an average daily consumption of 5 mL of drinking water and an average body weight of 30 g per mouse, drinking water was prepared with a concentration of 3 mg/mL of UBQ. The solutions were renewed three times a week. At the end of the treatment, the mice were weighed and put under deep anaesthesia through inhalation of 2% isoflurane in pure oxygen. Blood and tissue samples were collected, and the mice were sacrificed through cervical dislocation. The hearts and femoral quadriceps were quickly removed, cleaned from the surrounding structures, and thoroughly washed in PBS to remove all blood, then weighed. The tissues were quickly frozen in isopentane, cooled in liquid nitrogen, and stored at –80 °C until used for CoQ_{10} extraction.

2.15. Solid State NMR

To allow the characterization of Coenzyme Q_{10} inside the Ubiqsome® formulation, solid state NMR (ssNMR) measurements were performed on a Bruker Avance NEO WB with wide bore magnet (89 mm) operating at a ^{1}H frequency of 400 MHz. Crystalline bare CoQ_{10}, Ubiqsome® and the Phytosome® vector were analysed. The chemical shift for all nuclei was referenced to the ^{13}C signal of adamantane at 38.46 ppm. A 1.9 mm cross polarization-magic angle spinning (CP MAS) probe was used for the characterization employing a zirconia rotor with a VESPEL turbine. One dimensional ^{13}C-^{1}H spectra were acquired through cross polarization (CP) by exciting the ^{1}H nuclei and transferring the magnetization to the heteronucleus. The spin rotation frequency was set to 15 KHz. The 90° pulse duration for ^{13}C was 2.94 μs. The contact time for CP was set to 2.5 ms. Spectra from the analysed samples were collected.

2.16. Raman spectroscopy

Raman spectra of crystallin CoQ_{10} (referred to as CoQ_{10}), Ubiqsome® and Phytosome® (vector) were collected before and after dissolution in tap water for 5 days. Spectra were collected at t=0 (immediately dissolved powders) and t=5 (5 days after dissolution) in triplicate, using a Bruker MultiRam FT-Raman spectrometer, which features a cooled Ge-diode detector. The excitation source utilized was an Nd3+-YAG laser operating at 1064 nm, configured in a backscattering arrangement (180°). The diameter of the focused laser beam was approximately 100 μm, with a spectral resolution of 4 cm^{-1} and a laser power of around 100 mW at the sample. Each spectrum represented the average of 5000 acquisitions. The attribution of the bands was performed on the basis of the existing literature [175] [176] [177].

2.17. Simulated digestion

2.5 g of CoQ_{10} and UBQ were subjected to simulated digestion, following the "INFOGEST static *in vitro* simulation of gastrointestinal food digestion" protocol [178]. Volumes were annotated to calculate the theoretical final concentration of CoQ_{10} in the digested samples. 300 μl of digested and undigested samples (approximately 30 mM) were used for CoQ_{10} extraction (see paragraph 2.5.1.). The dry extracts were resuspended in 4 ml of ethanol and diluted 1:200 prior to the injection. 20 μL of samples were injected into a two-pump HPLC system equipped with photodiode array detector (Agilent, Santa Cruz, CA, USA) and a C18 column (Kinetex, Phenomenex, 5 μm 100 A, 150 × 4.6 mm), using an ethanol/water mobile phase (96:4, v/v) at a 0.8 mL/min flow rate. CoQ_{10} peaks at λ = 275 nm were identified and quantified by interpolating the area under the curve with a calibration curve. Results were compared to the expected (calculated) outcomes.

2.18. Statistical analysis

The statistical analysis was performed using GraphPad Prism (Version 8, San Diego, CA, USA). The values are expressed as means ± standard error of the mean (SEM). The significance of results was obtained using the Brown-Forsythe ANOVA test. A probability level of $p < 0.05$ was considered to be statistically significant.

3. Results

3.1. Atorvastatin induces mitochondrial dysfunction by lowering CoQ_{10} levels and by targeting Complex I and III in the mitochondrial chain.

3.1.1. Atorvastatin reduces cell viability

We investigated the effect of Atorvastatin treatment on HDF viability using the MTT test. Cells were incubated with 3 μM, 30 μM, 50 μM, and 100 μM of Atorvastatin in the presence or absence of different concentrations of UBQ for 24 hours. The MTT test revealed a dose-dependent reduction in cell viability after Atorvastatin treatment. The UBQ supplementation was partially able to rescue cell viability at 10 nM. (Figure 9), while showing toxicity at higher concentrations.

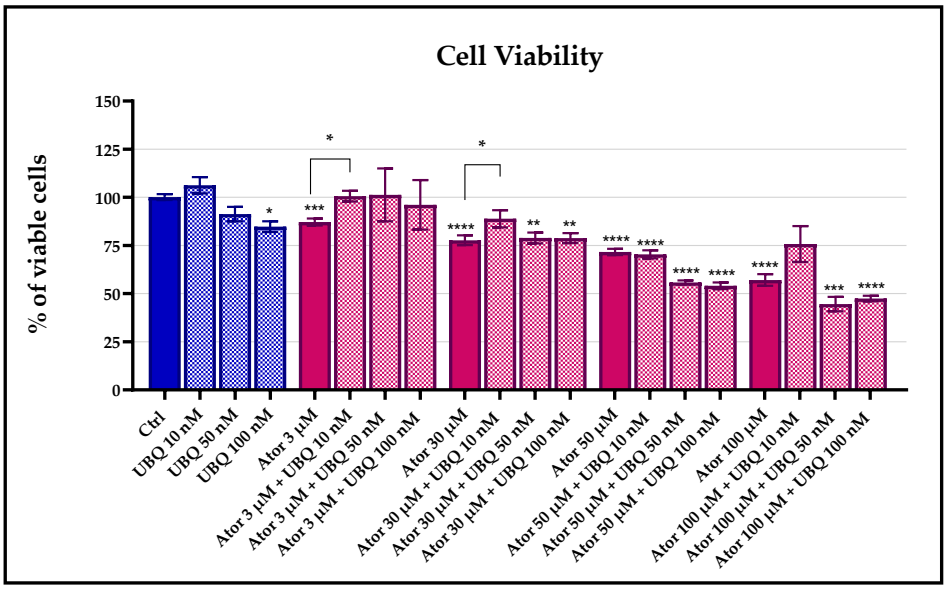

*Figure 9. Cell viability of human dermal fibroblasts following 24 hours-treatment with Atorvastatin (3, 30, 50, or 100 μM) alone or in combination with Ubiqsome® (10, 50, or 100 nM), as determined by MTT assay. Data represent the percentage of viable cells relative to untreated controls and are expressed as mean ± SEM (n = 5). Statistical significance was assessed using Brown-Forsythe ANOVA (*p ≤ 0.05; **p ≤ 0.01; ***p ≤ 0.001; ****p ≤ 0.0001). Abbreviations: Ator = Atorvastatin; UBQ = Ubiqsome®.*

3.1.2. Atorvastatin induces mitochondrial disfunction

We first quantified CoQ_{10} concentrations in HDF after Atorvastatin treatment by HPLC, and observed a drastic drop at all concentrations of Atorvastatin tested (Figure 10), indicating a

decreased biosynthesis of the molecule. This is in line with the on-target effect of the statins, which lower CoQ_{10} concentrations by inhibiting the HMG-CoA reductase.

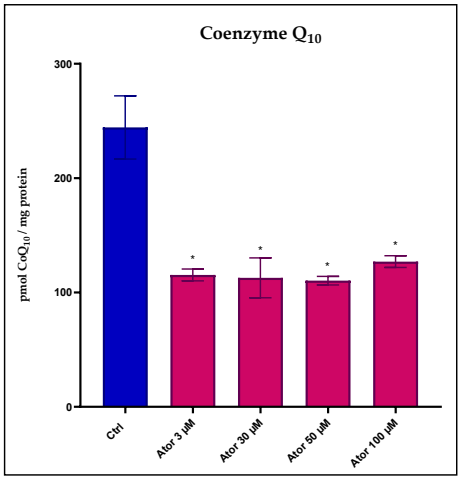

*Figure 10. CoQ_{10} levels after 24 hours-treatment with 30 µM Atorvastatin and 10 nM UBQ. Data are mean ± SEM (n = 3). Statistical significance was assessed using Brown-Forsythe ANOVA (*p ≤ 0.05; **p ≤ 0.01). Abbreviations: Ator = Atorvastatin.*

Given the importance of CoQ_{10} in maintaining the efficiency of the electron transport in the mitochondrial chain, we investigated the effect of Atorvastatin on the mitochondrial functionality by measuring the Oxygen consumption rate (OCR, Figure 11 A) in fibroblasts using the Seahorse XF24 Extracellular Flux Analyzer. The basal and ATP-linked respirations were significantly reduced by 3, 30, 50 and 100 µM Atorvastatin treatment, leaving oligomycin-related respirations unaltered; the co-supplementation with 10 nM of UBQ was able to restore the altered parameters to control levels. UBQ alone had no effect on the OCR for the considered parameters (Figure 11 B,C,D).

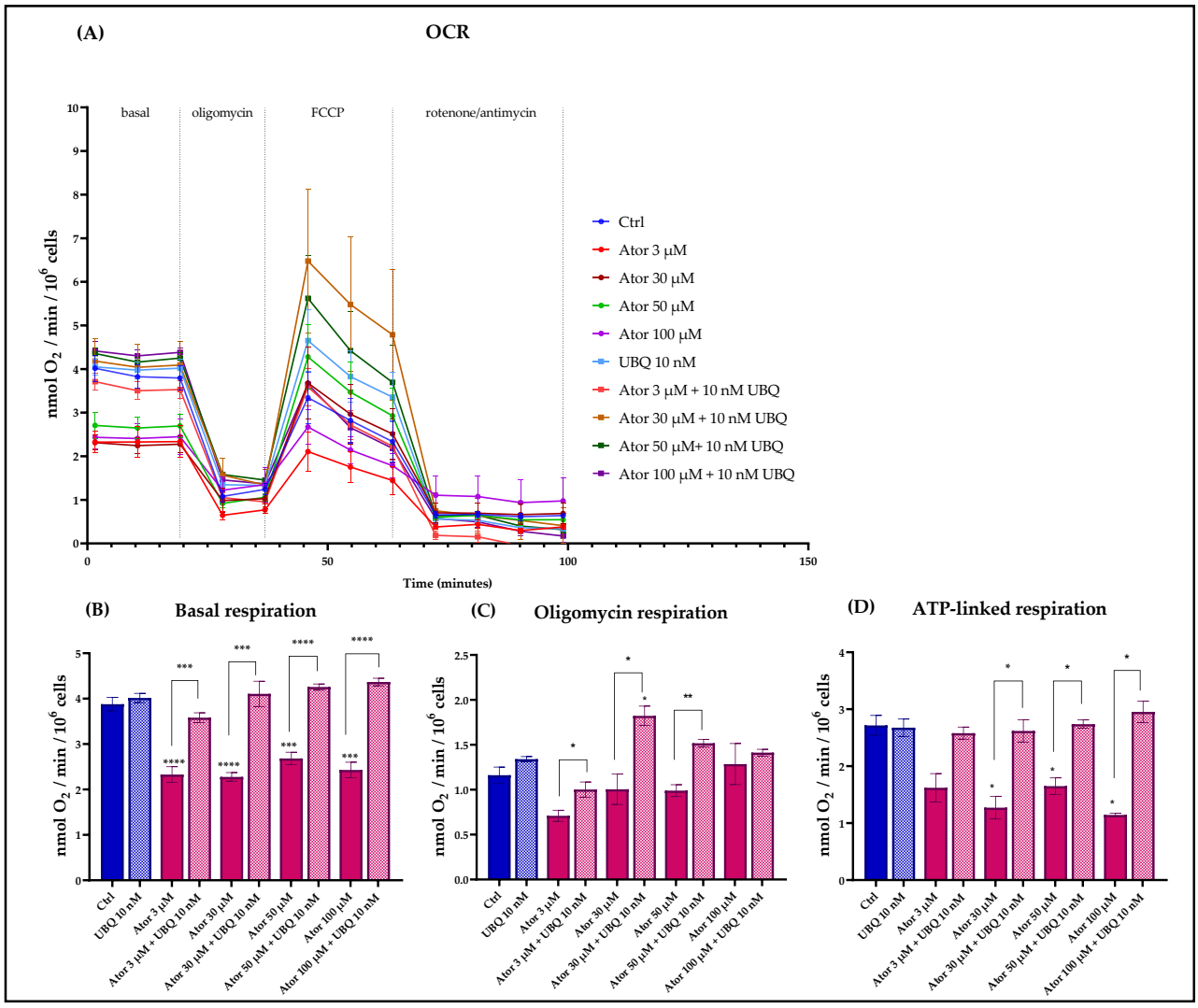

*Figure 11. Oxygen consumption rate in cells treated with various concentrations of Atorvastatin with and without supplementation with 10 nM UBQ for 24 hours. (A) Representative OCR pro-file, (B) Basal respiration, (C) respiration in the presence of oligomycin, (D) ATP-linked respiration calculated as the difference between basal respiration and oligomycin-respiration. Data are mean ± SEM (n = 3). Statistical significance was assessed using Brown-Forsythe ANOVA (*p ≤ 0.05; **p ≤ 0.01). Abbreviations: Ator = Atorvastatin; UBQ = Ubiqsome®.*

We decided to pursue the experiments at 30 µM of Atorvastatin, as at this concentration of drug, we both observed a decrease in viability (~25%) and in mitochondrial functionality.

To confirm the dysfunction at the mitochondrial level, we extracted adenine nucleotides from HDF treated with 30 µM Atorvastatin, 10 nM UBQ or both for 24 hours, and quantified ATP and ADP by liquid chromatography (HPLC). We observed a significant decrease in ATP content and ATP/ADP

ratio, with an increase in ADP, following treatment with Atorvastatin. Supplementation with UBQ partially but significantly recovered the bioenergetic impairment (Figure 12).

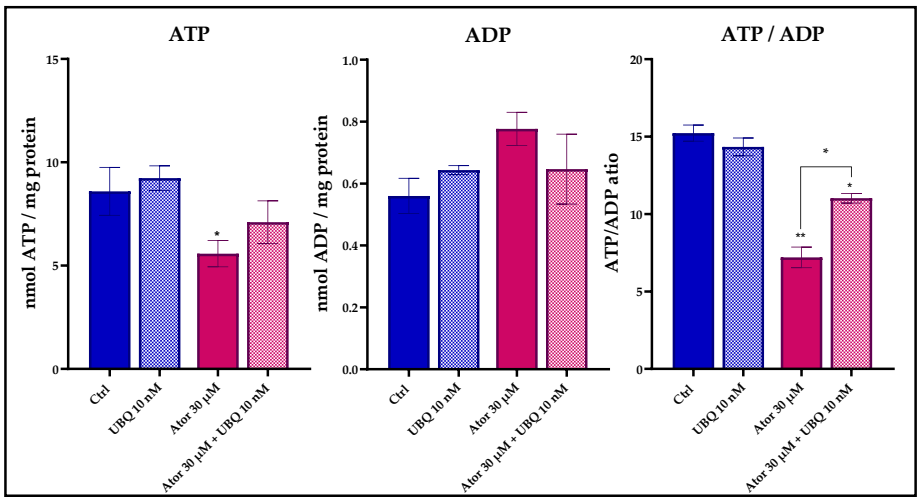

*Figure 12. ATP, ADP and ATP/ADP ratio after 24 hours-treatment with 30 µM Atorvastatin and 10 nM UBQ. Data are mean ± SEM (n = 3). Statistical significance was assessed using Brown-Forsythe ANOVA (*p ≤ 0.05; **p ≤ 0.01). Abbreviations: Ator = Atorvastatin; UBQ = Ubiqsome®.*

The uptake of CoQ_{10} after co-supplementation with 10 nM of UBQ was confirmed by measuring CoQ_{10} content by HPLC (Figure 13).

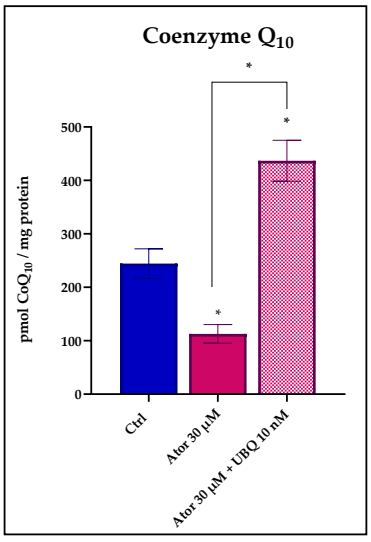

*Figure 13. CoQ_{10} levels after 24 hours-treatment with 30 µM Atorvastatin and 10 nM UBQ. Data are mean ± SEM (n = 3). Statistical significance was assessed using Brown-Forsythe ANOVA (*p ≤ 0.05; **p ≤ 0.01). Abbreviations: Ator = Atorvastatin; UBQ = Ubiqsome®.*

Mitochondrial mass was measured by means of citrate synthase activity, which is considered a reliable marker to estimate total mitochondrial content. Despite the observed impairment of the mitochondrial function, the overall mitochondrial mass is not altered after treatment with Atorvastatin, as indicated by the unaltered citrate synthase activity (Figure 14).

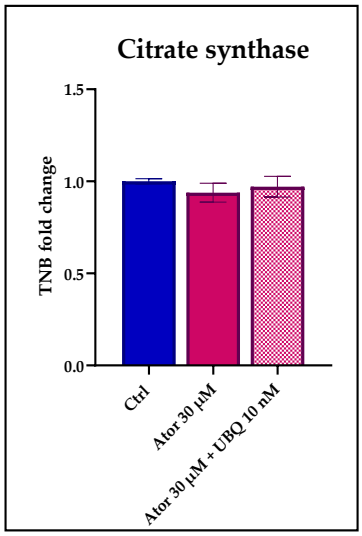

*Figure 14. Mitochondrial mass after 24 hours-treatment with 30 µM Atorvastatin with and without 10 nM UBQ detected as DTNB reduction to TNB. Data are mean ± SEM (n = 3). Statistical significance was assessed using Brown-Forsythe ANOVA (*p ≤ 0.05; **p ≤ 0.01). Abbreviations: Ator = Atorvastatin; UBQ = Ubiqsome®.*

Moreover, RT-PCR analysis confirmed that the expression of CS and other genes central to mitochondrial function (namely SDH, PGC1α and ETFDH) was not significantly altered in HDF after Atorvastatin treatment (Figure 15).

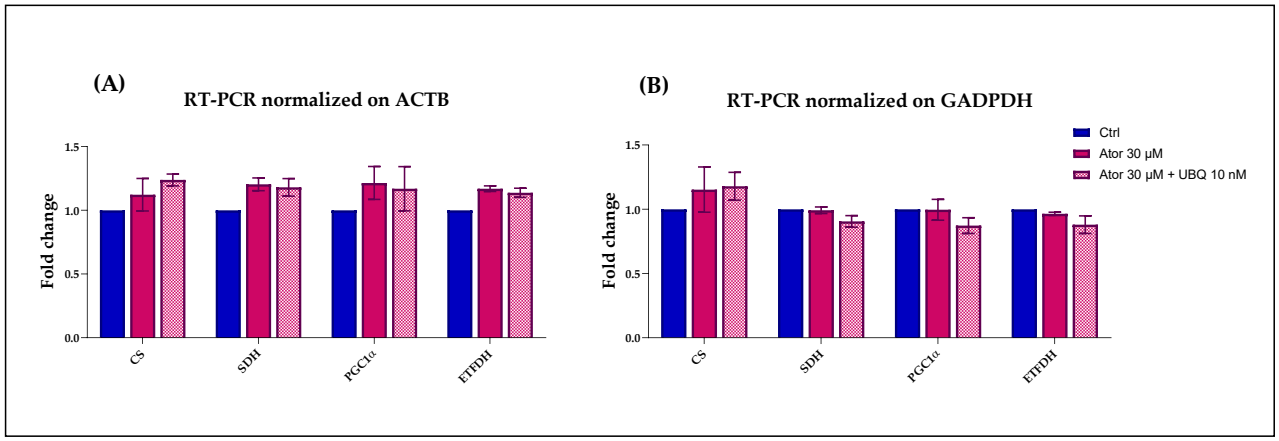

Figure 15. Real Time PCR analysis in human dermal fibroblasts following a 6-hour treatment with 30 μM of Atorvastatin alone or in combination with 10 nM Ubiqsome®. The Y-axis reports 2-ΔΔCt values corresponding to gene expression normalized to controls. Data represent relative gene expressions of citrate synthase, succinate dehydrogenase, peroxisome proliferator-activated receptor gamma coactivator 1-alpha, and electron-transferring-flavoprotein dehydrogenase, normalized on β-Actin (A) and GAPDH (B). Data are expressed as mean ± SEM (n = 3). Statistical significance was assessed using Tukey's multiple comparisons test. Abbreviations: Ator = Atorvastatin; UBQ = Ubiqsome®; CS = citrate synthase; SDH = succinate dehydrogenase; PGC-1α = peroxisome proliferator-activated receptor gamma coactivator 1-alpha; ETFDH = electron-transferring-flavoprotein dehydrogenase.

Lactate levels were measured in the collected media at 3 and 6 hours after replacing the Atorvastatin and UBQ supplemented media with fresh media. Atorvastatin-treated cells showed an increased release of lactate in the medium, compared to controls, and displayed a higher rate of production between the two considered time points. UBQ slightly decreased the production of lactate between the 3 and 6 hours considered. These results suggest that the Atorvastatin-treated cells were relying more on glycolysis for energy production rather than oxidative phosphorylation, which is in line with the observed mitochondrial dysfunction (Figure 16).

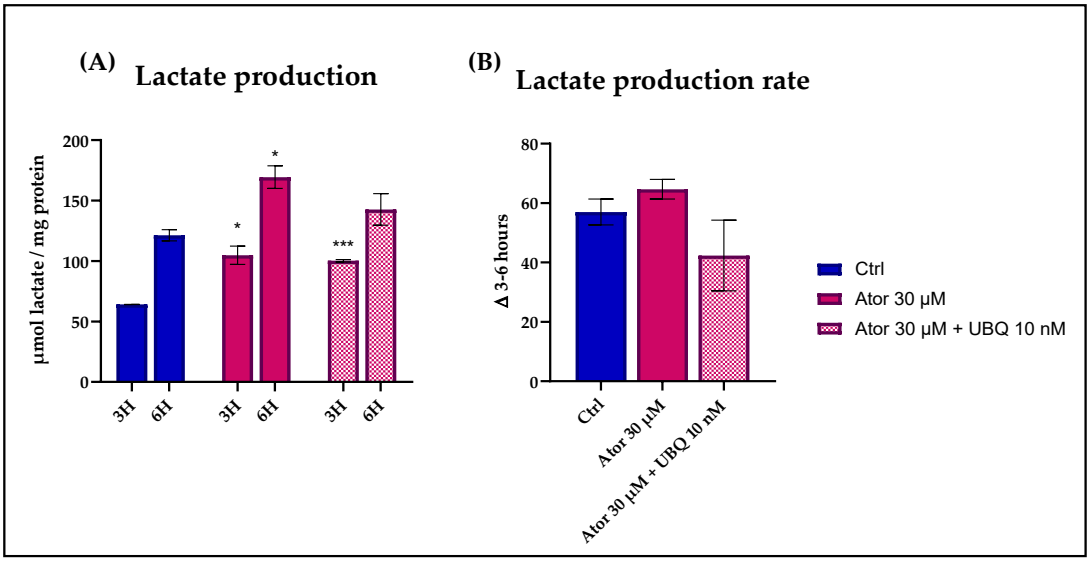

Figure 16. Lactate production of HDF treated with 30 µM of Atorvastatin alone or in combination with 10 nM Ubiqsome® . Lactate in the media was collected after 3 and 6 hours of replacing the media with fresh ones (A), and the rate of production was calculated as the difference in lactate content between the 6 and the 3 hours (B).

3.1.3. Atorvastatin impairs the mitochondrial electron transport chain in permeabilized HDF

To study the effect of Atorvastatin on the ETC, we measured Complex I and Complex II-driven respirations in digitonin-permeabilized HDF, after treatment with 30 µM Atorvastatin for 24 hours, using the Seahorse XF24 Extracellular Flux Analyzer. Complex I-dependent OCR was measured in the presence of glutamate and malate, inhibiting Complex II with malonate; Complex II-dependent respiration was assessed after the addition of succinate, inhibiting Complex I with rotenone. In both cases, Atorvastatin-treated cells showed a decrease in basal respiration, which could be due to the decrease in endogenous CoQ_{10} levels. Co-treatment with 10 nM UBQ and 30 µM Atorvastatin recovers the oxygen consumption both in the presence of gluta-mate/malate and succinate (Figure 17 A,B).

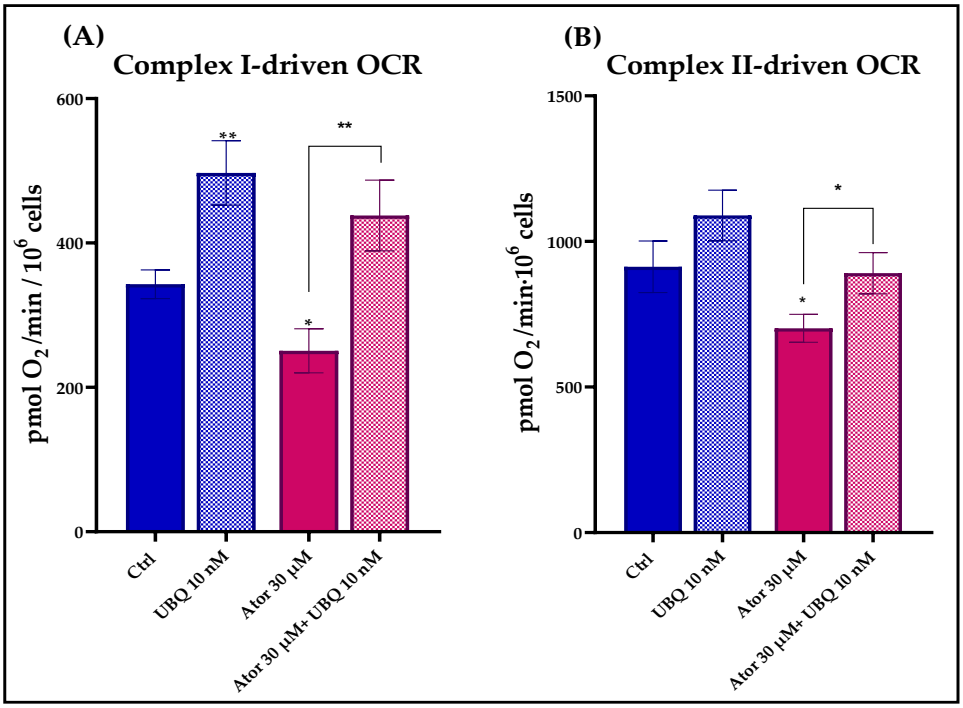

*Figure 17. Mitochondrial respiratory activity in permeabilized human dermal fibroblasts following 24 hours-treatment with 30 µM Atorvastatin alone or in combination with 10 nM UBQ. (A) Complex I-driven and (B) Complex II-driven oxygen consumption rates were measured by high-resolution respirometry. Data are expressed as mean ± SEM (n = 3). Statistical significance was assessed using Brown-Forsythe ANOVA (*p ≤ 0.05; **p ≤ 0.01). Abbreviations: Ator = Atorvastatin; UBQ = Ubiqsome®.*

In order to understand if the inhibitory effect could be direct on enzymes of the ETC, permeabilized HDF were acutely treated with Atorvastatin, during OCR measurement with a Seahorse instrument. A similar impairment of the OCR was observed in the Complex I and Complex II-driven respirations (Figure 18). To account for any effects due to volume differences in the wells, the same volume of respiration medium was added as a control, which showed no impact on the OCR.

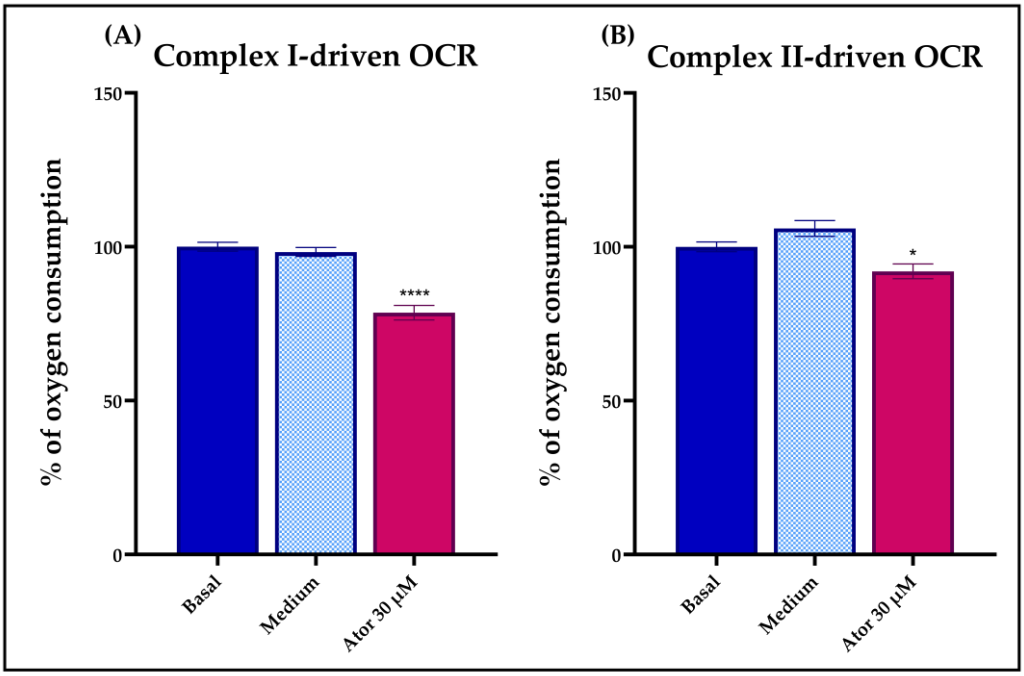

*Figure 18. Mitochondrial respiratory activity in permeabilized human dermal fibroblasts following acute treatment with 30 µM Atorvastatin. (A) Complex I-driven and (B) Complex II-driven oxygen consumption rates were measured by high-resolution respirometry. Data are expressed as mean ± SEM (n = 3). Statistical significance was assessed using Brown-Forsythe ANOVA (*p ≤ 0.05; ****p ≤ 0.0001). Abbreviations: Ator = Atorvastatin.*

3.1.4. Atorvastatin impairs the mitochondrial electron transport chain activity in isolated mitochondria

Since the inhibitory effect on the OCR seemed to be immediate and directed to the mitochondria (Figure 17 and 18), we assessed the effect of Atorvastatin on the ETC activity in isolated mouse liver mitochondria, finding a dose-dependent inhibition of both NADH-O_2 and Succinate-O_2 activities with similar IC_{50} value (98.07 µM and 95.43 µM respectively), as reported in Figure 19 A and B.

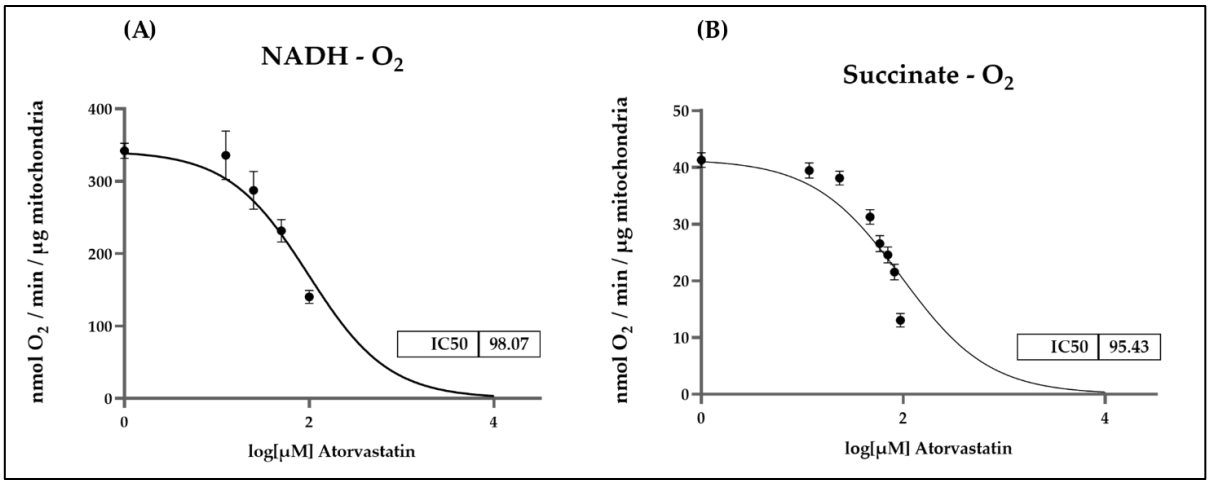

Figure 19. Dose-dependent effects of Atorvastatin on mitochondrial respiratory chain function in isolated mouse liver mitochondria. (A) NADH–O_2 activity measured at various concentrations of Atorvastatin. NADH oxidation was monitored spectrophotometrically at λ=340 nm. (B) Succinate–O_2 activity in the presence of different concentrations of Atorvastatin, assessed by oxygen consumption using a Clark-type oxygen electrode.

To identify which ETC enzyme might be directly affected by Atorvastatin, we tested the activity of functionally isolated Complex I using either decyl-ubiquinone (DB), a CoQ_{10} analogue, or ferricyanide ($[Fe(CN)_6]^{3-}$) as electron acceptors. Atorvastatin inhibited the NADH-DB reductase activity (hydrogenase module), while rotenone insensitive NADH-$[Fe(CN)_6]^{3-}$ (dehydrogenase module) activity remained unaffected (Figure 20 A, B). Notably, the activity of functionally isolated Complex II, tested in the presence of succinate, DB, and DCPIP as electron acceptor, was not affected by Atorvastatin. (Figure 20 C).

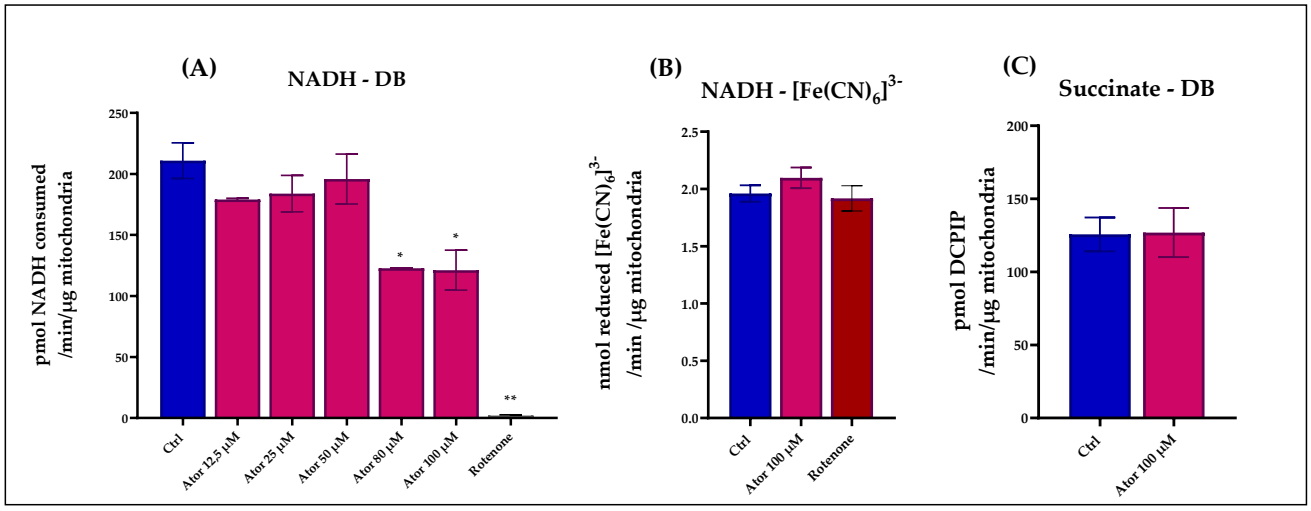

*Figure 20. (A) Functionally isolated Complex I activity in the presence of different concentrations of Atorvastatin in mitochondria energized with NADH and using decyl-ubiquinone (DB) or (B) ferricyanide ($[Fe(CN)_6]^{3-}$)as electron acceptors. NADH oxidation and $[Fe(CN)_6]^{3-}$ reduction were monitored spectrophotometrically at λ=340 nm and λ=420 nm, respectively. (C) Functionally isolated Complex II activity measured in the presence of different concentrations of Atorvastatin. Mitochondria were energized with succinate and the reduction of the electron acceptor DCPIP (in the presence of DB) was followed at λ=600 nm. Data are presented as mean ± SEM. Statistical analysis was performed using the Brown-Forsythe ANOVA test (*p ≤ 0.05). Abbreviations: Ator = Atorvastatin; DB = decyl-ubiquinone; $[Fe(CN)_6]^{3-}$ = ferricyanide.*

3.1.5. Effect of Atorvastatin on ROS levels in HDF

Given the controversial role attributed to statins as pro-oxidant or anti-oxidant drugs, and given the observed mitochondrial dysfunction, we tested the production of ROS in HDF following treatment with Atorvastatin. General ROS levels were measured using CM-H_2DCFDA, lipid peroxidation with the STY-BODIPY probe, and mitochondrial superoxide with MitoSOX Red.

HDF showed an increased fluorescence signal deriving from the oxidation of the CM-H_2DCFDA probe, after treatment for 24 hours with 30 µM Atorvastatin, indicating an increase in reactive oxygen species production, while the co-treatment with 10 nM UBQ reduced the general oxidative stress. Moreover, UBQ treatment decreased the hydrogen peroxide-induced oxidative stress, which was used as a positive control (Figure 21 A, B).

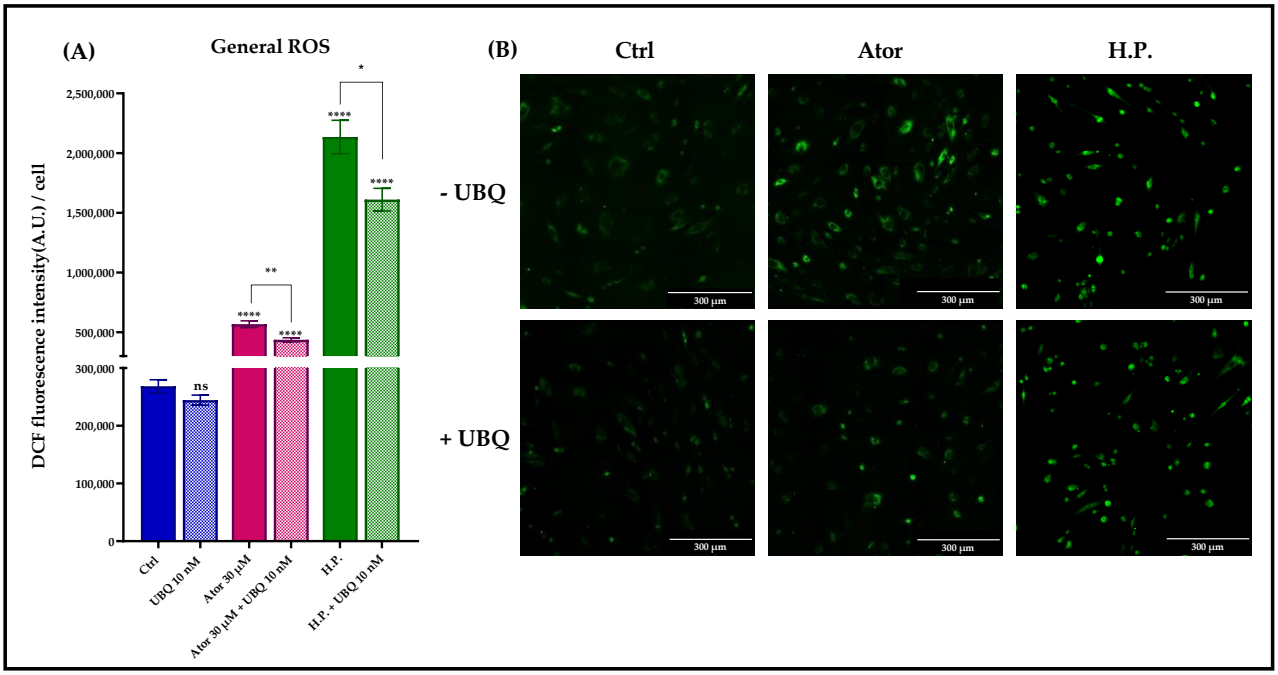

*Figure 21. Evaluation of oxidative stress in HDF after treatment with 30 µM Atorvastatin and supplementation with 10 nM UBQ. (A) General ROS detected by means of DCF epifluorescence and (B) relative images acquired by widefield fluorescence (Scale bar: 300 µm). Data are mean ± SEM. Statistical analysis was performed using the Brown-Forsythe ANOVA test (*p ≤ 0.05; **p ≤ 0.01; ***p ≤ 0.001; ****p ≤ 0.0001). Abbreviations: Ator = Atorvastatin; UBQ = Ubiqsome®; H.P. = Hydrogen Peroxide.*

Lipid peroxidation was evaluated using the STY-BODIPY dye in cells treated with 30 µM of Atorvastatin and/or 10 nM UBQ; RSL3, a selective inhibitor of glutathione peroxidase 4 was used as a positive control. We found no discernible effect on the levels of lipid peroxidation induced by Atorvastatin. However, UBQ treatment conferred protection against lipid membrane peroxidation in both control and RSL3-treated cells (Figure 22 A, B).

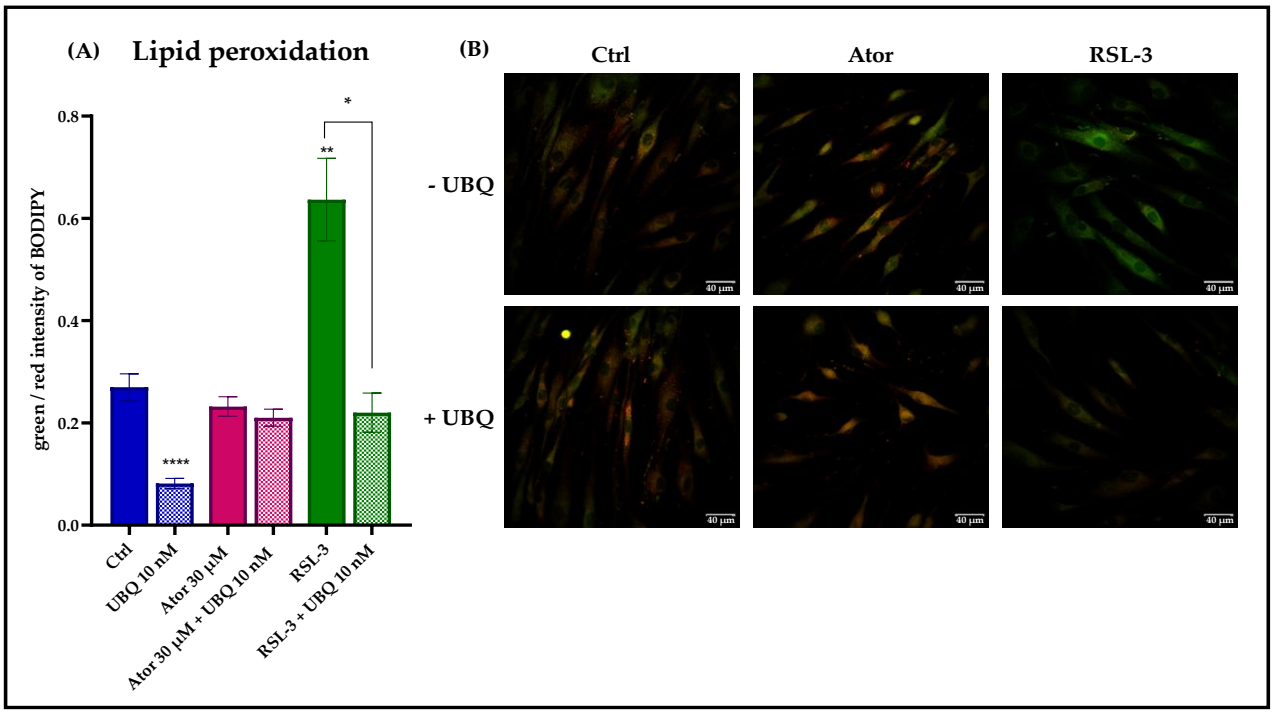

*Figure 22. Evaluation of oxidative stress in HDF membranes after treatment with 30 µM Atorvastatin and supplementation with 10 nM UBQ. (A) Lipid peroxidation quantitation expressed as green/red ratio of Bodipy fluorescence intensity acquired by confocal microscopy and (B) representative images (Scale bar: 40 µm). Data are mean ± SEM. Statistical analysis was performed using the Brown-Forsythe ANOVA test (*p ≤ 0.05; **p ≤ 0.01; ***p ≤ 0.001; ****p ≤ 0.0001). Abbreviations: Ator = Atorvastatin; UBQ = Ubiqsome®.*

Finally, to investigate the mitochondrial contribution in Atorvastatin-induced ROS, we measured mitochondrial superoxide production using the MitoSOX Red probe in HDF treated with 30 µM Atorvastatin, with and without UBQ for 24 hours; rotenone was used as a positive control. Atorvastatin treatment significantly increased mitochondrial ROS production, which was diminished by 10 nM UBQ co-treatment (Figure 23 A, B).

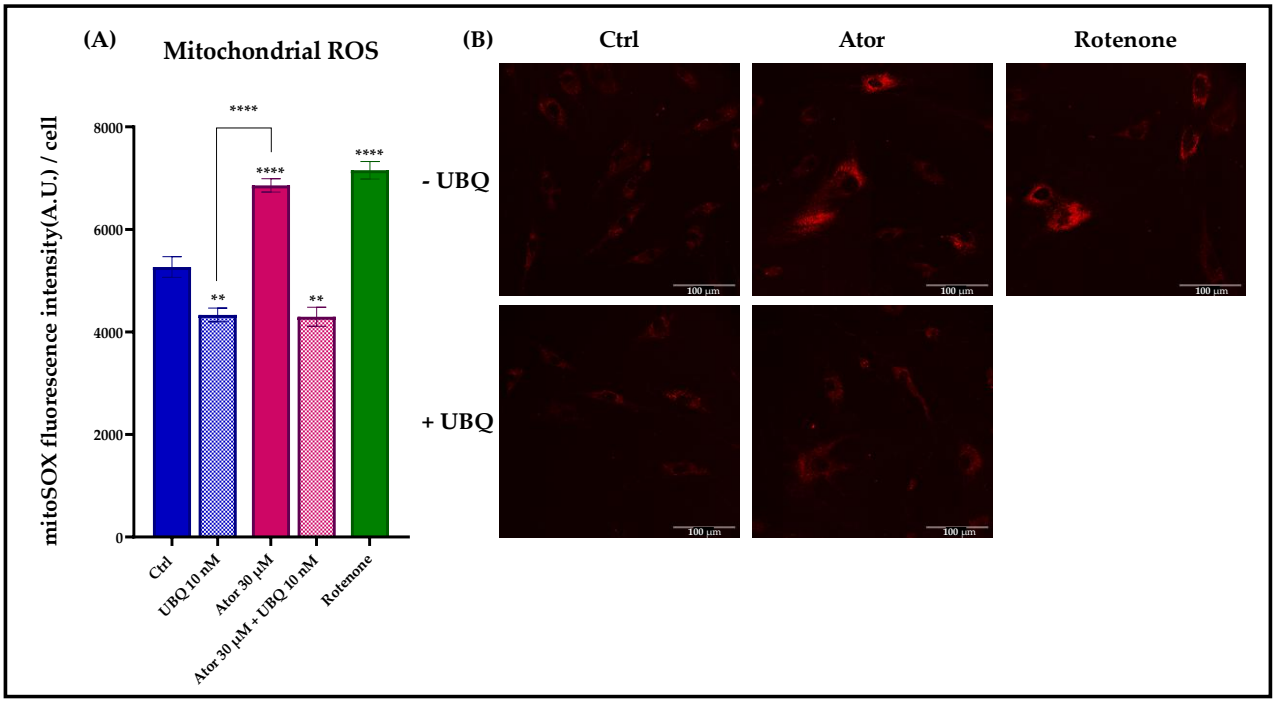

*Figure 23. Evaluation of oxidative stress in HDF mitochondria after treatment with 30 µM Atorvastatin and supplementation with 10 nM UBQ. (A) Mitochondrial ROS detected with Mito-SOX Red by confocal microscopy and (B) representative images (Scale bar: 100 µm:). Data are mean ± SEM. Statistical analysis was performed using the Brown-Forsythe ANOVA test (*p ≤ 0.05; **p ≤ 0.01; ***p ≤ 0.001; ****p ≤ 0.0001). Abbreviations: Ator = Atorvastatin; UBQ = Ubiqsome®.*

3.1.6. Effect of Atorvastatin on ROS levels in isolated mitochondria

As Complexes I and III of the ETC are considered the major ROS producers, we titrated ROS production in freeze-thawed isolated mouse mitochondria incubated with NADH or succinate in the presence of different concentrations of Atorvastatin. DCF fluorescence detected over time showed that Atorvastatin had no effect on ROS production using NADH as electron donor, while radical species increased slightly using succinate (Figure 24 A, B).

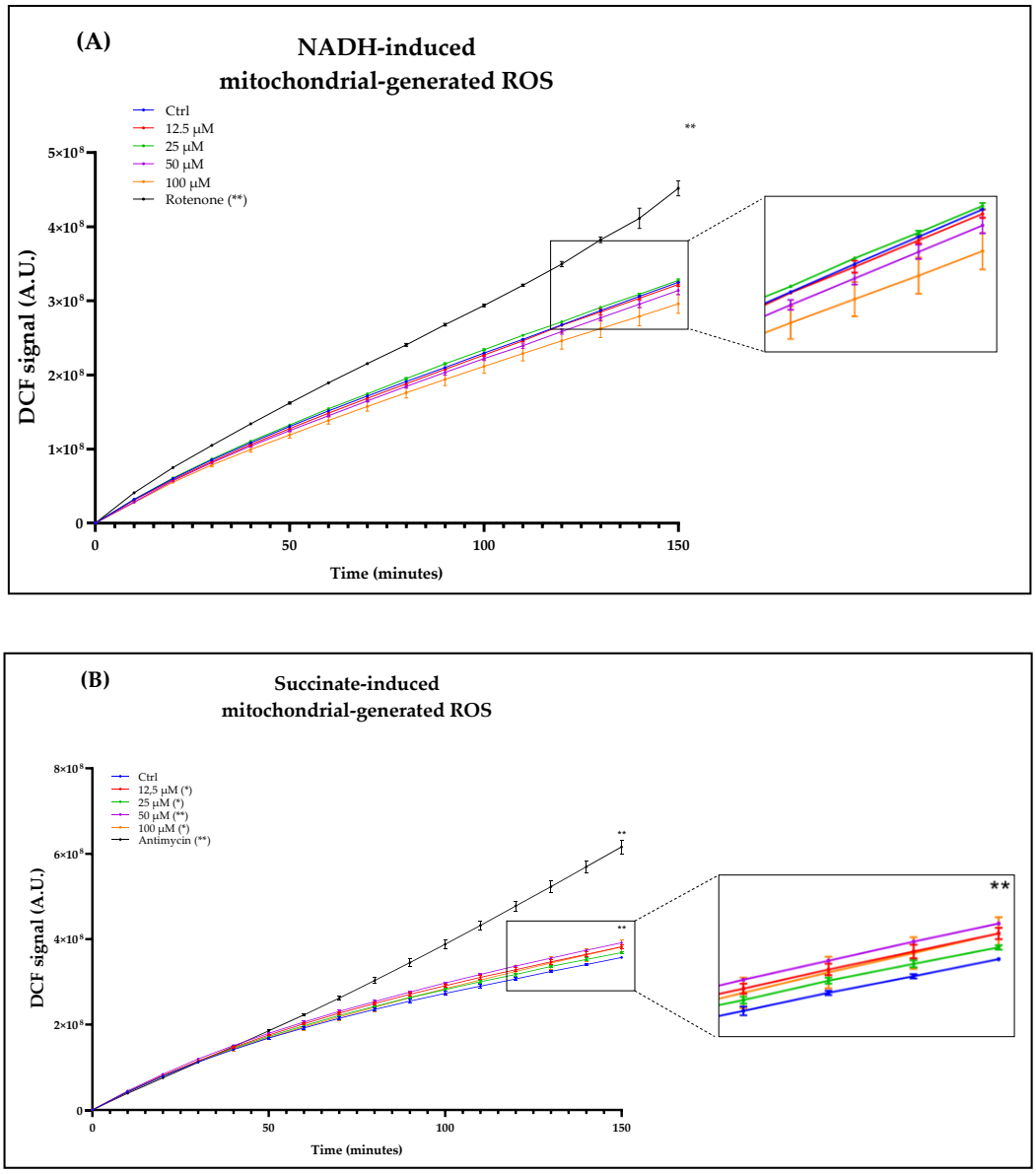

*Figure 24. ROS production in isolated mouse liver mitochondria incubated with Atorvastatin. Mitochondria were incubated with 12.5, 25, 50, 100 µM Atorvastatin and 5 µM DCFDA, energized with NADH (A) or succinate (B). Fluorescence was detected using a multi-plate reader every 5 minutes. Data are mean ± SEM. Statistical analysis was performed using the Brown-Forsythe ANOVA test (*p ≤ 0.05; **p ≤ 0.01). Abbreviations: Ator = Atorvastatin.*

Nonetheless, ROS production at the mitochondrial level was observed in intact cells (Figure 23 A, B). We attributed the observed discrepancy to the fact that Atorvastatin could induce mitochondrial ROS differently, unlike complexes inhibitors such as rotenone or antimycin that induce ROS generation during direct electron transfer across the ETC. K. Wojcicki et al. [179] observed a marked

production of ROS in State 4 mitochondria energized with succinate but not with malate+pyruvate, which suggests a mechanism of reverse electron transfer. Thus we decided to test the hypothesis that Atorvastatin, a known inhibitor of the Qo centre in Complex III, could induce ROS generation by a reverse electron transfer (RET) through Complex I in cells supplemented with succinate. The analysis of fluorescence of MitoSOX Green showed an increase in mROS in Atorvastatin-treated HDF as shown in Figure 25. Notably, co-treatment of HDF with Atorvastatin and rotenone reduced mROS to control levels.

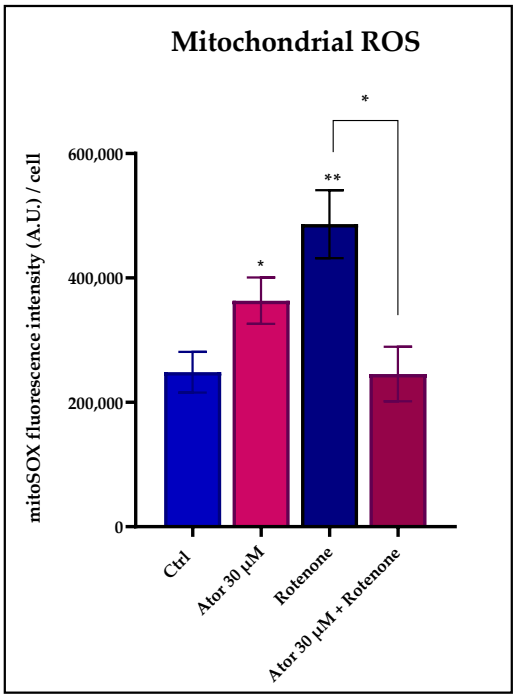

*Figure 25. Atorvastatin induces ROS production via Reverse Electron Transport. Quantitation of MitoSOX Green in cells treated with 30 µM Atorvastatin, 5 µM rotenone or both, and energized with 20 mM succinate. Data are mean ± SEM. Statistical analysis was performed using the Brown-Forsythe ANOVA test (*p ≤ 0.05; **p ≤ 0.01). Abbreviations: Ator = Atorvastatin.*

3.1.7. CoQ_{10}-deficient cells are more resistant to Atorvastatin treatment.

Atorvastatin was also tested in HDF retrieved from a patient (P118) with a homozygous mutation in the enzyme COQ7, which catalyses the hydroxylation of the 5-demethoxyubiquinone-10 (DMQ10), an intermediate in the CoQ_{10} biosynthesis. These cells contain very low levels of endogenous CoQ_{10},

with an increase in DMQ_{10} content, and display impaired OCR and respiratory parameters; moreover, in these cells the mevalonate pathway is downregulated, and cholesterol levels are lower than controls [161]. The MTT assay showed that treatment with Atorvastatin impacted less on the viability of these mutant cells, showing a higher LD50, compared to control wild type HDF (Figure 26).

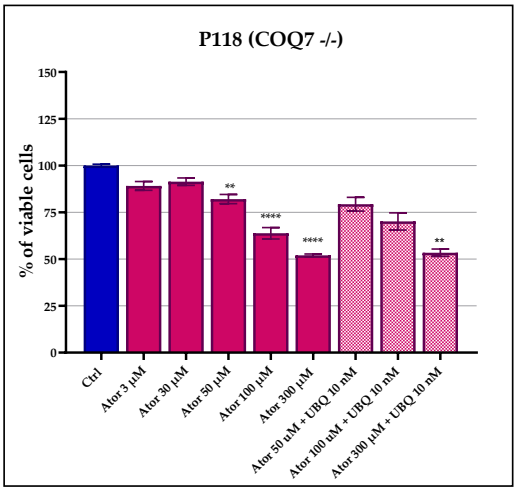

*Figure 26. Cell viability of COQ7-deficient HDF from patient P118, following 24 hours-treatment with Atorvastatin (3, 30, 50, 100 or 300 µM) alone or in combination with Ubiqsome® (10, 50, or 100 nM), as determined by MTT assay. Data represent the percentage of viable cells relative to untreated controls and are expressed as mean ± SEM (n = 5). Statistical significance was assessed using Brown-Forsythe ANOVA (**p ≤ 0.01; ****p ≤ 0.0001). Abbreviations: Ator = Atorvastatin; UBQ = Ubiqsome®.*

A possible explanation to this result is that where CoQ_{10} biosynthesis is already disrupted, the mevalonate pathway is downregulated, and the mitochondrial chain is not functional [161], Atorvastatin wouldn't impact in cell viability as in normal conditions.

3.2. Ubiqsome® has beneficial effects in *in vitro* and *in vivo* models of CDKL5 deficiency disorder.

3.2.1. Ubiqsome reduces oxidative stress in SH-*CDKL5*-KO cells

Since oxidative stress is a characteristic trait of the CDD phenotype, we evaluated the effect of UBQ supplementation on oxidative stress in a human neuronal cell model of CDKL5 deficiency (SH-*CDKL5*-KO). The DCF fluorescence showed a marked increase in total ROS production in KO cells, reduced by the supplementation of 100 nM of UBQ (Figure 27 A).

SH-*CDKL5*-KO cells showed a decrease of the reduced/oxidized glutathione ratio (GSH/GSSG) compared to parental cells, confirming a higher oxidative stress status. Treatment with 100 nM of UBQ significantly increased the GSH/GSSG ratio in KO cells, suggesting a protective effect, whereas no effect was observed in parental cells (Figure 27 B).

Lastly, SH-*CDKL5*-KO cells displayed an increase in mitochondrial ROS, as detected by probing the cells with MitoSox Green, which was diminished by UBQ (Figure 27 C,D).

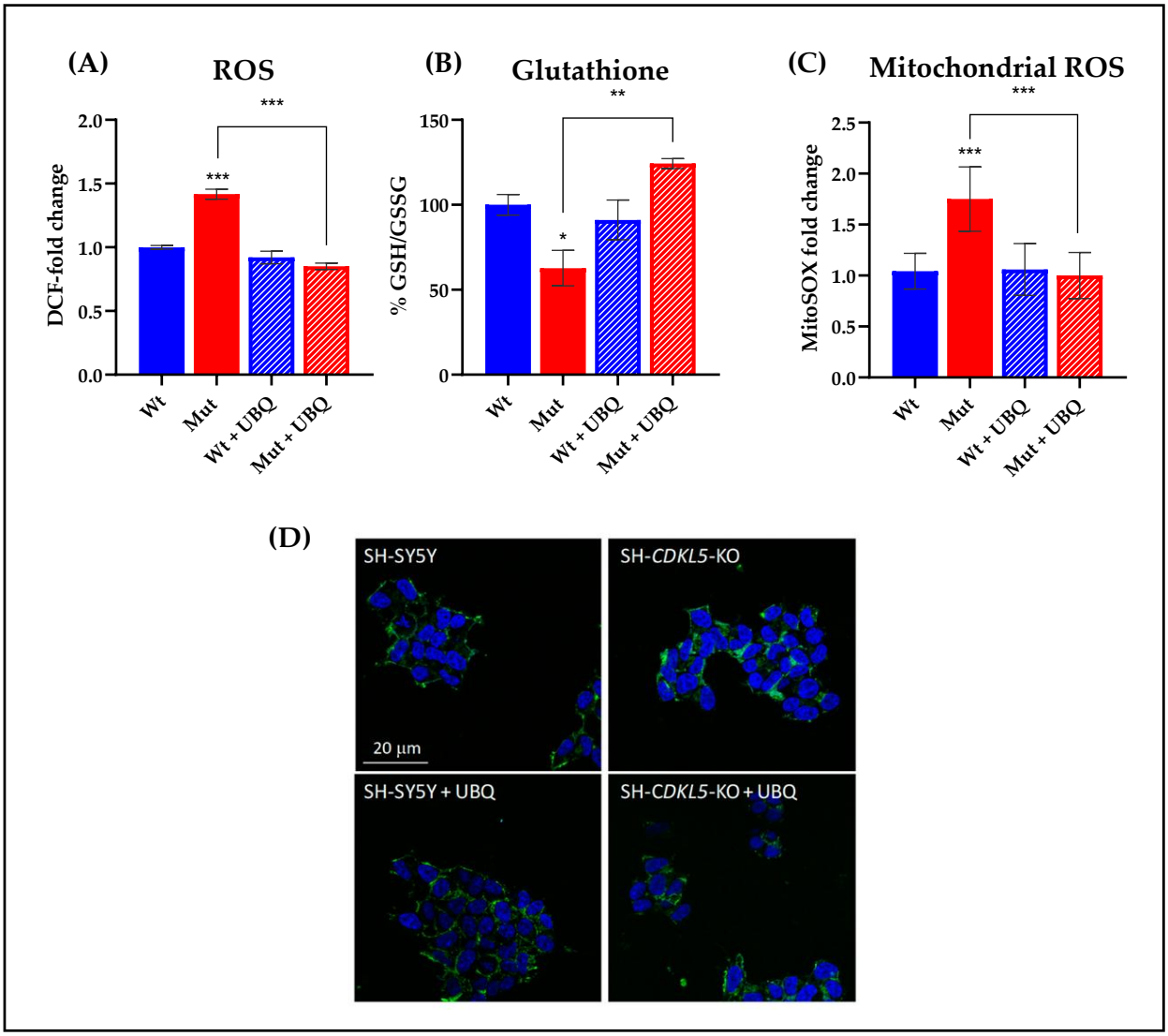

*Figure 27. Effect of treatment with UBQ on oxidative stress in SH-CDKL5-KO cells. (A) Oxidative stress determination in SH-SY5Y and SH-CDKL5-KO cells by DCF fluorescence. (B) Evaluation of reduced/oxidized glutathione ratio (GSH/GSSG) in SH-SY5Y and SH-CDKL5-KO before and after treatment with UBQ. (C) Oxidative stress determination in mitochondria of SH-SY5Y and SH-CDKL5-KO cells before and after treatment with UBQ, using MitoSOX Green. (D) Representative images of cells stained with MitoSOX Green and DAPI (blue). Data are mean ± SEM. Statistical analysis was performed using the Brown-Forsythe ANOVA test (*p ≤ 0.05; **p ≤ 0.01; *** p < 0.001). Abbreviations: UBQ = Ubiqsome®; Wt = SH-CDKL5; Mut = SH-CDKL5-KO.*

To note, parental and KO cells displayed no difference in CoQ_{10} content, measured by HPLC, nor in the OCR, measured by polarography (Figure 28 A, B). On the other hand, CoQ_{10} quantitation demonstrated a good uptake by both cell lines (Figure 28 A).

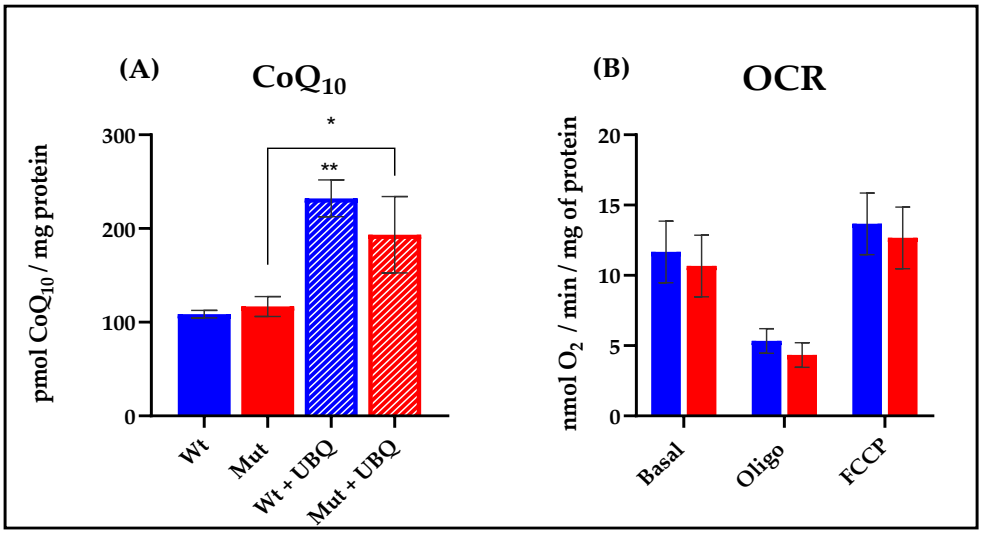

*Figure 28. Coenzyme Q_{10} quantitation by HPLC in the SH-SY5Y and SH-CDKL5-KO cells before and after supplementation with UBQ (A); OCR of SH-SY5Y and SH-CDKL5-KO cells (B). Data are mean ± SEM. Statistical analysis was performed using the Brown-Forsythe ANOVA test (*p ≤ 0.05; **p ≤ 0.01). Abbreviations: UBQ = Ubiqsome®; Wt = SH-CDKL5; Mut = SH-CDKL5-KO.*

3.2.2. Ubiqsome® is well uptaken *in vivo* and is effective in reducing oxidative stress

Coenzyme Q_{10} supplementation remains a challenge because of its scarce biodistribution in the peripheral tissues. The formulated CoQ_{10} product, Ubiqsome®, has demonstrated superior cellular uptake and intracellular delivery compared to crystalline CoQ_{10}, enhancing its bioavailability within target cells. To evaluate a beneficial effect of Ubiqsome® *in vivo*, we supplemented healthy ($Cdkl5^{+/+}$) and $Cdkl5^{+/-}$ mice, 6–8-month-old, with this product, in order to reduce the oxidative stress induced by the mutation. Mice were orally administered (dissolved in drinking water) with 500 mg/kg/die of formulated CoQ_{10} for two weeks. A group of vehicle-treated $Cdkl5^{+/-}$ and $Cdkl5^{+/+}$ female mice were used as treatment controls. The estimation of daily consumption of water for the vehicle- and UBQ-treated groups showed no treatment or genotype differences (4.5 ± 0.5 mL/day), suggesting a similar UBQ intake between $Cdkl5^{+/+}$ and $Cdkl5^{+/-}$ mice. We first investigated if the UBQ was absorbed, by measuring CoQ_{10} and CoQ_9 content in the plasmas of vehicle and UBQ-treated mice. Mutant mice showed a decrease in CoQ_{10} content (~ 55%) compared to healthy controls, while no difference was observed in the CoQ_9 content. UBQ supplementation successfully raised both CoQ_9

and CoQ_{10} content in plasma, suggesting that it was well absorbed in the intestine. However, the increase was evident for the wild type mice (+164% CoQ_9, + 85% CoQ_{10}), than for the mutant ones (+20% CoQ_9, +13% CoQ_{10}).

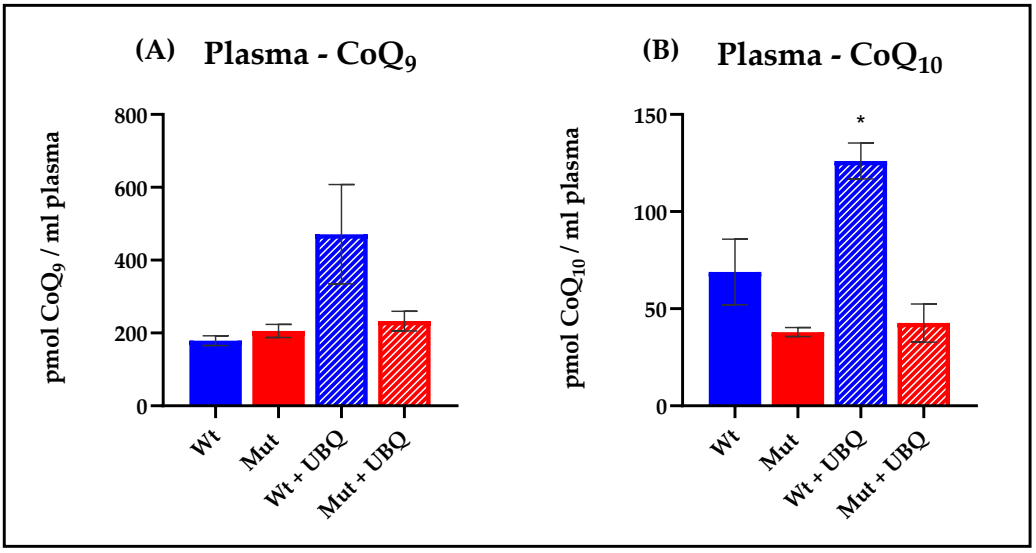

*Figure 29. Coenzyme Q_9 and Q_{10} content in plasma of Cdkl5$^{+/+}$ and Cdkl5$^{+/-}$ mice, before and after oral supplementation of UBQ, 500 mg/kg/die for two weeks. Statistical analysis was performed using the Brown-Forsythe ANOVA test (*p ≤ 0.05). Abbreviations: UBQ = Ubiqsome®; Wt = Cdkl5$^{+/+}$; Mut = Cdkl5$^{+/-}$.*

Tissues of mutant and control mice, treated with vehicle or UBQ, were analysed for CoQ content, before and after supplementation, in order to investigate its endogenous levels in the different conditions, and to assess to what extent this formulation could deliver CoQ_{10} in peripheral tissues. We found that heart tissues didn't display differences in CoQ content between control and mutant mice, and UBQ supplementation did not alter this outcome (Figure 30 A,B). Muscles (femoral quadriceps) from mutant mice seemed to show a lower CoQ content, nonetheless, UBQ did not alter these parameters (Figure 30 C,D).

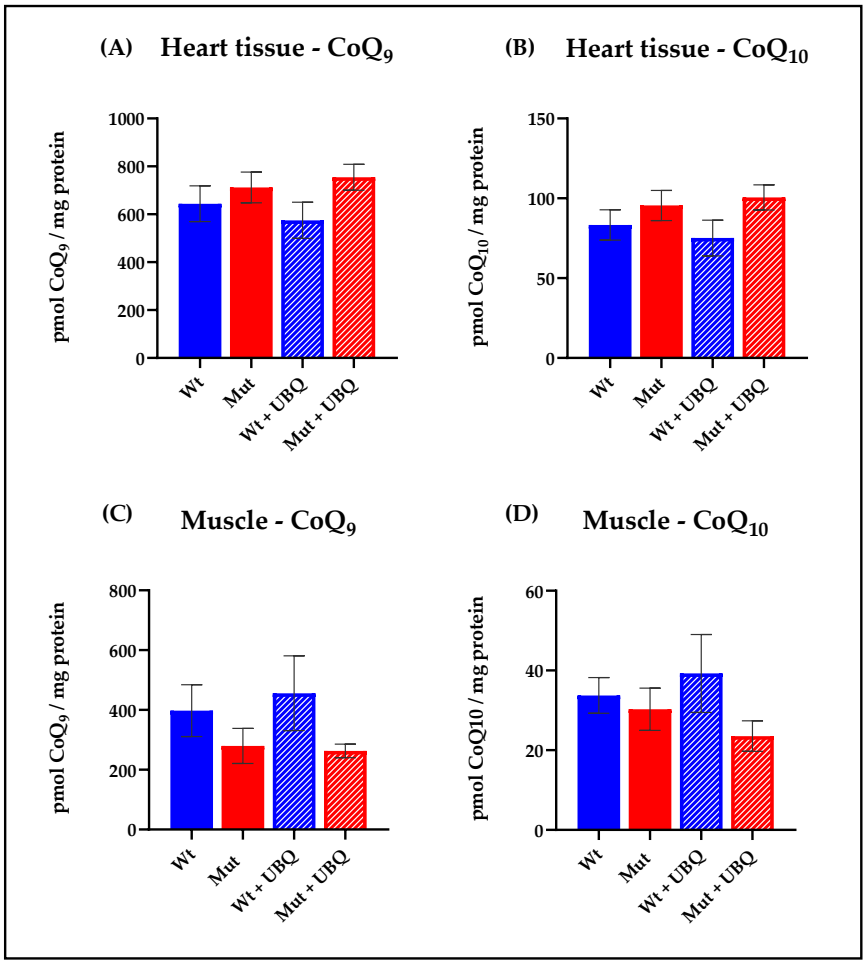

*Figure 30. CoQ_9 and CoQ_{10} contents from hearts (A,B) and muscles (C,D) from Cdkl5$^{+/+}$ and Cdkl5$^{+/-}$ mice after two weeks of Ubiqsome® supplementation. Statistical analysis was performed using the Brown-Forsythe ANOVA test (*p ≤ 0.05). Abbreviations: UBQ = Ubiqsome®; Wt = Cdkl5$^{+/+}$; Mut = Cdkl5$^{+/-}$.*

Since Cdkl5$^{+/-}$ female mice are characterized by typical signs of heart aging, which can manifest as oxidative stress, we investigated lipid peroxidation in those tissues, by measuring levels of MDA, which is a byproduct of lipid peroxidation. Despite the lack of a detectable CoQ increase, MDA quantitation revealed an increase in oxidative stress in the cardiac tissue of mutant mice compared to controls, decreased by UBQ treatment, suggesting that CoQ_{10} may have reached the organ (Figure 31).

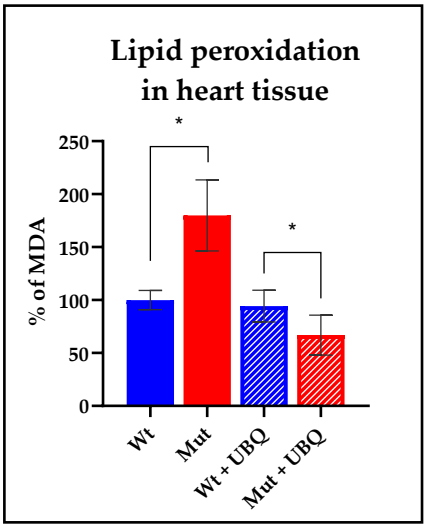

*Figure 31. Lipid peroxidation by means of MDA content. Data are shown as percentage of MDA. Statistical analysis was performed using the Brown-Forsythe ANOVA test (*p ≤ 0.05). Abbreviations: UBQ = Ubiqsome®; Wt = Cdkl5$^{+/+}$; Mut = Cdkl5$^{+/-}$.*

3.3. Ubiqsome® maintains CoQ_{10} chemical properties, is stable in water, and resistant to digestion.

3.3.1. CoQ_{10} in the formulation maintains its crystallin structure

Solid state NMR (ssNMR) analyses of crystalline bare CoQ_{10}, Ubiqsome® and the Phytosome® vector revealed that CoQ_{10} preserves its crystalline structure inside the formulation. The spectrum of Ubiqsome® exhibits characteristic peaks corresponding to crystalline Coenzyme Q_{10} as well as signals from the Phytosome® vector, suggesting that both carrier and solute maintain the original structures, and that no covalent bonds are formed during the preparation process (Figure 32 A,B).

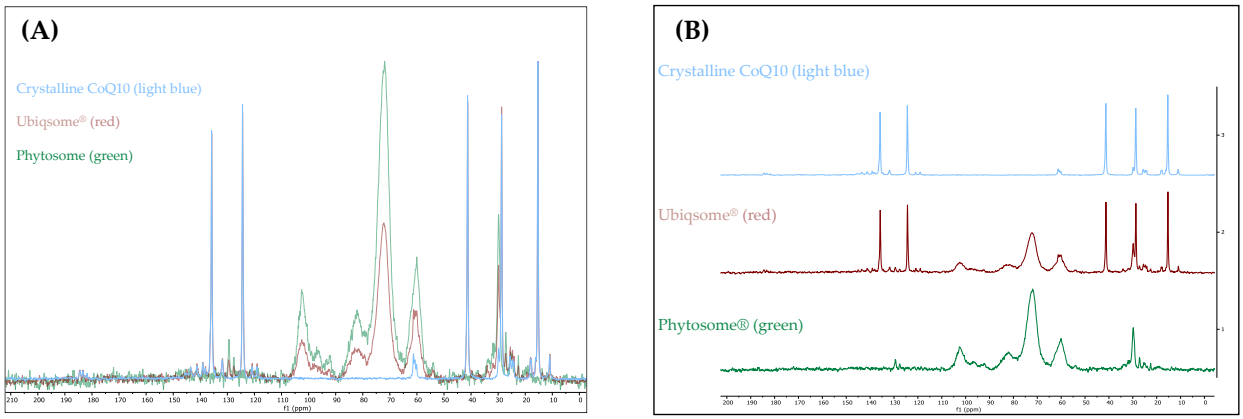

Figure 32. NMR spectra of crystalline CoQ_{10} (light blue), Ubiqsome® (red) and Phytosome® (green). (A) superimposed and (B) stacked spectra revealing peak correspondences.

3.3.2. CoQ_{10} and Ubiqsome® exhibit long-term stability in aqueous solutions and withstand simulated digestive conditions

Considering the results from *in vivo* studies, we decided to test the stability of crystalline and formulated CoQ_{10} in tap water, as well as the Phytosome® vector, through Raman spectroscopy. Samples were analysed right after dissolution (t=0) and after 5 days (t=5). Comparison of the spectra indicated there was no difference in the intensity and position of all peaks at the two different times, for what concerns CoQ_{10} (Figure 33).

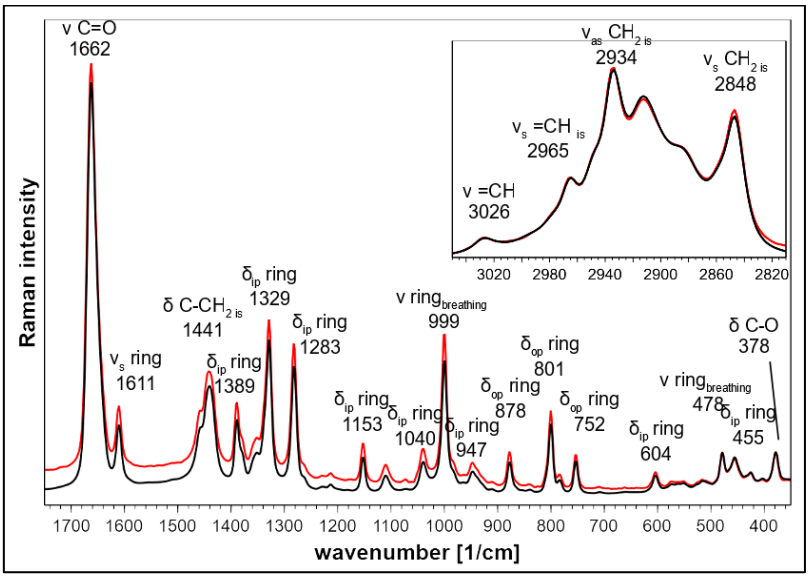

Figure 33. Raman spectra of crystallin CoQ_{10} at t = 0 days (black line) and t = 5 days (red line) in the 1750-350 cm^{-1} spectral range. In the inset, the Raman spectra in the 3050-2800 cm^{-1} spectral range, relative to CH stretching vibrations. ν: stretching vibrations; δ: bending vibrations; s: symmetrical vibrations; as: anti-symmetrical vibrations; ip: in-plane vibrations; op: out-of-plane vibrations; is: vibrations involving the isoprenic moiety of CoQ_{10}.

In the Ubiqsome® formulation all the observed bands are attributable to CoQ_{10}, without any sensible change in their position (Figure 34).

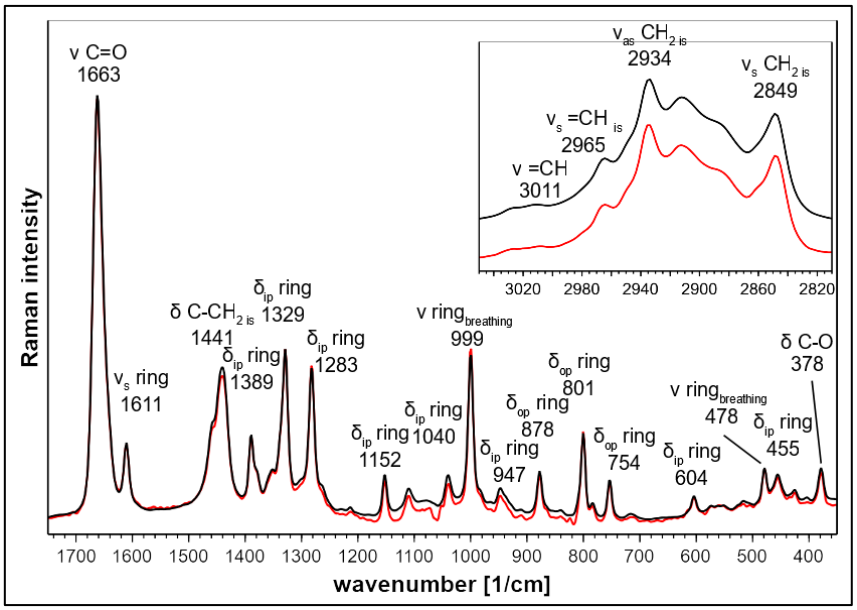

Figure 34. Raman spectra of UBQ at t = 0 days (black line) and t = 5 days (red line) in the 1750-350 cm^{-1} spectral range. In the inset, the Raman spectra in the 3050-2800 cm^{-1} spectral range, relative to CH stretching vibrations. ν: stretching vibrations; δ: bending vibrations; s: symmetrical vibrations; as: anti-symmetrical vibrations; ip: in-plane vibrations; op: out-of-plane vibrations; is: vibrations involving the isoprenic moiety of CoQ_{10}.

Spectra of the Phytosome® vector evidenced some differences at t=5, compared to t=0: in particular, some intensity ratios can be regarded as marker of the interaction between the alkyl chains of fatty acids composing the phospholipids. In fact, the intensity ratio between the band at 2925 cm^{-1} and the band at 2852 cm^{-1} (both attributed to CH vibration), increased at t=5, indicating a decrease of the hydrophobic interactions between alkyl chains [180]. The intensity ration between the bands at 1660 cm^{-1} (C=C) and 1440 cm^{-1} (C-H), and indicating the unsaturation degree of alkyl chains, remained unaffected at t=5. Raman spectra at t=5 also showed some peaks attributed to impurities (i.e., chlorophylls, carotenoids and anthocyanins) which showed peaks at 1610, 1512, 1360 and 1050 cm^{-1} [181]. The presence of these pigments (or their degradation) induced a marked increase of the fluorescence background of t=5 Raman spectrum as showed in Figure 35: the apparent intensity increase in the spectrum at t=5 can be attributed to the increased fluorescence emission by those pigments. These small changes detected in the Raman spectra of Phytosome® were not detected in the Ubiqsome® spectra, due to the strong Raman emission of CoQ_{10} molecules, which completely overlap and mask the typical peaks of phospholipids, that could be detected only thanks to difference spectra (Figure 35).

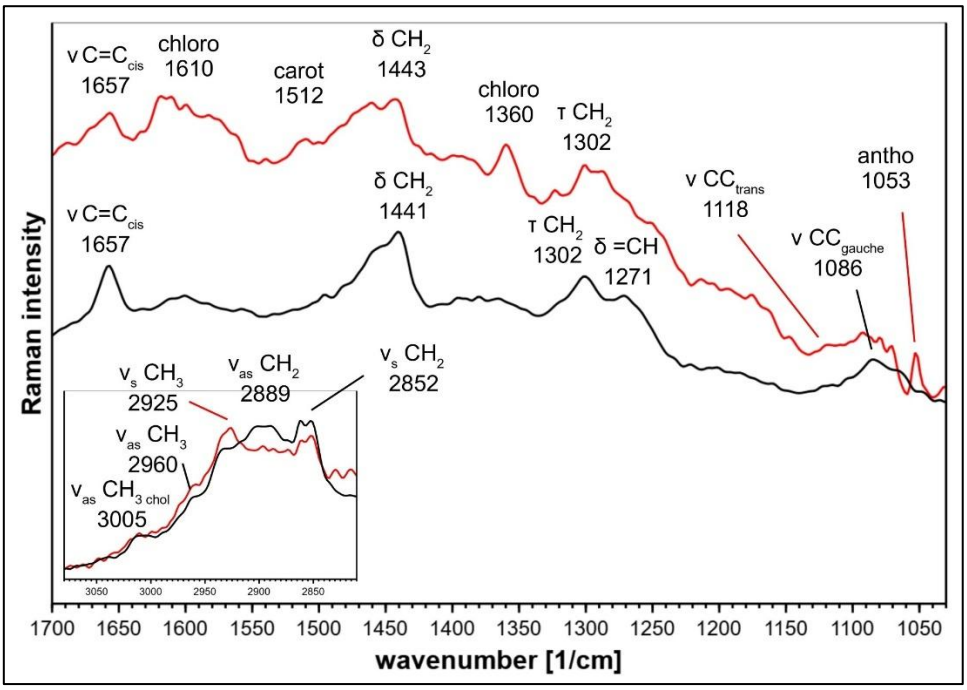

Figure 35. Raman spectra of Phytosome® at t = 0 days (black line) and t = 5 days (red line) in the 1750-350 cm-1 spectral range. In the inset, the Raman spectra in the 3005-2850 cm-1 spectral range, relative to CH stretching vibrations. ν: stretching vibrations; δ: bending vibrations; s: symmetrical vibrations; as: anti-symmetrical vibrations; cis: cis conformation; trans: trans conformation; gauche: gauche conformation; chol: choline moiety.

In order to better detect the variations between UBQ and CoQ_{10} at t=0 days and t=5 days, the difference spectra (UBQ – CoQ_{10}) were calculated and considered (blue line). Difference spectra show negative and positive peaks: negative peaks can all be attributed to CoQ_{10}, (UBQ contains approximately 20% of CoQ_{10}). Conversely, positive peaks are attributable to lipids of the formulation and are indicated in Figures 36 and 37. Most of those peaks changed their position compared to pure Phytosome® (i.e., bands at 3013-3009, 1371-1366, 1301-1300, 1267-1265, and 1084-1080 cm-1), indicating a chemical interaction between lipids and CoQ_{10} that affects the hydrophobic interactions between CH2 and CH3 groups of fatty acid acyl chains and of the choline head group (the 3013-3009 cm^{-1} band).

Interestingly, at t=0, the CoQ_{10} bands at 999 (ring breathing vibration) and 801 (out-of-plane bending) cm^{-1} showed a different behaviour (not only a simple decrease), which highlights that CoQ_{10} also is

slightly interacting with lipids in the formulation: as a matter of fact, both bands decrease their width in the formulated CoQ_{10}. This effect was not detected at t = 5 days.

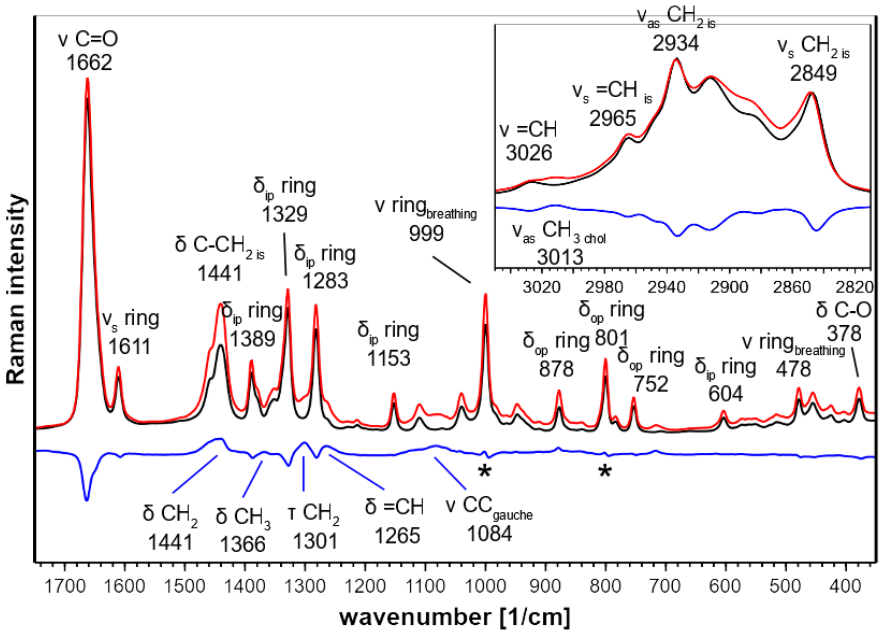

Figure 36. Raman spectra of CoQ_{10} (black line); UBQ (red line) at t = 0 days and their difference spectrum (UBQ- CoQ_{10}, blue line) in the 1750-350 cm^{-1} spectral range. In the inset, the Raman spectra in the 3050-2800 cm^{-1} spectral range, relative to CH stretching vibrations. ν: stretching vibrations; δ: bending vibrations; s: symmetrical vibrations; as: anti-symmetrical vibrations; ip: in-plane vibrations; op: out-of-plane vibrations; is: vibrations involving the isoprenic moiety of CoQ_{10}; gauche: gauche conformation; chol: choline moiety. Asterisks indicate CoQ_{10} bands affected by the interaction with lipids and discussed in the text.

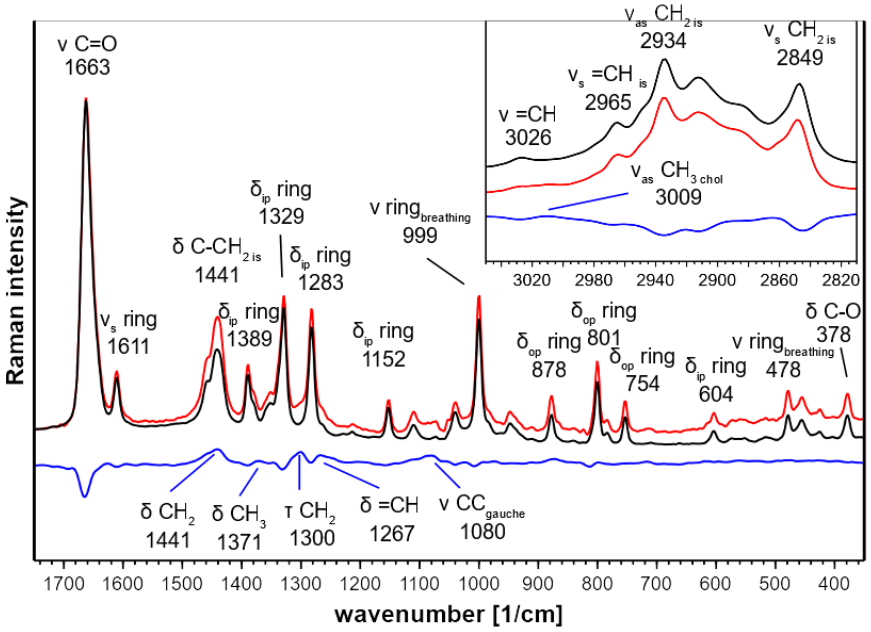

Figure 37. Raman spectra of CoQ10 (black line); UBQ (red line) at t = 5 days and their difference spectrum (UBQ- CoQ10, blue line) in the 1750-350 cm-1 spectral range. In the inset, the Raman spectra in the 3050-2800 cm-1 spectral range, relative to CH stretching vibrations. ν: stretching vibrations; δ: bending vibrations; s: symmetrical vibrations; as: anti-symmetrical vibrations; ip: in-plane vibrations; op: out-of-plane vibrations; is: vibrations involving the isoprenic moiety of CoQ10; gauche: gauche conformation; chol: choline moiety.

The simulated digestion had apparently no impact in the structure of bare or formulated CoQ10, as HPLC analyses only revealed the presence of one peak, with the expected retention time, and with an area under the curve matching the expected amounts (Figure 38).

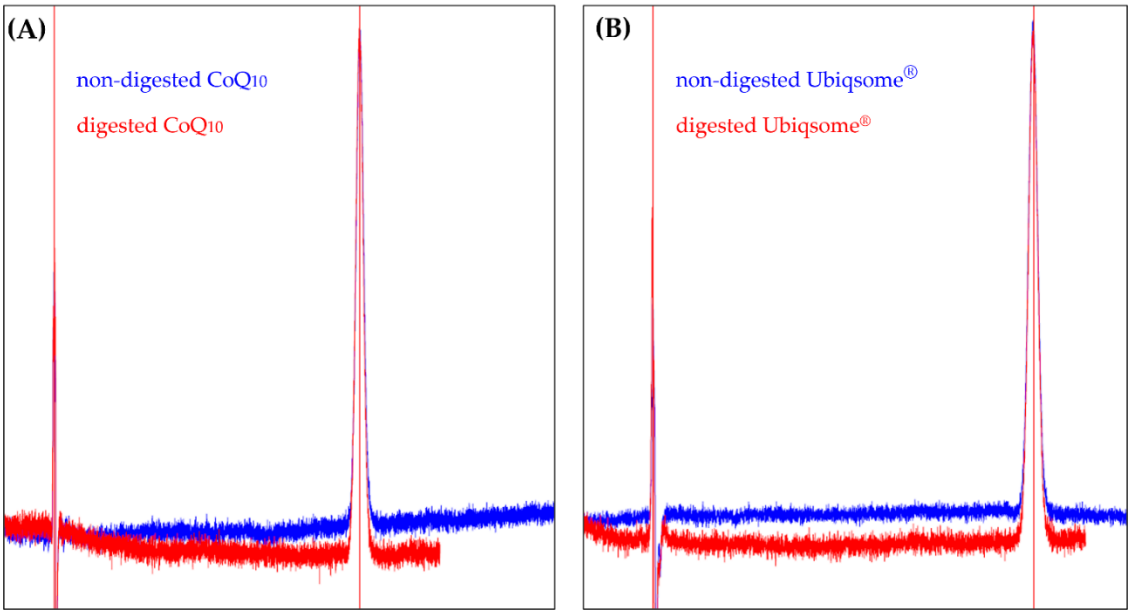

Figure 38. Representative HPLC chromatograms of crystalline CoQ10 (A) and UBQ-extracted CoQ10 (B) before (blue) and after (red) simulated digestion.

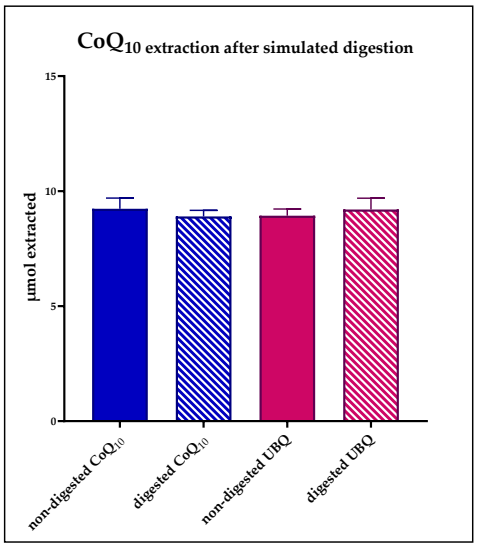

Figure 39. Quantitation of the extracted CoQ10 before and after simulated digestion.

4. Discussion

4.1. Ubiqsome® ameliorates bioenergetic impairment induced by Atorvastatin

Statin therapy is broadly used for both primary and secondary prevention of cardiovascular diseases, as its efficacy in lowering circulating LDL-cholesterol significantly decreases the insurgence of major cardiovascular events and microvascular complications [182]. Although being considered overall safe, with a benefit/risk ratio that justifies their prescription, statins are associated with multiple side effects, particularly muscle-related symptoms, such as pain and weakness, that undermine the patients' compliance with therapy. Therapy efficiency and side effects can vary significantly between patients [183], and *in vitro* outcomes are also controversial, likely depending on the cell model used [184] [185]. This study provides significant insights in-to the impact of Atorvastatin, a commonly prescribed statin, on the mitochondrial functions of human dermal fibroblasts (HDF). Atorvastatin-treated HDF displayed impaired OCR, a decrease in ATP/ADP ratio, and increased oxidative stress. It is assumed that statin-related symptoms are caused by a reduction of Coenzyme Q_{10}, which is biosynthesized through the mevalonate pathway. We observed a drastic reduction in total CoQ_{10} content after Atorvastatin treatment, but it is not clear whether the bioenergetic impairment is due to CoQ_{10} deficiency in the ETC, or because of a lowering of antioxidant defences, or both. We evaluated the efficacy of Ubiqsome®, a formulated CoQ_{10}, in alleviating these alterations. Our results demonstrated that co-supplementation of CoQ_{10} in Atorvastatin-treated cells is efficient in recovering the altered parameters, in terms of ROS protection, ETC efficiency, OCR sustained by gluta-mate/malate and succinate, and ATP/ADP ratio. However, seeing the plethora of statin-associated symptoms [186], it would be oversimplified to state that Atorvastatin-induced side effects only rely on CoQ_{10} deficiency. We observed a direct inhibition on functionally isolated Complex I at the CoQ_{10} binding site level. Complex I can be functionally divided into three modules: the dehydrogenase module, the hydrogenase module and the proton pump module [187] [188]. Atorvastatin

seems to inhibit Complex I activity at the hydrogenase level, since the oxidation of NADH in the presence of the CoQ analogue decyl-ubiquinone (DB) is lowered, while the rotenone-insensitive NADH-$[Fe(CN)_6]^{3-}$ reaction occurring at the dehydrogenase module of Complex I was not affected. In a previous study from our laboratory, Fato et al. [174] demonstrated that Complex I inhibitors can be classified into two groups based on their ability to induce reactive oxygen species (ROS). Class A inhibitors, such as rotenone, piericidin A and rolliniastatin 1 and 2, enhance ROS production during forward electron transport. In contrast, class B inhibitors, such as stigmatellin, mucidin, and capsaicin (that are considered classical inhibitors of Complex III at the "O" center), at high concentrations target Complex I and block it in a conformation that prevents ROS generation during forward electron transfer. Our findings suggest that the mechanism by which Atorvastatin inhibits Complex I is not rotenone-like, since Atorvastatin did not increase ROS production in isolated mitochondria energized with NADH. Since Atorvastatin, a lactone containing statin, blocks the "O" centre of Complex III, preventing ROS generation [102], we hypothesized that the marked increase in mitochondrial ROS observed in Atorvastatin-treated cells (Figure 23 A,B) should be attributed to reverse electron flow through Complex I. To validate the occurrence of RET, we supplemented cells with succinate (a membrane-permeable metabolite) in the presence of Atorvastatin. This treatment led to an increase in ROS production, which was significantly reduced by rotenone treatment (Figure 25). Furthermore, our findings are consistent with those reported by Wojcicki et al. [179], who observed that Atorvastatin and Simvastatin increased ROS production in non-phosphorylating (State 4) mitochondria energized with succinate. In contrast, ROS levels remained low in phosphorylating (State 3) mitochondria energized with either malate-pyruvate (as NADH source) or succinate. Taken together, the results presented in this paper, along with evidence from the literature, suggest a mechanism by which Atorvastatin affects mitochondrial function. This mechanism involves the ability of the molecule to inhibit Complex III by targeting the "O" centre and to alter Complex I

activity. Atorvastatin inhibition may induce a Complex I conformation that prevents the direct transfer of electrons from NADH to molecular oxygen. However, in the presence of elevated levels of $CoQH_2$, Atorvastatin treatment may promote reverse electron transfer (RET), leading to increased ROS pro-duction [189]. This exacerbation of oxidative stress can impair mitochondrial function and compromise cell homeostasis, switching the metabolism to a more glycolytic one, apparently leaving unaltered the mitochondrial mass and the expression of genes involved in mitochondrial function.

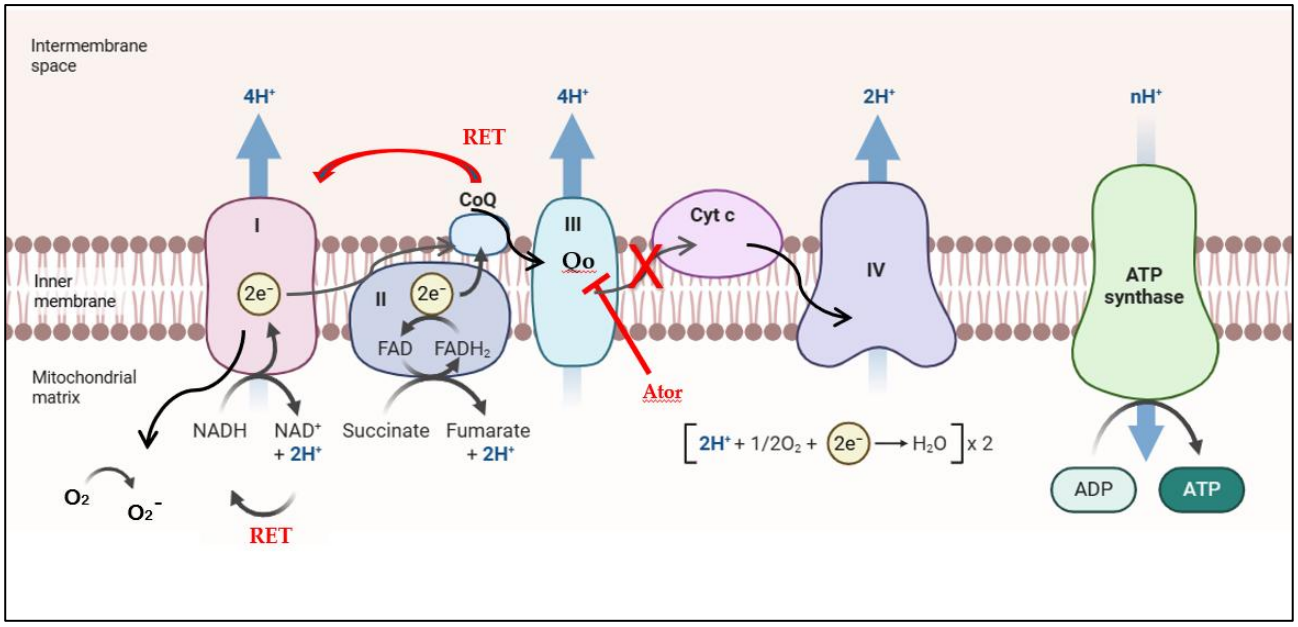

Figure 40. Schematic representation of the proposed mechanism of mitochondrial ROS generation induced by Atorvastatin in the presence of succinate: the reverse electron transport (RET) determines ROS generation via Complex I.

4.2. Ubiqsome® ameliorate oxidative stress in a *CDKL5*-deficient model

Despite the uptake of CoQ_{10} after UBQ supplementation *in vitro*, and its efficacy in reducing oxidative stress in SH-*CDKL5*-KO cells, the *in vivo* supplementation led to contrasting results. UBQ was well absorbed in the intestine, as plasma analysis revealed a higher content of both CoQ_9 and CoQ_{10} after supplementation, especially in control mice; however, peripheral tissues showed no change in CoQ levels, in both control and mutant mice. Nonetheless, UBQ was effective in reducing oxidative stress in cardiac tissues.

In order to comprehend what limits the uptake of Coenzyme Q_{10} by tissues, we analysed the stability of the formulation after dissolution in tap water, to mimic the conditions of administration *in vivo*; Raman spectroscopy, conducted by Professor Michele Di Foggia, revealed no changes in the structure of CoQ_{10} both in the crystalline and formulated samples after 5 days in water and light exposure, as the characteristic peaks were retained in the samples. We also questioned whether pH fluctuations and digestive enzymes presence could interfere with the structure of the molecule, thus crystalline and formulated CoQ_{10} underwent an *in vitro* simulated digestion, but no significant alterations were noticed during the HPLC analysis. Lastly, we asked the team of Professor Daniele Cortecchia (University of Bologna) to investigate whether CoQ_{10} maintained its crystalline structure after being dissolved in the formulation. The analysis revealed that no chemical interactions were occurring between CoQ_{10} and the phospholipids, and that CoQ_{10} maintained its crystalline structure, which may represent a limit in a drug delivery contest, since amorphous-structured molecules are usually better up taken than their crystallin counterparts [190].

5. Bibliography

1. Mensah GA, Roth GA, Fuster V. The Global Burden of Cardiovascular Diseases and Risk Factors: 2020 and Beyond. Journal of the American College of Cardiology. 2019;74(20):2529-2532. doi:10.1016/j.jacc.2019.10.009

2. Global, regional, and national age-sex-specific mortality for 282 causes of death in 195 countries and territories, 1980–2017: a systematic analysis for the Global Burden of Disease Study 2017 - The Lancet. Accessed August 19, 2025. https://www.thelancet.com/journals/lancet/article/PIIS0140-6736(18)32203-7/fulltext

3. Yusuf S, Hawken S, Ounpuu S, et al. Effect of potentially modifiable risk factors associated with myocardial infarction in 52 countries (the INTERHEART study): case-control study. Lancet. 2004;364(9438):937-952. doi:10.1016/S0140-6736(04)17018-9

4. Grundy SM, Stone NJ, Bailey AL, et al. 2018 AHA/ACC/AACVPR/AAPA/ABC/ACPM/ADA/AGS/APhA/ASPC/NLA/PCNA Guideline on the Management of Blood Cholesterol: A Report of the American College of Cardiology/American Heart Association Task Force on Clinical Practice Guidelines. Circulation. 2019;139(25). doi:10.1161/CIR.0000000000000625

5. Ference BA, Ginsberg HN, Graham I, et al. Low-density lipoproteins cause atherosclerotic cardiovascular disease. 1. Evidence from genetic, epidemiologic, and clinical studies. A consensus statement from the European Atherosclerosis Society Consensus Panel. Eur Heart J. 2017;38(32):2459-2472. doi:10.1093/eurheartj/ehx144

6. Ference BA, Ginsberg HN, Graham I, et al. Low-density lipoproteins cause atherosclerotic cardiovascular disease. 1. Evidence from genetic, epidemiologic, and clinical studies. A consensus statement from the European Atherosclerosis Society Consensus Panel. Eur Heart J. 2017;38(32):2459-2472. doi:10.1093/eurheartj/ehx144

7. The Role of Lipids and Lipoproteins in Atherosclerosis - Endotext - NCBI Bookshelf. Accessed September 3, 2025. https://www.ncbi.nlm.nih.gov/books/NBK343489/

8. Sabatine MS, Wiviott SD, Im K, Murphy SA, Giugliano RP. Efficacy and Safety of Further Lowering of Low-Density Lipoprotein Cholesterol in Patients Starting With Very Low Levels. JAMA Cardiol. 2018;3(9):823-828. doi:10.1001/jamacardio.2018.2258

9. Roth GA, Mensah GA, Johnson CO, et al. Global Burden of Cardiovascular Diseases and Risk Factors, 1990–2019: Update From the GBD 2019 Study. Journal of the American College of Cardiology. 2020;76(25):2982-3021. doi:10.1016/j.jacc.2020.11.010

10. Pirillo A, Norata GD. The burden of hypercholesterolemia and ischemic heart disease in an ageing world. Pharmacological Research. 2023;193:106814. doi:10.1016/j.phrs.2023.106814

11. Feb 16 LR, 2024. What Your Cholesterol Levels Mean. www.heart.org. Accessed August 19, 2025. https://www.heart.org/en/health-topics/cholesterol/about-cholesterol/what-your-cholesterol-levels-mean

12. Civeira F, Arca M, Cenarro A, Hegele RA. A mechanism-based operational definition and classification of hypercholesterolemia. Journal of Clinical Lipidology. 2022;16(6):813-821. doi:10.1016/j.jacl.2022.09.006

13. Ojeda-Granados C, Campisi E, Barchitta M, Agodi A. Genetic, lifestyle and metabolic factors contributing to cardiovascular disease in the Italian population: a literature review. Front Nutr. 2024;11. doi:10.3389/fnut.2024.1379785

14. Li YH, Shih CL. 2025 Consensus on the Clinical Pathway of Blood Cholesterol Management in Taiwan. Acta Cardiol Sin. 2025;41(2):161-165. doi:10.6515/ACS.202503_41(2).20250215A

15. Ravnskov U, de Lorgeril M, Diamond DM, et al. LDL-C does not cause cardiovascular disease: a comprehensive review of the current literature. Expert Rev Clin Pharmacol. 2018;11(10):959-970. doi:10.1080/17512433.2018.1519391

16. Collaborators CTT (CTT). Efficacy of cholesterol-lowering therapy in 18 686 people with diabetes in 14 randomised trials of statins: a meta-analysis. The Lancet. 2008;371(9607):117-125. doi:10.1016/S0140-6736(08)60104-X

17. Collaboration CTT (CTT). Efficacy and safety of more intensive lowering of LDL cholesterol: a meta-analysis of data from 170 000 participants in 26 randomised trials. The Lancet. 2010;376(9753):1670-1681. doi:10.1016/S0140-6736(10)61350-5

18. LaRosa JC, Grundy SM, Kastelein JJP, Kostis JB, Greten H. Safety and Efficacy of Atorvastatin-Induced Very Low-Density Lipoprotein Cholesterol Levels in Patients With Coronary Heart Disease (a Post Hoc Analysis of the Treating to New Targets [TNT] Study)†. American Journal of Cardiology. 2007;100(5):747-752. doi:10.1016/j.amjcard.2007.03.102

19. Wang W, Hu M, Liu H, et al. Global Burden of Disease Study 2019 suggests that metabolic risk factors are the leading drivers of the burden of ischemic heart disease. Cell Metabolism. 2021;33(10):1943-1956.e2. doi:10.1016/j.cmet.2021.08.005

20. Patel J, Sharma T, Allan C, Curnew G. Use of Lifestyle Modifications for Management of a Patient with Severely High Total Cholesterol (> 14 mmol/L) and Triglycerides (> 40 mmol/L). Journal of Lifestyle Medicine. 2021;11(1):43-46. doi:10.15280/jlm.2021.11.1.43

21. Harris MI. Hypercholesterolemia in diabetes and glucose intolerance in the U.S. population. Diabetes Care. 1991;14(5):366-374. doi:10.2337/diacare.14.5.366

22. Warden BA, Fazio S, Shapiro MD. Familial Hypercholesterolemia: Genes and Beyond. In: Feingold KR, Ahmed SF, Anawalt B, et al., eds. Endotext. MDText.com, Inc.; 2000. Accessed August 19, 2025. http://www.ncbi.nlm.nih.gov/books/NBK343488/

23. Overproduction of Very Low–Density Lipoproteins Is the Hallmark of the Dyslipidemia in the Metabolic Syndrome | Arteriosclerosis, Thrombosis, and Vascular Biology. Accessed August 20, 2025. https://www.ahajournals.org/doi/10.1161/atvbaha.107.160192

24. Talmud PJ, Shah S, Whittall R, et al. Use of low-density lipoprotein cholesterol gene score to distinguish patients with polygenic and monogenic familial hypercholesterolaemia: a case-control study. The Lancet. 2013;381(9874):1293-1301. doi:10.1016/S0140-6736(12)62127-8

25. Medeiros AM, Alves AC, Bourbon M. APOB/APOA1 ratio and APOC2 are the best biomarkers to distinguish familial hypercholesterolemia from other dyslipidaemia. Atherosclerosis. 2017;263:e61. doi:10.1016/j.atherosclerosis.2017.06.206

26. Mikhailova SV, Ivanoshchuk DE, Shirokova NS, Shakhtshneider EV. Polymorphism of the APOA5 gene in patients with primary hyperlipidemia. Complex Issues of Cardiovascular Diseases. 2020;9(2):38-44. doi:10.17802/2306-1278-2020-9-2-38-44

27. Khalil YA, Rabès JP, Boileau C, Varret M. APOE gene variants in primary dyslipidemia. Atherosclerosis. 2021;328:11-22. doi:10.1016/j.atherosclerosis.2021.05.007

28. Iwamoto S, Boonvisut S, Makishima S, Ishizuka Y, Watanabe K, Nakayama K. The role of TRIB1 in lipid metabolism; from genetics to pathways. Biochem Soc Trans. 2015;43(5):1063-1068. doi:10.1042/BST20150094

29. Dijk W, Di Filippo M, Kooijman S, et al. Identification of a Gain-of-Function LIPC Variant as a Novel Cause of Familial Combined Hypocholesterolemia. Circulation. 2022;146(10):724-739. doi:10.1161/CIRCULATIONAHA.121.057978

30. Cicero AFG, Cincione IR. Chapter 23 - Secondary (acquired) hypercholesterolemia. In: Bukiya AN, Dopico AM, eds. Cholesterol. Academic Press; 2022:609-621. doi:10.1016/B978-0-323-85857-1.00016-X

31. Won H, Bae JH, Lim H, Kang M, Kim M, Lee SH. 2024 KSoLA consensus on secondary dyslipidemia. Korean J Intern Med. 2024;39(5):717-730. doi:10.3904/kjim.2024.156

32. Feingold KR. Guidelines for the Management of High Blood Cholesterol. In: Feingold KR, Ahmed SF, Anawalt B, et al., eds. Endotext. MDText.com, Inc.; 2000. Accessed August 20, 2025. http://www.ncbi.nlm.nih.gov/books/NBK305897/

33. 2018 AHA/ACC/AACVPR/AAPA/ABC/ACPM/ADA/AGS/APhA/ASPC/NLA/PCNA Guideline on the Management of Blood Cholesterol: A Report of the American College of Cardiology/American Heart Association Task Force on Clinical Practice Guidelines | Circulation. Accessed August 20, 2025. https://www.ahajournals.org/doi/10.1161/cir.0000000000000625

34. ESC Guidelines on Dyslipidaemias (Management of). Accessed September 23, 2025. https://www.escardio.org/Guidelines/Clinical-Practice-Guidelines/Dyslipidaemias-Management-of#

35. Feingold KR. Cholesterol Lowering Drugs. In: Feingold KR, Ahmed SF, Anawalt B, et al., eds. Endotext. MDText.com, Inc.; 2000. Accessed August 21, 2025. http://www.ncbi.nlm.nih.gov/books/NBK395573/

36. Agnello F, Ingala S, Laterra G, Scalia L, Barbanti M. Novel and Emerging LDL-C Lowering Strategies: A New Era of Dyslipidemia Management. Journal of Clinical Medicine. 2024;13(5):1251. doi:10.3390/jcm13051251

37. Catapano AL, Graham I, Backer GD, et al. 2016 ESC/EAS Guidelines for the Management of Dyslipidaemias: The Task Force for the Management of Dyslipidaemias of the European Society of Cardiology (ESC) and European Atherosclerosis Society (EAS) Developed with the special contribution of the European Association for Cardiovascular Prevention & Rehabilitation (EACPR). Atherosclerosis. 2016;253:281-344. doi:10.1016/j.atherosclerosis.2016.08.018

38. 2013 ACC/AHA Guideline on the Treatment of Blood Cholesterol to Reduce Atherosclerotic Cardiovascular Risk in Adults | Circulation. Accessed August 21, 2025. https://www.ahajournals.org/doi/10.1161/01.cir.0000437738.63853.7a

39. Bruckert E, Giral P, Tellier P. Perspectives in cholesterol-lowering therapy: the role of ezetimibe, a new selective inhibitor of intestinal cholesterol absorption. Circulation. 2003;107(25):3124-3128. doi:10.1161/01.CIR.0000072345.98581.24

40. Telford DE, Sutherland BG, Edwards JY, Andrews JD, Barrett PHR, Huff MW. The molecular mechanisms underlying the reduction of LDL apoB-100 by ezetimibe plus simvastatin. J Lipid Res. 2007;48(3):699-708. doi:10.1194/jlr.M600439-JLR200

41. Frontiers | Regulation of PCSK9 Expression and Function: Mechanisms and Therapeutic Implications. Accessed August 21, 2025. https://www.frontiersin.org/journals/cardiovascular-medicine/articles/10.3389/fcvm.2021.764038/full

42. Shin D, Kim S, Lee H, et al. PCSK9 stimulates Syk, PKCδ, and NF-κB, leading to atherosclerosis progression independently of LDL receptor. Nat Commun. 2024;15(1):2789. doi:10.1038/s41467-024-46336-2

43. Schachter M. Chemical, pharmacokinetic and pharmacodynamic properties of statins: an update. Fundam Clin Pharmacol. 2005;19(1):117-125. doi:10.1111/j.1472-8206.2004.00299.x

44. Bansal AB, Cassagnol M. HMG-CoA Reductase Inhibitors. In: StatPearls. StatPearls Publishing; 2025. Accessed August 23, 2025. http://www.ncbi.nlm.nih.gov/books/NBK542212/

45. Bucher NLR, Overath P, Lynen F. β-hydroxy-β-methylglutaryl coenzyme a reductase, cleavage and condensing enzymes in relation to cholesterol formation in rat liver. Biochimica et Biophysica Acta. 1960;40:491-501. doi:10.1016/0006-3002(60)91390-1

46. Endo A, Kuroda M, Tsujita Y. ML-236A, ML-236B, AND ML-236C, NEW INHIBITORS OF CHOLESTEROGENESIS PRODUCED BY PENICILLIUM CITRINUM. J Antibiot. 1976;29(12):1346-1348. doi:10.7164/antibiotics.29.1346

47. A gift from nature: the birth of the statins | Nature Medicine. Accessed September 23, 2025. https://www.nature.com/articles/nm1008-1050

48. Haruyama H, Kuwano H, Kinoshita T, Terahara A, Nishigaki T, Tamura C. Structure Elucidation of the Bioactive Metabolites of ML-236B (Mevastatin) Isolated from Dog Urine. Chemical & Pharmaceutical Bulletin. 1986;34(4):1459-1467. doi:10.1248/cpb.34.1459

49. Endo A. The origin of the statins. International Congress Series. 2004;1262:3-8. doi:10.1016/j.ics.2003.12.099

50. Mevinolin: a highly potent competitive inhibitor of hydroxymethylglutaryl-coenzyme A reductase and a cholesterol-lowering agent. | PNAS. Accessed August 23, 2025. https://www.pnas.org/doi/abs/10.1073/pnas.77.7.3957

51. Endo A. The discovery and development of HMG-CoA reductase inhibitors. Journal of Lipid Research. 1992;33(11):1569-1582. doi:10.1016/S0022-2275(20)41379-3

52. Schachter M. Chemical, pharmacokinetic and pharmacodynamic properties of statins: an update. Fundam Clin Pharmacol. 2005;19(1):117-125. doi:10.1111/j.1472-8206.2004.00299.x

53. Moore BM, Cook GA. Chapter 33 - Medicinal chemistry and pharmacology of statins. In: Bukiya AN, Dopico AM, eds. Cholesterol. Academic Press; 2022:903-926. doi:10.1016/B978-0-323-85857-1.00012-2

54. Murphy C, Deplazes E, Cranfield CG, Garcia A. The Role of Structure and Biophysical Properties in the Pleiotropic Effects of Statins. Int J Mol Sci. 2020;21(22):8745. doi:10.3390/ijms21228745

55. Murphy C, Deplazes E, Cranfield CG, Garcia A. The Role of Structure and Biophysical Properties in the Pleiotropic Effects of Statins. Int J Mol Sci. 2020;21(22):8745. doi:10.3390/ijms21228745

56. Istvan ES, Deisenhofer J. Structural Mechanism for Statin Inhibition of HMG-CoA Reductase. Science. 2001;292(5519):1160-1164. doi:10.1126/science.1059344

57. Istvan ES, Deisenhofer J. Structural Mechanism for Statin Inhibition of HMG-CoA Reductase. Science. 2001;292(5519):1160-1164. doi:10.1126/science.1059344

58. Istvan ES, Deisenhofer J. Structural mechanism for statin inhibition of HMG-CoA reductase. Science. 2001;292(5519):1160-1164. doi:10.1126/science.1059344

59. McTaggart F, Buckett L, Davidson R, et al. Preclinical and clinical pharmacology of rosuvastatin, a new 3-hydroxy- 3-methylglutaryl coenzyme A reductase inhibitor1. The American Journal of Cardiology. 2001;87(5, Supplement 1):28-32. doi:10.1016/S0002-9149(01)01454-0

60. Molecular mechanism for inhibition of 3-hydroxy-3-methylglutaryl CoA (HMG-CoA) reductase by rosuvastatin | Biochemical Society Transactions | Portland Press. Accessed August 23, 2025. https://portlandpress.com/biochemsoctrans/article-abstract/31/3/528/63539/Molecular-mechanism-for-inhibition-of-3-hydroxy-3?redirectedFrom=fulltext

61. Fong CW. Statins in therapy: understanding their hydrophilicity, lipophilicity, binding to 3-hydroxy-3-methylglutaryl-CoA reductase, ability to cross the blood brain barrier and metabolic stability based on electrostatic molecular orbital studies. Eur J Med Chem. 2014;85:661-674. doi:10.1016/j.ejmech.2014.08.037

62. LogP vs LogD - What is the Difference? - ACD/Labs. Accessed August 21, 2025. https://www.acdlabs.com/blog/partitioning-logp-or-logd-are-you-using-measuring-the-right-descriptor/

63. Kelley BJ, Glasser S. Cognitive effects of statin medications. CNS Drugs. 2014;28(5):411-419. doi:10.1007/s40263-014-0147-5

64. Shitara Y, Sugiyama Y. Pharmacokinetic and pharmacodynamic alterations of 3-hydroxy-3-methylglutaryl coenzyme A (HMG-CoA) reductase inhibitors: Drug–drug interactions and interindividual differences in transporter and metabolic enzyme functions. Pharmacology & Therapeutics. 2006;112(1):71-105. doi:10.1016/j.pharmthera.2006.03.003

65. Fujino H, Nakai D, Nakagomi R, Saito M, Tokui T, Kojima J. Metabolic stability and uptake by human hepatocytes of pitavastatin, a new inhibitor of HMG-CoA reductase. Arzneim-Forsch Drug Res. 2004;54(7):382-388. doi:10.1055/s-0031-1296988

66. Lau YY, Okochi H, Huang Y, Benet LZ. Multiple Transporters Affect the Disposition of Atorvastatin and Its Two Active Hydroxy Metabolites: Application of in Vitro and ex Situ Systems. The Journal of Pharmacology and Experimental Therapeutics. 2006;316(2):762-771. doi:10.1124/jpet.105.093088

67. Schneck DW, Birmingham BK, Zalikowski JA, et al. The effect of gemfibrozil on the pharmacokinetics of rosuvastatin. Clinical Pharmacology & Therapeutics. 2004;75(5):455-463. doi:10.1016/j.clpt.2003.12.014

68. Sirtori CR. Tissue selectivity of hydroxymethylglutaryl coenzyme a (HMG CoA) reductase inhibitors. Pharmacology & Therapeutics. 1993;60(3):431-459. doi:10.1016/0163-7258(93)90031-8

69. Lennernäs H. Clinical Pharmacokinetics of Atorvastatin. Clin Pharmacokinet. 2003;42(13):1141-1160. doi:10.2165/00003088-200342130-00005

70. In vitro comparative inhibition profiles of major human drug metabolising cytochrome P450 isozymes (CYP2C9, CYP2D6 and CYP3A4) by HMG-CoA reductase inhibitors | European Journal of Clinical Pharmacology. Accessed August 23, 2025. https://link.springer.com/article/10.1007/s002280050094

71. White CM. A Review of the Pharmacologic and Pharmacokinetic Aspects of Rosuvastatin. The Journal of Clinical Pharmacology. 2002;42(9):963-970. doi:10.1177/009127000204200902

72. Clinical Pharmacokinetics of Pravastatin | Clinical Pharmacokinetics. Accessed August 23, 2025. https://link.springer.com/article/10.2165/00003088-200039060-00002

73. Moore BM, Cook GA. Chapter 33 - Medicinal chemistry and pharmacology of statins. In: Bukiya AN, Dopico AM, eds. Cholesterol. Academic Press; 2022:903-926. doi:10.1016/B978-0-323-85857-1.00012-2

74. Mullen PJ, Yu R, Longo J, Archer MC, Penn LZ. The interplay between cell signalling and the mevalonate pathway in cancer. Nat Rev Cancer. 2016;16(11):718-731. doi:10.1038/nrc.2016.76

75. The interplay between cell signalling and the mevalonate pathway in cancer | Nature Reviews Cancer. Accessed October 7, 2025. https://www.nature.com/articles/nrc.2016.76

76. Petras SF, Lindsey S, Harwood HJ. HMG-CoA reductase regulation: use of structurally diverse first half-reaction squalene synthetase inhibitors to characterize the site of mevalonate-derived nonsterol regulator production in cultured IM-9 cells. J Lipid Res. 1999;40(1):24-38.

77. Transon C, Leemann T, Dayer P. In vitro comparative inhibition profiles of major human drug metabolising cytochrome P450 isozymes (CYP2C9, CYP2D6 and CYP3A4) by HMG-CoA reductase inhibitors. Eur J Clin Pharmacol. 1996;50(3):209-215. doi:10.1007/s002280050094

78. A Receptor-Mediated Pathway for Cholesterol Homeostasis | Science. Accessed August 23, 2025. https://www.science.org/doi/10.1126/science.3513311

79. Effects of Statins on High-Density Lipoproteins: A Potential Contribution to Cardiovascular Benefit - PMC. Accessed September 23, 2025. https://pmc.ncbi.nlm.nih.gov/articles/PMC2493531/

80. Sorrentino S, Landmesser U. Nonlipid-lowering effects of statins. Curr Treat Options Cardiovasc Med. 2005;7(6):459-466. doi:10.1007/s11936-005-0031-1

81. Shitara Y, Sugiyama Y. Pharmacokinetic and pharmacodynamic alterations of 3-hydroxy-3-methylglutaryl coenzyme A (HMG-CoA) reductase inhibitors: Drug–drug interactions and interindividual differences in transporter and metabolic enzyme functions. Pharmacology & Therapeutics. 2006;112(1):71-105. doi:10.1016/j.pharmthera.2006.03.003

82. Cholesterol Treatment Trialists' (CTT) Collaboration, Baigent C, Blackwell L, et al. Efficacy and safety of more intensive lowering of LDL cholesterol: a meta-analysis of data from 170,000 participants in 26 randomised trials. Lancet. 2010;376(9753):1670-1681. doi:10.1016/S0140-6736(10)61350-5

83. Ruscica M, Ferri N, Banach M, Sirtori CR, Corsini A. Side effects of statins: from pathophysiology and epidemiology to diagnostic and therapeutic implications. Cardiovasc Res. 2022;118(17):3288-3304. doi:10.1093/cvr/cvac020

84. Trust the Blinded Randomized Evidence That Statin Therapy Rarely Causes Symptomatic Side Effects | Circulation. Accessed August 23, 2025. https://www.ahajournals.org/doi/10.1161/CIRCULATIONAHA.118.036846

85. Prevalence of statin intolerance: a meta-analysis | European Heart Journal | Oxford Academic. Accessed August 23, 2025. https://academic.oup.com/eurheartj/article/43/34/3213/6529098

86. Rosenson RS, Baker SK, Jacobson TA, Kopecky SL, Parker BA, The National Lipid Association's Muscle Safety Expert Panel null. An assessment by the Statin Muscle Safety Task Force: 2014 update. J Clin Lipidol. 2014;8(3 Suppl):S58-71. doi:10.1016/j.jacl.2014.03.004

87. Statin-associated muscle symptoms: impact on statin therapy—European Atherosclerosis Society Consensus Panel Statement on Assessment, Aetiology and

Management | European Heart Journal | Oxford Academic. Accessed September 23, 2025. https://academic.oup.com/eurheartj/article/36/17/1012/2465952?login=false

88. Ward NC, Watts GF, Eckel RH. Statin Toxicity. Circ Res. 2019;124(2):328-350. doi:10.1161/CIRCRESAHA.118.312782

89. Catapano AL. Statin-Induced Myotoxicity: Pharmacokinetic Differences among Statins and the Risk of Rhabdomyolysis, with Particular Reference to Pitavastatin. Current Vascular Pharmacology. 10(2):257-267. doi:10.2174/157016112799305021

90. Draeger A, Monastyrskaya K, Mohaupt M, et al. Statin therapy induces ultrastructural damage in skeletal muscle in patients without myalgia. The Journal of Pathology. 2006;210(1):94-102. doi:10.1002/path.2018

91. Flint OP, Masters BA, Gregg RE, Durham SK. Inhibition of cholesterol synthesis by squalene synthase inhibitors does not induce myotoxicity in vitro. TOXICOL APPL PHARMACOL. 1997;145(1):91-98. doi:10.1006/taap.1997.8131

92. Moriarty PM, Thompson PD, Cannon CP, et al. Efficacy and safety of alirocumab vs ezetimibe in statin-intolerant patients, with a statin rechallenge arm: The ODYSSEY ALTERNATIVE randomized trial. J Clin Lipidol. 2015;9(6):758-769. doi:10.1016/j.jacl.2015.08.006

93. Statin-mediated disruption of Rho GTPase prenylation and activity inhibits respiratory syncytial virus infection | Communications Biology. Accessed August 23, 2025. https://www.nature.com/articles/s42003-021-02754-2

94. Greenwood J, Steinman L, Zamvil SS. Statin therapy in autoimmunity: From protein prenylation to immunomodulation. Nat Rev Immunol. 2006;6(5):10.1038/nri1839. doi:10.1038/nri1839

95. Thompson PD, Clarkson P, Karas RH. Statin-Associated Myopathy. J Am Med Assoc. 2003;289(13):1681-1690. doi:10.1001/jama.289.13.1681

96. Marcoff L, Thompson PD. The Role of Coenzyme Q10 in Statin-Associated Myopathy. JACC. 2007;49(23):2231-2237. doi:10.1016/j.jacc.2007.02.049

97. Lalani SR, Vladutiu GD, Plunkett K, Lotze TE, Adesina AM, Scaglia F. Isolated Mitochondrial Myopathy Associated With Muscle Coenzyme Q10 Deficiency. Arch Neurol. 2005;62(2):317-320. doi:10.1001/archneur.62.2.317

98. Folkers K, Langsjoen P, Willis R, et al. Lovastatin decreases coenzyme Q levels in humans. Proceedings of the National Academy of Sciences. 1990;87(22):8931-8934. doi:10.1073/pnas.87.22.8931

99. Laaksonen R, Jokelainen K, Sahi T, Tikkanen MJ, Himberg JJ. Decreases in serum ubiquinone concentrations do not result in reduced levels in muscle tissue during

short-term simvastatin treatment in humans. CLIN PHARMACOL THER. 1995;57(1):62-66. doi:10.1016/0009-9236(95)90266-X

100. High-dose statins and skeletal muscle metabolism in humans: A randomized, controlled trial - Päivä - 2005 - Clinical Pharmacology & Therapeutics - Wiley Online Library. Accessed August 23, 2025. https://ascpt.onlinelibrary.wiley.com/doi/abs/10.1016/j.clpt.2005.03.006

101. Pierno S, Didonna MP, Cippone V, et al. Effects of chronic treatment with statins and fenofibrate on rat skeletal muscle: a biochemical, histological and electrophysiological study. Br J Pharmacol. 2006;149(7):909-919. doi:10.1038/sj.bjp.0706917

102. Schirris TJJ, Renkema GH, Ritschel T, et al. Statin-Induced Myopathy Is Associated with Mitochondrial Complex III Inhibition. Cell Metabolism. 2015;22(3):399-407. doi:10.1016/j.cmet.2015.08.002

103. Liu JC, Lei SY, Zhang DH, et al. The pleiotropic effects of statins: a comprehensive exploration of neurovascular unit modulation and blood–brain barrier protection. Mol Med. 2024;30:256. doi:10.1186/s10020-024-01025-0

104. Ahmadi M, Amiri S, Pecic S, et al. Pleiotropic effects of statins: A focus on cancer. Biochimica et Biophysica Acta (BBA) - Molecular Basis of Disease. 2020;1866(12):165968. doi:10.1016/j.bbadis.2020.165968

105. Kato S, Smalley S, Sadarangani A, et al. Lipophilic but not hydrophilic statins selectively induce cell death in gynaecological cancers expressing high levels of HMGCoA reductase. J Cell Mol Med. 2010;14(5):1180-1193. doi:10.1111/j.1582-4934.2009.00771.x

106. Apostolopoulou M, Corsini A, Roden M. The role of mitochondria in statin-induced myopathy. Eur J Clin Invest. 2015;45(7):745-754. doi:10.1111/eci.12461

107. Evidence for a role of human organic anion transporters in the muscular side effects of HMG-CoA reductase inhibitors. ClinPGx. Accessed September 5, 2025. https://www.clinpgx.org/literature/3013381

108. Banach M, Serban C, Ursoniu S, et al. Statin therapy and plasma coenzyme Q10 concentrations--A systematic review and meta-analysis of placebo-controlled trials. Pharmacol Res. 2015;99:329-336. doi:10.1016/j.phrs.2015.07.008

109. Rundek T, Naini A, Sacco R, Coates K, DiMauro S. Atorvastatin Decreases the Coenzyme Q10 Level in the Blood of Patients at Risk for Cardiovascular Disease and Stroke. Arch Neurol. 2004;61(6):889-892. doi:10.1001/archneur.61.6.889

110. Qu H, Guo M, Chai H, Wang WT, Gao ZY, Shi DZ. Effects of Coenzyme Q10 on Statin-Induced Myopathy: An Updated Meta-Analysis of Randomized Controlled Trials. J Am Heart Assoc. 2018;7(19):e009835. doi:10.1161/JAHA.118.009835

111. Quinzii CM, Hirano M, DiMauro S. CoQ10 deficiency diseases in adults. Mitochondrion. 2007;7(Suppl):S122-S126. doi:10.1016/j.mito.2007.03.004

112. Zaleski AL, Taylor BA, Thompson PD. Coenzyme Q10 as Treatment for Statin-Associated Muscle Symptoms—A Good Idea, but…. Advances in Nutrition. 2018;9(4):519S-523S. doi:10.1093/advances/nmy010

113. Wang Y, Lilienfeldt N, Hekimi S. Understanding coenzyme Q. Physiol Rev. 2024;104(4):1533-1610. doi:10.1152/physrev.00040.2023

114. Kalén A, Appelkvist EL, Chojnacki T, Dallner G. Nonaprenyl-4-hydroxybenzoate transferase, an enzyme involved in ubiquinone biosynthesis, in the endoplasmic reticulum-Golgi system of rat liver. J Biol Chem. 1990;265(2):1158-1164.

115. Pelosi L, Morbiato L, Burgardt A, et al. COQ4 is required for the oxidative decarboxylation of the C1 carbon of coenzyme Q in eukaryotic cells. Molecular Cell. 2024;84(5):981-989.e7. doi:10.1016/j.molcel.2024.01.003

116. Guerra RM, Pagliarini DJ. Coenzyme Q biochemistry and biosynthesis. Trends in Biochemical Sciences. 2023;48(5):463-476. doi:10.1016/j.tibs.2022.12.006

117. Wong HS, Dighe PA, Mezera V, Monternier PA, Brand MD. Production of superoxide and hydrogen peroxide from specific mitochondrial sites under different bioenergetic conditions. J Biol Chem. 2017;292(41):16804-16809. doi:10.1074/jbc.R117.789271

118. Ubiquinone Binding and Reduction by Complex I-Open Questions and Mechanistic Implications - PubMed. Accessed October 7, 2025. https://pubmed.ncbi.nlm.nih.gov/33996767/

119. Okoye CN, Koren SA, Wojtovich AP. Mitochondrial complex I ROS production and redox signaling in hypoxia. Redox Biol. 2023;67:102926. doi:10.1016/j.redox.2023.102926

120. Spandidos Publications: International Journal of Molecular Medicine. Accessed October 26, 2025. https://www.spandidos-publications.com/ijmm

121. Control of mitochondrial superoxide production by reverse electron transport at complex I - Journal of Biological Chemistry. Accessed October 26, 2025. https://www.jbc.org/article/S0021-9258(20)39969-5/fulltext

122. Quinone binding sites of cyt bc complexes analysed by X-ray crystallography and cryogenic electron microscopy | Biochemical Society Transactions | Portland Press. Accessed October 26, 2025.

https://portlandpress.com/biochemsoctrans/article/50/2/877/231101/Quinone-binding-sites-of-cyt-bc-complexes-analysed

123. Structural analysis of cytochrome bc1 complexes: Implications to the mechanism of function - ScienceDirect. Accessed October 26, 2025. https://www.sciencedirect.com/science/article/pii/S0005272812010833?via%3Dihub

124. Crofts AR. The Cytochrome bc1 Complex: Function in the Context of Structure. Annual Review of Physiology. 2004;66(Volume 66, 2004):689-733. doi:10.1146/annurev.physiol.66.032102.150251

125. Ohnishi T, Salerno JC. Conformation-driven and semiquinone-gated proton-pump mechanism in the NADH-ubiquinone oxidoreductase (complex I). FEBS Lett. 2005;579(21):4555-4561. doi:10.1016/j.febslet.2005.06.086

126. Crofts AR. The cytochrome bc1 complex: function in the context of structure. Annu Rev Physiol. 2004;66:689-733. doi:10.1146/annurev.physiol.66.032102.150251

127. Nierobisz LS, Hentz NG, Felts JV, Mozdziak PE. Fiber Phenotype and Coenzyme Q10 Content in Turkey Skeletal Muscles. Cells Tissues Organs. 2010;196(6):382-394. doi:10.1159/000319550

128. Taylor BA, Panza G, Thompson PD. Increased Creatine Kinase with Statin Treatment May Identify Statin-Associated Muscle Symptoms. Int J Cardiol. 2016;209:12-13. doi:10.1016/j.ijcard.2016.02.028

129. Ballard KD, Parker BA, Capizzi JA, et al. Increases in Creatine Kinase with Atorvastatin Treatment are Not Associated with Decreases in Muscular Performance. Atherosclerosis. 2013;230(1):121-124. doi:10.1016/j.atherosclerosis.2013.07.001

130. Rahman S, Clarke CF, Hirano M. 176th ENMC International Workshop: Diagnosis and treatment of Coenzyme Q10 deficiency. Neuromuscul Disord. 2012;22(1):76-86. doi:10.1016/j.nmd.2011.05.001

131. Casagrande D, Waib PH, Jordão Júnior AA. Mechanisms of action and effects of the administration of Coenzyme Q10 on metabolic syndrome. Journal of Nutrition & Intermediary Metabolism. 2018;13:26-32. doi:10.1016/j.jnim.2018.08.002

132. Kubo H, Yamamoto Y, Fujisawa A. Orally ingested ubiquinol-10 or ubiquinone-10 reaches the intestinal tract and is absorbed by the small intestine of mice mostly in its original form. J Clin Biochem Nutr. 2023;72(2):101-106. doi:10.3164/jcbn.22-91

133. Coenzyme Q10: Absorption, tissue uptake, metabolism and pharmacokinetics: Free Radical Research: Vol 40 , No 5 - Get Access. Accessed September 24, 2025. https://www.tandfonline.com/doi/full/10.1080/10715760600617843

134. Vitetta L, Leong A, Zhou J, Dal Forno S, Hall S, Rutolo D. The Plasma Bioavailability of Coenzyme Q10 Absorbed from the Gut and the Oral Mucosa. J Funct Biomater. 2018;9(4):73. doi:10.3390/jfb9040073

135. Batiha O, Hamzeh D, Alfaqih MA, Nawafleh M, Khanjar H, Al-zoubi E. The interaction between a genetic variant in the NQO1 gene and environmental influences involving coenzyme Q10 has a significant impact on sperm motility. Acta Biomedica Atenei Parmensis. 2024;95(5):e2024166-e2024166. doi:10.23750/abm.v95i5.16314

136. Fischer A, Schmelzer C, Rimbach G, Niklowitz P, Menke T, Döring F. Association between genetic variants in the Coenzyme Q10 metabolism and Coenzyme Q10 status in humans. BMC Res Notes. 2011;4:245. doi:10.1186/1756-0500-4-245

137. Miles MV. The uptake and distribution of coenzyme Q10. Mitochondrion. 2007;7 Suppl:S72-77. doi:10.1016/j.mito.2007.02.012

138. Zhang Q, Xia M, Zheng C, et al. The Cocrystal of Ubiquinol: Improved Stability and Bioavailability. Pharmaceutics. 2023;15(10):2499. doi:10.3390/pharmaceutics15102499

139. Weis M, Mortensen SA, Rassing MR, Møller-Sonnergaard J, Poulsen G, Rasmussen SN. Bioavailability of four oral coenzyme Q10 formulations in healthy volunteers. Mol Aspects Med. 1994;15 Suppl:s273-280. doi:10.1016/0098-2997(94)90038-8

140. News. Accessed September 24, 2025. https://www.pharmanord.eu/news/therefore-q10-in-soybean-oil---no-one-else-was-nearly-as-good

141. Hertel-Storm P, Sindberg C. BIOAVAILABILITY OF COENZYME Q 10 FORMULATED WITH PALM OIL IS EQUIVALENT WITH A SIMILAR SOY OIL FORMULATION (Conference Poster Abstract). Accessed September 24, 2025. https://www.academia.edu/25193144/BIOAVAILABILITY_OF_COENZYME_Q_10_FORMULATED_WITH_PALM_OIL_IS_EQUIVALENT_WITH_A_SIMILAR_SOY_OIL_FORMULATION_Conference_Poster_Abstract_

142. Masotta NE, Martinefski MR, Lucangioli S, Rojas AM, Tripodi VP. High-dose coenzyme Q10-loaded oleogels for oral therapeutic supplementation. Int J Pharm. 2019;556:9-20. doi:10.1016/j.ijpharm.2018.12.003

143. Chaudhary AA, Fareed M, Khan SUD, et al. Exploring the therapeutic potential of lipid-based nanoparticles in the management of oral squamous cell carcinoma. Explor Target Antitumor Ther. 2024;5(6):1223-1246. doi:10.37349/etat.2024.00272

144. Bergamini C, Moruzzi N, Sblendido A, Lenaz G, Fato R. A Water Soluble CoQ10 Formulation Improves Intracellular Distribution and Promotes Mitochondrial Respiration in Cultured Cells. PLOS ONE. 2012;7(3):e33712. doi:10.1371/journal.pone.0033712

145. Novel Lipid-Based Formulation to Enhance Coenzyme Q10 Bioavailability: Preclinical Assessment and Phase 1 Pharmacokinetic Trial. Accessed September 24, 2025. https://www.mdpi.com/1999-4923/17/4/414

146. Karimi N, Ghanbarzadeh B, Hamishehkar H, Keivani F, Pezeshki A, Gholian MM. Phytosome and Liposome: The Beneficial Encapsulation Systems in Drug Delivery and Food Application. Applied Food Biotechnology. 2015;2(3):17-27. doi:10.22037/afb.v2i3.8832

147. Koppula S, Shaik B, Maddi S. Phytosomes as a New Frontier and Emerging Nanotechnology Platform for Phytopharmaceuticals: Therapeutic and Clinical Applications. Phytotherapy Research. 2025;39(5):2217-2249. doi:10.1002/ptr.8465

148. Kapse MV, Mulla JAS. Unlocking the potential of phytosomes: a review of formulation techniques, evaluation methods, and emerging applications. Acta Materia Medica. 2024;3:509-520. doi:10.15212/AMM-2024-0055

149. Rizzardi N, Liparulo I, Antonelli G, et al. Coenzyme Q10 Phytosome Formulation Improves CoQ10 Bioavailability and Mitochondrial Functionality in Cultured Cells. Antioxidants (Basel). 2021;10(6):927. doi:10.3390/antiox10060927

150. Cicero AFG, Fogacci F, Di Micoli A, Veronesi M, Borghi C. Noninvasive instrumental evaluation of coenzyme Q10 phytosome on endothelial reactivity in healthy nonsmoking young volunteers: A double-blind, randomized, placebo-controlled crossover clinical trial. Biofactors. 2022;48(5):1160-1165. doi:10.1002/biof.1839

151. Fehr S, Wilson M, Downs J, et al. The CDKL5 disorder is an independent clinical entity associated with early-onset encephalopathy. Eur J Hum Genet. 2013;21(3):266-273. doi:10.1038/ejhg.2012.156

152. Jakimiec M, Paprocka J, Śmigiel R. CDKL5 Deficiency Disorder-A Complex Epileptic Encephalopathy. Brain Sci. 2020;10(2):107. doi:10.3390/brainsci10020107

153. Bertani I, Rusconi L, Bolognese F, et al. Functional Consequences of Mutations in CDKL5, an X-linked Gene Involved in Infantile Spasms and Mental Retardation *. Journal of Biological Chemistry. 2006;281(42):32048-32056. doi:10.1016/S0021-9258(19)84118-2

154. Zhu YC, Xiong ZQ. Molecular and Synaptic Bases of CDKL5 Disorder. Dev Neurobiol. 2019;79(1):8-19. doi:10.1002/dneu.22639

155. Van Bergen NJ, Massey S, Stait T, et al. Abnormalities of mitochondrial dynamics and bioenergetics in neuronal cells from CDKL5 deficiency disorder. Neurobiol Dis. 2021;155:105370. doi:10.1016/j.nbd.2021.105370

156. Crane FL. Biochemical functions of coenzyme Q10. J Am Coll Nutr. 2001;20(6):591-598. doi:10.1080/07315724.2001.10719063

157. Disturbed redox homeostasis and oxidative stress: Potential players in the developmental regression in Rett syndrome - ScienceDirect. Accessed October 8, 2025. https://www.sciencedirect.com/science/article/abs/pii/S0149763418306900?via%3Dihub

158. Pastor-Maldonado CJ, Suárez-Rivero JM, Povea-Cabello S, et al. Coenzyme Q10: Novel Formulations and Medical Trends. International Journal of Molecular Sciences. 2020;21(22):8432. doi:10.3390/ijms21228432

159. Avelar-Freitas BA, Almeida VG, Pinto MCX, et al. Trypan blue exclusion assay by flow cytometry. Braz J Med Biol Res. 2014;47:307-315. doi:https://doi.org/10.1590/1414-431X20143437

160. Lowry OH, Rosebrough NJ, Farr AL, Randall RJ. Protein measurement with the Folin phenol reagent. J Biol Chem. 1951;193(1):265-275.

161. New variants expand the neurological phenotype of COQ7 deficiency - Fabra - 2024 - Journal of Inherited Metabolic Disease - Wiley Online Library. Accessed October 4, 2025. https://onlinelibrary.wiley.com/doi/10.1002/jimd.12776

162. Loi M, Trazzi S, Fuchs C, et al. Increased DNA Damage and Apoptosis in CDKL5-Deficient Neurons. Mol Neurobiol. 2020;57(5):2244-2262. doi:10.1007/s12035-020-01884-8

163. van Meerloo J, Kaspers GJL, Cloos J. Cell Sensitivity Assays: The MTT Assay. In: Cree IA, ed. Cancer Cell Culture: Methods and Protocols. Humana Press; 2011:237-245. doi:10.1007/978-1-61779-080-5_20

164. Coenzyme Q biosynthesis inhibition induces HIF-1α stabilization and metabolic switch toward glycolysis - Liparulo - 2021 - The FEBS Journal - Wiley Online Library. Accessed October 4, 2025. https://febs.onlinelibrary.wiley.com/doi/10.1111/febs.15561

165. Jones DP. Determination of pyridine dinucleotides in cell extracts by high-performance liquid chromatography. Journal of Chromatography B: Biomedical Sciences and Applications. 1981;225(2):446-449. doi:10.1016/S0378-4347(00)80293-5

166. Takada M, Ikenoya S, Yuzuriha T, Katayama K. [17] Simultaneous determination of reduced and oxidized ubiquinones. In: Methods in Enzymology. Vol 105. Oxygen Radicals in Biological Systems. Academic Press; 1984:147-155. doi:10.1016/S0076-6879(84)05020-5

167. Kruger NJ. The Bradford Method For Protein Quantitation. In: Walker JM, ed. The Protein Protocols Handbook. Humana Press; 2009:17-24. doi:10.1007/978-1-59745-198-7_4

168. Larsen S, Nielsen J, Hansen CN, et al. Biomarkers of mitochondrial content in skeletal muscle of healthy young human subjects. J Physiol. 2012;590(Pt 14):3349-3360. doi:10.1113/jphysiol.2012.230185

169. Bergamini C, Fato R, Biagini G, et al. Mitochondrial changes induced by natural and synthetic asbestos fibers: studies on isolated mitochondria. Cell Mol Biol (Noisy-le-grand). 2007;52 Suppl:OL905-913.

170. Spinazzi M, Casarin A, Pertegato V, Salviati L, Angelini C. Assessment of mitochondrial respiratory chain enzymatic activities on tissues and cultured cells. Nat Protoc. 2012;7(6):1235-1246. doi:10.1038/nprot.2012.058

171. Askerlund P, Larsson C, Widell S. Localization of donor and acceptor sites of NADH dehydrogenase activities using inside-out and right-side-out plasma membrane vesicles from plants. FEBS Letters. 1988;239(1):23-28. doi:10.1016/0014-5793(88)80538-6

172. Pedrera L, Prieto Clemente L, Dahlhaus A, et al. Ferroptosis triggers mitochondrial fragmentation via Drp1 activation. Cell Death Dis. 2025;16(1):40. doi:10.1038/s41419-024-07312-2

173. Reilly CA, Aust SD. Measurement of lipid peroxidation. Curr Protoc Toxicol. 2001;Chapter 2:Unit 2.4. doi:10.1002/0471140856.tx0204s00

174. Fato R, Bergamini C, Bortolus M, et al. Differential effects of mitochondrial Complex I inhibitors on production of reactive oxygen species. Biochimica et Biophysica Acta (BBA) - Bioenergetics. 2009;1787(5):384-392. doi:10.1016/j.bbabio.2008.11.003

175. Raman spectra of isotopic derivatives of p-benzoquinone: revised vibrational assignments | The Journal of Physical Chemistry. Accessed September 30, 2025. https://pubs.acs.org/doi/10.1021/j100160a035

176. Raman scattering in bilayers of saturated phosphatidylcholines. Experiment and theory | Biochemistry. Accessed September 30, 2025. https://pubs.acs.org/doi/10.1021/bi00543a016

177. Roche Y, Peretti P, Bernard S. DSC and Raman studies of the side chain length effect of ubiquinones on the thermotropic phase behavior of liposomes. Thermochimica Acta. 2006;447(1):81-88. doi:10.1016/j.tca.2006.05.009

178. Brodkorb A, Egger L, Alminger M, et al. INFOGEST static in vitro simulation of gastrointestinal food digestion. Nat Protoc. 2019;14(4):991-1014. doi:10.1038/s41596-018-0119-1

179. Wojcicki K, Budzinska A, Jarmuszkiewicz W. Effects of Atorvastatin and Simvastatin on the Bioenergetic Function of Isolated Rat Brain Mitochondria. International Journal of Molecular Sciences. 2024;25(15):8494. doi:10.3390/ijms25158494

180. Quantitative Correlation of Raman Spectral Indicators in Determining Conformational Order in Alkyl Chains | The Journal of Physical Chemistry A. Accessed October 29, 2025. https://pubs.acs.org/doi/10.1021/jp014311n

181. Saletnik A, Saletnik B, Zaguła G, Puchalski C. Raman Spectroscopy for Plant Disease Detection in Next-Generation Agriculture. Sustainability. 2024;16(13):5474. doi:10.3390/su16135474

182. Mach F, Baigent C, Catapano AL, et al. 2019 ESC/EAS Guidelines for the management of dyslipidaemias: lipid modification to reduce cardiovascular risk: The Task Force for the management of dyslipidaemias of the European Society of Cardiology (ESC) and European Atherosclerosis Society (EAS). European Heart Journal. 2020;41(1):111-188. doi:10.1093/eurheartj/ehz455

183. Shi Z, Han S. Personalized statin therapy: Targeting metabolic processes to modulate the therapeutic and adverse effects of statins. Heliyon. 2025;11(1):e41629. doi:10.1016/j.heliyon.2025.e41629

184. Gbelcová H, Rimpelová S, Jariabková A, et al. Highly variable biological effects of statins on cancer, non-cancer, and stem cells in vitro. Sci Rep. 2024;14(1):11830. doi:10.1038/s41598-024-62615-w

185. Ahmadi Y, Fard JK, Ghafoor D, Eid AH, Sahebkar A. Paradoxical effects of statins on endothelial and cancer cells: the impact of concentrations. Cancer Cell Int. 2023;23(1):43. doi:10.1186/s12935-023-02890-1

186. Khatiwada N, Hong Z. Potential Benefits and Risks Associated with the Use of Statins. Pharmaceutics. 2024;16(2):214. doi:10.3390/pharmaceutics16020214

187. Friedrich T, Dekovic DK, Burschel S. Assembly of the Escherichia coli NADH:ubiquinone oxidoreductase (respiratory complex I). Biochim Biophys Acta. 2016;1857(3):214-223. doi:10.1016/j.bbabio.2015.12.004

188. Brandt U. Energy Converting NADH: Quinone Oxidoreductase (Complex I). Annual Review of Biochemistry. 2006;75(Volume 75, 2006):69-92. doi:10.1146/annurev.biochem.75.103004.142539

189. Goncalves RLS, Wang ZB, Riveros JK, et al. CoQ imbalance drives reverse electron transport to disrupt liver metabolism. Nature. 2025;643(8073):1057-1065. doi:10.1038/s41586-025-09072-1

190. Schittny A, Huwyler J, Puchkov M. Mechanisms of increased bioavailability through amorphous solid dispersions: a review. Drug Deliv. 2019;27(1):110-127. doi:10.1080/10717544.2019.1704940

Financed by the European Union—Next Generation EU—Mission 4, Component 2, Investment 3.3 (DM 352/2022), CUP J33C22001530009 and by Indena S.p.A. (Milano)